

Actinide Transmutation in Nuclear Reactors

J. Bultman

May 8, 1995

Actinide Transmutation in Nuclear Reactors

PROEFSCHRIFT

ter verkrijging van de graad van doctor
aan de Technische Universiteit Delft,
op gezag van de Rector Magnificus Prof. ir. K.F. Wakker,
in het openbaar te verdedigen ten overstaan van een commissie,
door het College van Dekanen aangewezen,
op dinsdag 17 januari 1995 te 13.30 uur
door

Jan Hendrik BULTMAN

doctorandus in de natuurkunde
geboren te Renkum

Dit proefschrift is goedgekeurd door de promotor:
Prof. dr. ir. H. van Dam

Toegevoegd promotor: Dr. ir. J.E. Hoogenboom.

The work described in this thesis has been performed at the Netherlands Energy Research Foundation (ECN), Petten.

CIP-GEGEVENS KONINKLIJKE BIBLIOTHEEK, DEN HAAG

Bultman, Jan Hendrik

Actinide Transmutation in Nuclear Reactors

Jan Hendrik Bultman.- Petten: Netherlands Energy Research Foundation (ECN)

Thesis Delft University of Technology. -I11.

With ref. - With summary in Dutch.

ISBN 90-9007889-4

NUGI 812

Subject headings: Nuclear Reactors, Nuclear Waste, Transmutation

Copyright ©1995 by J.H. Bultman

Voorwoord

Kernafval speelt in menige discussie over kernenergie een grote rol. In discussies tussen mij en mijn ouders leidde dit tot onoverbrugbare meningsverschillen. ECN heeft mij de mogelijkheid gegeven wat dieper op deze materie in te gaan en naar een oplossing van dit probleem te zoeken. Het resultaat van deze zoekactie ligt voor u, in de vorm van een proefschrift.

Dit heb ik niet alleen gedaan. Dr. Harm Gruppelaar heeft de zoekactie ingeleid en vanaf het begin heeft Dr. Ir. Ton Janssen mij op het goede pad gehouden, later bijgestaan door Dr. Ir. Jan Leen Kloosterman. Jan Leen heeft aan de wieg gestaan, zoals zoveel ECN'ers, van mijn vierde hoofdstuk. Professor Dr. Ir. H. Van Dam en Dr. Ir. J.E. Hoogenboom bedank ik voor hun inbreng en kritiek op mijn proefschrift. Hun werkcolleges hebben mij gevormd tot een zeer speciale reactorfysicus, namelijk één die alle opgaven van Duderstadt heeft volbracht.

Ik dank het ECN voor de financiering van dit project. Dit werk is een bijdrage aan het ECN-onderzoeksproject voor de energievoorziening van de toekomst, ENGINE. Een andere financier is de Gemeenschappelijke Kernenergiecentrale Nederland (GKN) te Dodewaard. Zij heeft een stage van acht maanden mogelijk gemaakt bij General Electric Nuclear Energy te San José, Californië.

I would like to thank my friends at General Electric Nuclear Energy of the Advanced Reactor Program; Dr. Jim Quinn and Dr. Pat Magee for giving me encouragement and freedom to operate; Dr. Christine Cockey and Dr. Tang Wu for teaching me to work with their codes and computers. Chris, Tang, Sarah, and Alan, thank you so much for acquainting me the principles of TGIF!

Tenslotte, bedank ik mijn vrienden, collega's, familieleden en ouders voor hun steun. Deze missie had ik nooit kunnen volbrengen zonder de toewijding van Willy en Beth.

Jan Bultman

Contents

Voorwoord	iii
Summary	ix
Samenvatting	x
Nomenclature	xiii
List of Symbols	xiv
List of Definitions	xv
List of Abbreviations	xix
1 Introduction	1
1.1 Nuclear Energy and Waste	1
1.2 Motivation to Perform this Work	4
1.3 What this Thesis Covers	6
2 Nuclear Waste and Nuclear Waste Reduction	9
2.1 Introduction	9
2.2 Waste Parameters	10
2.3 Waste Production and Reduction Factors	13
2.3.1 Fuel and Waste Amounts and Flows	13
2.3.2 Definitions to Evaluate Waste Production and Reduction	16
2.4 On Reducing LWR Waste by Recycling in LWRs	17

2.4.1	Introduction	17
2.4.2	Calculational Method	19
2.4.3	Plutonium Recycling in LWRs	20
2.4.4	Transuranics Recycling in LWRs	22
2.4.5	Uranium Recycling in LWRs	24
2.4.6	Transuranics Waste Produced by Equilibrium LWRs	26
2.5	Energy Scenarios and Waste Production	26
2.5.1	Energy Scenarios	28
2.5.2	Reactor Designs	29
2.5.3	Waste and Energy Production	31
2.6	Physics Aspects of Burner Design	36
2.6.1	Burner Design Objective	36
2.6.2	Waste and Enrichment	37
2.6.3	Transmutation Efficiency of a Transuranics Fueled Reactor	39
2.7	Conclusions	41
3	LWR Waste Reduction with ALMR Burners	43
3.1	Introduction	43
3.2	The ALMR system	45
3.3	Design Approach	48
3.4	Calculational Methods	51
3.4.1	Multigroup Cross Section Generation	52
3.4.2	Flux Solution and Burnup Calculations	54
3.4.3	Reactivity Control Requirement and Control Rod Worth Calculation	55
3.4.4	Void Worth and Reactivity Parameters	55
3.5	Influence of Design Parameters on Actinide Burning	57
3.5.1	Introduction	57
3.5.2	Partial Derivatives of the Performance Parameters to the Design Parameters	58
3.5.3	Correlations between the Coefficients for Cycle Length and Number of Batches	61

3.5.4	Burner Optimization within Performance Constraints . . .	62
3.6	Metallic and Oxide Fueled ALMR Burners	69
3.6.1	Optimization Process and Core Description	69
3.6.2	Comparison of the Metallic and Oxide Fueled Burners . . .	71
3.6.3	Reactivity Control	73
3.6.4	Void Worth and Reactivity Parameters of the Optimized Burner Designs	74
3.6.5	Safety Parameters	79
3.7	Conclusions	86
4	Molten Salt Transmuter	89
4.1	Introduction	89
4.2	History of the Molten Salt Reactor Development	92
4.3	Systems Description	93
4.3.1	Core	93
4.3.2	Reprocessing	94
4.3.3	Materials	94
4.3.4	Cooling	96
4.4	Calculational Methods	96
4.4.1	Neutron Balance	96
4.4.2	Calculation of Fission Product Densities	97
4.4.3	Calculation of the Actinide Densities	98
4.4.4	Core Calculation	100
4.4.5	Calculation of Reactivity Coefficients	100
4.5	Design of the Molten Salt Transmuter	100
4.5.1	Role of Fission Products	100
4.5.2	Flux Dependence	102
4.5.3	Fuel Volume Fraction Dependence	107
4.5.4	Transuranics Salt Fraction Dependence	111
4.5.5	Startup of the Molten Salt Transmuter	114
4.5.6	Discussion of the Results	114

4.6	Influence of Uncertainty in Actinide Cross Sections	115
4.6.1	Adjoint Computational Method	115
4.6.2	Method Verification	117
4.6.3	Reactivity and Core Size	118
4.7	Conclusions	121
5	Final Conclusions and Recommendations	123
	REFERENCES	130
A	EQUI: Calculation of Equilibrium Actinide Densities	131
A.1	Computational Method	131
A.2	Cross Section and Decay Data	134
A.3	Program Description	135
A.4	Verification of EQUI	137
A.4.1	Nuclide Densities	137
A.5	Conclusions	139
	Curriculum Vitae	140

Summary

The reduction of the transuranics part of nuclear waste is discussed in this thesis. Only the transuranics and not the fission products are discussed, because they represent the highest environmental hazard in the long term. A huge amount of 1,000 tonne of transuranics is already produced worldwide, and annually about 80 tonne of transuranics is added. This material can be used for nuclear energy production, for instance, as fuel for Advanced Liquid Metal Reactors (ALMRs), but to reduce this amount will be rather difficult as only $1.2 \text{ kg/MW}_e \cdot \text{y}$ can be fissioned maximally. To stabilize the amount of transuranics, one has to operate about 70 GW_e in burners; that is an increase of about 20% in installed nuclear power worldwide.

One can reduce the production of transuranics by recycling in the reactor which produces them. As is shown in chapter two of this thesis, only the plutonium isotopes can be recycled in Light Water Reactors (LWRs), because recycling of other transuranics will lead to a high production of short-lived and spontaneously fissioning actinides. These actinides make the reprocessing of fuel, which is necessary when recycling is applied, impossible with current techniques. The production of transuranics can be reduced by maximally a factor of four by recycling plutonium isotopes in LWRs.

Another approach to reduce transuranics is the use of special burners. In chapter two, we show that nuclear energy can be produced without an increase of the transuranics amount currently produced. For low reprocessing losses in the order of 0.1 %, energy can be produced in this way for many centuries.

The physics of transuranics transmutation is rather simple: reduce the production rate of transuranics by removing uranium from the fuel. Also, the time to reduce a certain amount of transuranics should be small, which can be accomplished by a high specific power. All other design criteria are related to issues of safety and technology. This is an important conclusion; it shows that previous studies' focus on burning capability, which can be raised to $1.2 \text{ kg/MW}_e \cdot \text{y}$ at the most, was irrelevant. One has to take safety and technological issues in consideration, which might reduce the burning capability.

Two important issues result from reactor operation without uranium. First, fissioned material is not replaced by fissile material formed by neutron capture in the fertile uranium. This leads to a large reactivity loss during a cycle. This loss should be compensated e.g. by control rods, which is in contradiction with modern safety philosophies. Second, the Doppler coefficient which may result from the broadening of neutron absorption resonances will be very different, changing the reactivity feedback. Unsafe reactor operation results when the reactivity feedback is positive or negative but small in absolute value.

The production of the short-lived and spontaneously fissioning actinides results from recycling transuranics. Production is limited when a fast spectrum reactor is used. Therefore, this type of reactor is discussed in chapter three of this thesis. However, for this commercially designed ALMR, one limits the transuranics enrichment to about 30%, which leads to a reduced burning capability of about $0.4 \text{ kg/MW}_e \cdot \text{y}$. Also, the inventory of transuranics is rather high, leading to several hundreds of years to reduce a certain amount of transuranics. Even with fertile material present, the burnup reactivity loss is increased, reducing safety. Another issue related to the standard fast reactor technology is the sodium void effect. This effect is reduced considerably for burner reactors, but is still positive for sodium voiding of the fuel region.

In this thesis, an optimization method is developed to maximize the burning capability of the ALMR while complying with all constraints imposed on the design for reliability and safety. This method leads to a maximal transuranics enrichment, which is being limited by constraints on reactivity. The enrichment can be raised by using the neutrons less efficiently by increasing leakage from the fuel.

With the developed optimization method, a metallic and an oxide fueled ALMR were optimized. Both reactors perform equally well considering the burning of transuranics. However, metallic fuel has a much higher heat conductivity coefficient, which in general leads to better safety characteristics.

In search of a more effective waste transmuter, a modified Molten Salt Reactor was designed for this study. A Molten Salt Reactor operates on a liquid fuel salt which makes continuous refueling possible, eliminating the issue of the burnup reactivity loss. Also, a prompt negative reactivity feedback is possible for an overmoderated reactor design, even when the Doppler coefficient is positive, due to the fuel expansion with fuel temperature increase. Furthermore, the molten salt fuel can be reprocessed based on a reduction process which is not sensitive to the short-lived spontaneously fissioning actinides.

In chapter four of this thesis, we show that the margins in which such a design can be operated are very limited. One has to take a fuel fraction higher than about 7%, and the minimum power is equal to about 1000 MW_t . This is due to a limit on the the power density salt and the high fraction of fissionable higher actinides. The salt power density and the production of these higher actinides are limited by an increase in fuel volume fraction due to the reduction in spectrum weighted microscopic cross sections. Higher fuel volume fractions leads to an increase in prompt negative reactivity feedback. Therefore, the conclusion of this work is that the safest way to operate the Molten Salt Transmuter is with a high fuel volume fraction to obtain a fast reactor. Operation as a thermal reactor is possible for a very limited range of parameters. Any underestimation of the

absorption rate of the fission products or the need for some overreactivity will make operation impossible. Operating a Molten Salt Transmuter will halve the inventory of transuranics in less than 10 years, which is more than a factor of four shorter than for the ALMR burners.

Actinidentransmutatie in Kernreactoren

Samenvatting

Reductie van het transuranen deel van nucleair afval wordt behandeld in dit proefschrift. Alleen de reductie van de hoeveelheid transuranen, en niet van de splijttingsprodukten, wordt beschouwd, omdat deze op de lange termijn het grootste milieurisico geven. Over de hele wereld is al een gigantische hoeveelheid van 1000 ton transuranen geproduceerd en jaarlijks wordt 80 ton transuranen toegevoegd. Echter, dit materiaal is nog steeds geschikt als brandstof in reactoren, bijvoorbeeld voor de Advanced Liquid Metal Reactor (ALMR), een reactorontwerp van General Electric. Reductie van deze grote hoeveelheid transuranen is echter moeilijker, omdat slechts 1,2 kg/MW_e.j verspleten kan worden. Om de hoeveelheid transuranen te stabiliseren, moet dan 70 GW_e aan verbrandercapaciteit worden opgesteld, wat een toename is van 20% aan geïnstalleerd vermogen.

De productie van transuranen kan worden afgeremd door de transuranen terug te voeren in de reactor die ze gemaakt heeft. In hoofdstuk twee wordt aangetoond dat alleen plutoniumisotopen op deze manier teruggevoerd kunnen worden in Licht Water Reactoren (LWR). Dit komt doordat als ook andere transuranen worden teruggevoerd, er een hoge concentratie aan kortlevende en spontaan splijtende actiniden wordt gevormd. Deze actiniden maken opwerken, noodzakelijk voor het terugvoeren van transuranen, op basis van huidige technieken onmogelijk. Als plutonium wordt teruggevoerd kan de groei van transuranen met maximaal een factor vier worden gereduceerd in LWRs.

Een mogelijkheid om transuranen te reduceren is door gebruik te maken van speciale verbranders. Op deze manier is het mogelijk om energie te produceren zonder dat de al geproduceerde hoeveelheid transuranen stijgt. Als de verliezen bij opwerking beperkt blijven tot 0.1% kan vele eeuwen energie worden geproduceerd zonder een toename van de hoeveelheid transuranenafval.

De fysica van transmutatie van transuranen is nogal eenvoudig: beperk de productiesnelheid van transuranen door het uranium uit de brandstof te verwijderen. Ook de tijd om een zekere hoeveelheid transuranen te verminderen moet klein zijn. Dit wordt bereikt met een hoog specifiek vermogen. Dit is een belangrijke conclusie; het toont aan dat de focus van vorige onderzoeken om een zo groot mogelijke verbrandingscapaciteit te krijgen irrelevant was. Die capaciteit is maximaal 1,2 kg/MW_e.j bij bedrijf zonder uranium. Echter, als veiligheid en technologie in beschouwing worden genomen zal de verbrandingscapaciteit lager liggen.

Twee belangrijke problemen treden op bij bedrijf zonder uranium. Ten eerste wordt verspleten materiaal niet vervangen door nieuw splijtbaar materiaal gevormd door

neutronenvangst in het moeilijk splijtbaar uranium. Daardoor wordt de verandering van reactiviteit gedurende een cyclus groot. Deze verandering van reactiviteit moet dan opgevangen worden met bijvoorbeeld regelstaven. Dit is in tegenspraak met de huidige veiligheidsfilosofie. Ten tweede zal de Doppler coefficient ten gevolge van de verbreding van resonanties in absorptie werkzame doorsneden veranderen, wat de reactiviteits-terugkoppeling beïnvloedt. De veiligheid van een systeem wordt zwaar aangetast wanneer de terugkoppeling positief of licht negatief is.

Momenteel is opwerking van brandstof niet mogelijk als de fractie kortlevende en spontaan-splijtende actiniden groot is. De produktie van de kortlevende en spontaan-splijtende isotopen is beperkt voor een reactor met een snel spectrum. Dit type reactor wordt daarom behandeld in hoofdstuk drie van dit proefschrift. Voor het behandelde commerciële reactorontwerp, de ALMR, is de verrijkingsgraad van transuranen beperkt tot 30% wat de mogelijkheid tot verbranding van transuranen reduceert tot 0,4 kg/MW_e.j. De transuraneninventaris is nogal hoog wat leidt tot een lange tijd om een bepaalde hoeveelheid transuranen te transmuteren. De verandering van reactiviteit gedurende een cyclus is hoog ondanks het uranium in de reactor. Dit heeft een nadelig effect op de veiligheid van het ontwerp. Een andere factor die een rol speelt bij standaard snelle reactortechnologie is het natriumdampbel-effect. In snelle reactoren leidt verwijdering van het natrium uit de kern tot een reactiviteitstoename, hetgeen zeer ongewenst is. Voor een verbrander is dit effect aanzienlijk kleiner door de grotere kans dat neutronen weglekken uit de kern.

In dit proefschrift is een methode ontwikkeld om de Advanced Liquid Metal Reactor te optimaliseren om een zo hoog mogelijke opbrand van transuranen te halen *binnen* de grenzen die gesteld zijn voor een veilig en betrouwbaar ontwerp. De methode leidt tot een maximale verrijkingsgraad aan transuranen, die wordt beperkt door eisen aan de reactiviteit. De verrijkingsgraad kan omhoog als de neutronen minder efficiënt worden gebruikt door een verhoogde lek uit de brandstof.

Met deze optimalisatiemethode zijn twee Advanced Liquid Metal Reactors ontwikkeld: één met metallische brandstof en één met oxidische brandstof. Het blijkt dat beide reactoren niet voor elkaar onderdoen wat betreft de opbrand van transuranen. Echter, de metallische brandstof heeft een veel hogere warmtegeleidingscoëfficiënt, wat in het algemeen leidt tot een beter gedrag tijdens ongevals-situaties.

Een betere verbrander is ontwikkeld op basis van een Gesmolten Zout Reactor. Deze reactor wordt bedreven met brandstof opgelost in een gesmolten zout. Een vloeibare brandstof maakt continu herladen van brandstof mogelijk waardoor geen verandering van reactiviteit gedurende een cyclus optreedt. Een prompt negatieve reactiviteits-terugkoppeling is ook mogelijk voor dit reactortype door te kiezen voor een overgemodereerd reactorontwerp. Dit komt door de uitzetting

van brandstof bij hogere temperatuur. Een bijkomend voordeel is dat opwerking mogelijk is volgens een reductieproces dat ongevoelig is voor aanwezigheid van kortlevende spontaan-splijtende actiniden. In dit proefschrift wordt aangetoond dat het gebied waarin deze reactor bedreven kan worden zeer beperkt is. De brandstof-volumefractie moet groter zijn dan 7% en het vermogen is minimaal 1000 MW_t. Dit komt door de limiet op de vermogensdichtheid in het zout en de hoge fractie aan absorberende, moeilijk-splijtende hogere actiniden. De vermogensdichtheid en de produktie van deze hogere actiniden wordt beperkt wanneer de brandstof-volumefractie wordt verhoogd, wat leidt tot vermindering van de spektrum-gemiddelde werkzame doorsneden. Grotere brandstof-volumefractie's leiden tevens tot een negatieve prompte reactiviteits-terugkoppeling. Daarom is de conclusie van dit onderzoek dat de Gesmolten Zout Verbrander moet worden bedreven met een brandstof-volumefractie groter dan 7%, hetgeen in feite leidt tot een snelle reactor. Bedrijf als thermische reactor is mogelijk voor een zeer beperkt gebied van parameters. Onderschatting van de absorptie van neutronen in splijtingsprodukten of de noodzaak van enige overreactiviteit zal bedrijf als thermische reactor onmogelijk maken. De tijd die nodig is voor een halvering van de transuranen-inventaris is minder dan tien jaar, hetgeen een aanzienlijke verbetering is ten opzichte van de ALMR, die tenminste veertig jaar nodig heeft.

NOMENCLATURE

List of Symbols

α_i	cross section variable
α_D	Doppler reactivity coefficient
α_H	axial fuel expansion reactivity coefficient
α_R	radial fuel expansion reactivity coefficient
α_{Na}	sodium density reactivity coefficient
α^{AC}	ratio of macroscopic capture cross section of the fuel and the macroscopic fission cross section
α^{FP}	ratio of macroscopic absorption cross section of the fission products and the macroscopic fission cross section
α^{PAR}	ratio of macroscopic absorption cross section of parasitic absorbers and the macroscopic fission cross section
α^{TOT}	ratio of total macroscopic absorption cross section and the macroscopic fission cross section
A	neutron interaction matrix
<i>A</i>	net power reactivity increment
\underline{b}	isotope feed vector
b_j	performance parameter j
β	delayed neutron fraction
<i>B</i>	power flow coefficient
B_g^2	geometric buckling
<i>C</i>	inlet temperature coefficient of reactivity
<i>D</i>	amount of fuel discharged from Advanced Reactors at the end of cycle (EOC)
<i>D</i>	diffusion coefficient
η	number of fission neutrons produced per absorption in the fuel
E_L	energy produced by LWRs
E_B	energy produced by Advanced Reactors
<i>f</i>	thermal utilization
<i>F</i>	in-core and out-of-core fuel inventory of Advanced Reactors
<i>F</i>	flow
ϕ	neutron flux
γ_i	yield for fission product i
γ_f	linear expansion coefficient of the fuel
γ_g	linear expansion coefficient of the grid
<i>H</i>	core height
<i>I</i>	inventory of LWRs

k	multiplication factor
k_{∞}	infinite multiplication factor
δk	burnup reactivity loss
l	prompt neutron lifetime
$\langle l \rangle$	average neutron lifetime
λ	decay constant
M^2	migration area
ν	number of neutrons produced per fission
\underline{N}	isotopic density vector
P	reactor power
P_{NL}	non-leakage probability
Q	amount discharged by LWRs
Q_f	part of LWR discharges which will be fed to the ARs
Q_d	part of LWR discharges which will be disposed of
R_j	response function
R	amount of fuel at BOC produced by reprocessing Advanced Reactors fuel
R	core radius
ρ	reactivity
$\rho_{material}$	material density
S_{ij}	relative sensitivity coefficient
Σ_a	macroscopic absorption cross section
σ_a	microscopic absorption cross section
Σ_c	macroscopic capture cross section
σ_c	microscopic capture cross section
Σ_f	macroscopic fission cross section
σ_f	microscopic fission cross section
τ	pump flow coastdown time constant
T	mean in-core residence time
T_{cyc}	cycle length
T_c	average coolant temperature
T_f	average fuel temperature
T_{in}	average inlet coolant temperature
T_{out}	average outlet coolant temperature
V	active core volume
W	amount of waste produced by Advanced Reactors
x_i	value of design parameter i
Z_i	radiotoxicity or radioactivity of isotope i

List of Definitions

Actinides	thorium and elements with higher atomic mass numbers
Activity	number of nuclear disintegrations in a quantity of radioactive material per unit of time; measured in becquerel (Bq)
ALI	Annual Limit on Intake is the activity in becquerels a radiological worker may inhale or ingest maximally to remain below the dose limit for workers, which is 0.02 Sv annually
ARA	all actinides except for Th-232, U-235, and U-238
Batch	number of assemblies loaded and discharged at the same time
Blanket	fertile material used for breeding fissile material
Bondarenko factor	ratio of resonance shielded cross section and infinitely diluted cross section
Break-even	production of fissile atoms equal to the consumption and loss of fissile atoms
Breeding ratio	conversion ratio when it is larger than one
Burnup reactivity loss	loss in reactivity during a cycle; symbol δk
Conversion ratio	ratio of the average rate of fissile atom production and consumption
Control rod worth	reactivity effect of the control rods
Critical	effective multiplication factor of one
Cycle length	time between two reloads of the reactor core
Delayed neutron fraction	fraction of the neutrons produced per fission which are produced by neutron decay of fission products
Denatured	sufficient U-238 added that uranium is not usable for atomic weapons
Design parameters	parameters which can be chosen by the designer
Doppler effect	increase in neutron absorption due to broadening of neutron absorption resonances with temperature

Dose conversion factor	factors to calculate the radiation dose due to ingested or inhaled isotopes measured in Sv/Bq
Duct dilation	the bowing of the assemblies reducing the ducts between the assemblies
Effective multiplication factor	ratio of neutron production rate and neutron loss rate; symbol k
Equilibrium	no change in isotopic density
Equilibrium cycle	reactor cycle which is the same from cycle to cycle
Fast reactor	reactor operated without a moderator
Fertile material	material which will become fissile after neutron capture
Fissionable isotopes	actinides which can not be fissioned by thermal neutrons
Fissile isotopes	actinides which can be fissioned by thermal neutrons
Fuel burnup	amount of energy produced per unit of mass during in-core residence time; measured in MWd/kg(HM)
Fuel utilization	energy produced per unit of mined uranium
In-core residence time	time an assembly is in-core, which equals cycle length times the number of batches
Inventory Transmutation Time	time to transmute an amount equal to the inventory
Infinite multiplication factor	multiplication factor of system assuming no neutron loss by leakage; symbol k_{∞}
Inventory	mass of all assemblies in-core and out-of-core
Isotope feed vector	isotope masses of an array of isotopes
Heavy Metal (HM)	actinide part of the fuel
Lanthanides	fission products with similar chemical behavior as the actinides
Linear power	power produced per fuel element per unit of length; measured in W/cm
Microscopic cross section	nuclide cross section in cm^2
Minor Actinides (MA)	all actinides with higher mass number than uranium except for plutonium
Macroscopic cross section	microscopic cross section times nuclide number density in cm^{-1}

Narrow resonance approximation	approximation for resonance selfshielding generally applicable for high energy resonances
Neutron lifetime	ratio of the neutron population and the neutron loss rate
Nuclear waste	material to be deposited in final storage
One-group cross section	spectrum weighted cross section value
Performance parameters	parameters which result from the choice in design parameters
Potential Waste	inventory of the nuclear fuel cycle
Power density	reactor power per unit of volume; measured in W/cm^3
Power peaking factor	ratio of maximum power density and average power density in core
Prompt super critical	effective multiplication factor larger than one plus the delayed neutron fraction
Radiotoxicity	toxicity due to the ionizing radiation of ingested or inhaled isotopes; symbol ALI
Rational approximation	approximation for the first-flight escape probability in lumped fuels
Reactivity	deviation of the multiplication factor from unity; symbol ρ
Reprocessing	separation of valuable and non-valuable isotopes
Reprocessing losses	losses of isotopes during reprocessing
Sodium void effect	reactivity effect of sodium voiding in a (fast) reactor
Specific power	reactor power per unit of heavy metal mass; measured in $\text{W}/\text{kg}(\text{HM})$
Subcritical	effective multiplication factor smaller than one
Supercritical	effective multiplication factor larger than one
Temperature defect	reactivity change from hot full power to zero power at refueling temperature
Thermal reactor	reactor operated with a neutron moderator
Thermal utilization	probability that if a neutron is absorbed it is absorbed in the fuel
Transmutation	nuclear transition by particle absorption

Transuranics	all elements with a higher mass number than uranium
Waste parameters	quantities characterizing nuclear waste and inventory
Waste Production Ratio	ratio of the waste produced by once-through LWRs and a certain reactor system per unit of energy
Waste Ratio	ratio of the material fed to the waste produced per unit of energy

List of Abbreviations

ALMR	Advanced Liquid Metal Reactor
ASME	American Society of Structural Mechanical Engineers
AR	Advanced Reactor
ARA	Artificial Radiotoxic Actinides
ATWS	Anticipated Transient Without Scram
BOC	Beginning Of Cycle
BOEC	Beginning Of Equilibrium Cycle
<i>BU</i>	burned amount
ENDF	Evaluated Nuclear Data File
EOC	End Of Cycle
EOEC	End Of Equilibrium Cycle
<i>FMSE</i>	fractional mean squared error
GE	General Electric
GEM	Gas Expansion Module
HM	Heavy Metal (all actinides)
HTGR	High Temperature Gas Cooled Reactor
IFR	Integral Fast Reactor
IHTS	Intermediate Heat Transport System
<i>ITT</i>	Inventory Transmutation Time
JEF	Joint Evaluated File
LANL	Los Alamos National Laboratory
LOFWS	Loss Of Flow Without Scram
LOHS	Loss Of Heat Sink
LWR	Light Water Reactor
MA	Minor Actinides
RVACS	Radiant Vessel Auxiliary Cooling System
TOP	Transient Over Power
TRU	Transuranics
<i>WR</i>	Waste Ratio
<i>WPR</i>	Waste Production Ratio

Chapter 1

Introduction

1.1 Nuclear Energy and Waste

Commercial nuclear energy production always has been controversial: the relation between nuclear energy and proliferation of atomic weapons technology, the question of what to do with nuclear waste, and the safety problems. All of these issues are currently investigated by the research institutes and the nuclear-energy related industry. This thesis addresses one of these issues, namely nuclear waste. You will find the results of a computational study on the possibilities to reduce nuclear waste from nuclear reactors.

Two types of potential nuclear waste produced in nuclear reactors can be distinguished: fission products and transuranium elements. Fission products are produced when fissile nuclides are fissioned by a neutron into two nuclei, releasing energy in the form of neutrons, neutrinos, photons, and kinetic movement. Transuranium elements are produced when a neutron is captured by the nucleus of uranium. In general, both types of products are radioactive due to energy excess, which is released by emitting nuclear particles and radiation which can be harmful for all living creatures.

In figure 1.1, the most important actinides are displayed as on a chart of the nuclides. The first actinide is thorium, which occurs as Th-232 in nature. Three other actinides occur in nature, namely U-234, U-235, and U-238. On this chart, one can see what happens upon irradiation. A neutron capture leads to a move to the right.

A	proton number	140	141	142	143	144	145	146	147	148	149	150	151	
96	Cm Curium	Cm 242		Cm 243		Cm 244		Cm 245		Cm 246		Cm 247		
		162.8 d α 6.113,6.069 ... SF σ 16 σ_f 5	28.5 y α 5.785,5.741 ... σ 225 σ_f 600	18.11 a α 5.805,5.763 ... SF σ 13.9 σ_f 1.2	8500 a α 5.362,5.304 ... σ 345 σ_f 2020	4730 a α 5.386,5.343 ... SF σ 1.3 σ_f 0.17	1.56E7 a α 4.869,5.266 ... σ 60 σ_f 90							
95	Am Americium	Am 241		Am 242		Am 243		Am 244		Am 245		Am 246		
		432.6 a α 5.486,5.443 ... SF σ 83.8,7.96,63.2	16 h β 0.6... σ 4600 σ 6000	7570 a α 5.275,5.233 ... SF σ 75,6 σ_f <0.07	26 m 161 h β 1.5... β 0.4... σ 1600 σ 1600	4730 a α 5.362,5.304 ... σ 345 σ_f 2020	1.56E7 a α 4.869,5.266 ... σ 60 σ_f 90							
94	Pu Plutonium	Pu 238		Pu 239		Pu 240		Pu 241		Pu 242		Pu 243		
		87.75 a α 5.499,5.456 ... SF σ 547 σ_f 6.5	2.411E4 a α 5.157,5.144 ... SF σ 268.8 σ_f 742.5	6550 a α 5.168,5.124 ... SF σ 289.5 σ_f 0.030	14.4 a α 5.499,0.002 ... SF σ 368 σ_f 1099	3.763E5 a α 4.901,4.856 ... SF σ 18.5 σ_f <0.2	4.956 h β 0.6... σ 60 σ_f 96	8.26E7 a α 4.894,5.46 ... SF σ 1.7	8.26E7 a α 4.894,5.46 ... SF σ 1.7	8.26E7 a α 4.894,5.46 ... SF σ 1.7	8.26E7 a α 4.894,5.46 ... SF σ 1.7	8.26E7 a α 4.894,5.46 ... SF σ 1.7	8.26E7 a α 4.894,5.46 ... SF σ 1.7	8.26E7 a α 4.894,5.46 ... SF σ 1.7
93	Np Neptunium	Np 237		Np 238		Np 239		Np 240		Np 241		Np 242		
		2.14E6 a α 4.788,4.771 ... SF σ 169.8 σ_f 0.019	2.117 d β 1.2... σ 2070	2.355 d β 0.4; 0.7... σ 31+14 σ_f <1	7.2 m 65 m β 2.2... β 0.9... σ 22	3.763E5 a α 4.901,4.856 ... SF σ 18.5 σ_f <0.2	4.956 h β 0.6... σ 60 σ_f 96	8.26E7 a α 4.894,5.46 ... SF σ 1.7	8.26E7 a α 4.894,5.46 ... SF σ 1.7	8.26E7 a α 4.894,5.46 ... SF σ 1.7	8.26E7 a α 4.894,5.46 ... SF σ 1.7	8.26E7 a α 4.894,5.46 ... SF σ 1.7	8.26E7 a α 4.894,5.46 ... SF σ 1.7	8.26E7 a α 4.894,5.46 ... SF σ 1.7
92	U Uranium	U 232		U 233		U 234		U 235		U 236		U 237		
		70.0 y α 5.520,5.463 ... SF σ 73.1 σ_f 75.2	1.592E5 a α 4.82,4.783 ... SF σ 47.7 σ_f 531.1	2.446E5 a α 4.75,4.713 ... SF σ 100.2 σ_f <0.65	7.038E8 a α 4.46,4.445 ... SF σ 98.3 σ_f 583.54	2.342E7 a α 4.59,4.445 ... SF σ 5.2	6.75 d β 0.2... σ 411 σ_f <0.35	2.35 m β 1.21,3... σ 22	2.35 m β 1.21,3... σ 22	2.35 m β 1.21,3... σ 22	2.35 m β 1.21,3... σ 22	2.35 m β 1.21,3... σ 22	2.35 m β 1.21,3... σ 22	2.35 m β 1.21,3... σ 22
91	Pa Protactinium	Pa 231		Pa 232		Pa 233		Pa 234		Pa 235		Pa 236		
		3.276E4 a α 5.014,4.952 ... SF σ 210 σ_f 0.010	1.31 d β 0.3; 1.3... σ 760 σ_f 700	27.0 d β 0.3; 0.6... σ 21+20 σ_f <0.1	1.17 m 6.70 h β 2.3... β 0.5... σ <500 β <5000	242 m β 1.4... σ 1.8 σ_f <0.01	6.75 d β 0.2... σ 411 σ_f <0.35	2.35 m β 1.21,3... σ 22	2.35 m β 1.21,3... σ 22	2.35 m β 1.21,3... σ 22	2.35 m β 1.21,3... σ 22	2.35 m β 1.21,3... σ 22	2.35 m β 1.21,3... σ 22	2.35 m β 1.21,3... σ 22
90	Th Thorium	Th 230		Th 231		Th 232		Th 233		Th 234		Th 235		
		7.538E4 a α 4.687,4.621 ... SF σ 23.2 σ_f 1.2 μ	25.52 h β 0.362,0.138 ... SF σ 160.1 σ_f 26.68	1.405E10 a α 4.012,3.397 ... SF σ 7.4,8 σ_f 9.9 μ	1.17 m 6.70 h β 2.3... β 0.5... σ <500 β <5000	24.10 d β 0.199,0.104 ... σ 1.8 σ_f <0.01	6.75 d β 0.2... σ 411 σ_f <0.35	2.35 m β 1.21,3... σ 22	2.35 m β 1.21,3... σ 22	2.35 m β 1.21,3... σ 22	2.35 m β 1.21,3... σ 22	2.35 m β 1.21,3... σ 22	2.35 m β 1.21,3... σ 22	2.35 m β 1.21,3... σ 22

Element number A+N
half life
decay type + energy [MeV]
abundance [%]/Spontaneous Fission
capture + fission thermal cross section [b]

Figure 1.1: Chart of the actinides

For instance, neutron capture in U-238 produces U-239. This isotope has a short half life for β decay (an electron is emitted), which leads to a move to the left and up; β decay of U-239 leads to Np-239, which will also emit an electron, which leads to Pu-239. Many actinides display α decay, which is displayed on the chart of the nuclides by two moves left and two moves down. For instance, α decay of Pu-239 leads to U-235. This chart of the nuclides is very important in this thesis; many times the production and decay of isotopes will be discussed. For a clear understanding of these processes, the chart is a necessity.

Three parameters determine the radiotoxicity of a nuclide:

1. the average time to emit the particles and/or radiation,
2. the residence time in biological systems. Some elements, once absorbed in the human body, will stay there forever, and others will not be absorbed. For instance, many of the transuranium elements easily attach to the red bone marrow, which is very sensitive to radiation.
3. the radiation type. Radioactive nuclei can emit four types of radiation: neutron radiation, β -radiation by electrons or positrons, α -radiation by helium nuclei, and gamma radiation, photons emitted by the nucleus, and X-rays, photons emitted by the atom.

Many of the transuranium isotopes decay via long decay chains with combinations of short-lived and long-lived isotopes. Therefore, nuclear waste has to be isolated from the biosphere for a long time period.

A possible solution to the nuclear waste problem is storage of the waste for a long time, for instance, in geological stable formations of salt or rock. Of course, the cask with the nuclear waste will eventually deteriorate and elements will disperse in the salt or rock formation. As long as the time for these elements to disperse to the biosphere is long enough that they decay, no extra radioactivity will enter the biosphere. Due to the very long time involved, it is difficult to guarantee everlasting isolation from biosphere, and that is one of the reasons why the public acceptance of this solution is low even if extensive calculations show a very small risk to future generations. Other reasons nature of the waste (radioactivity) and the nature of the risks involved. Therefore, other means to solve the waste problem are studied, for instance nuclear transmutation.

Transmutation is the change of one isotope into another isotope by nuclear methods, e.g. neutron absorption. By transmutation of long-lived elements to short-lived or stable elements, the time required for isolation of waste might be shortened considerably. Also, the contents of the geological repositories might be reduced,

and the possibly dispersed amount of elements might be reduced. So, transmutation might at least reduce the nuclear waste problem.

Transmutation usually involves interactions with neutrons which have to be supplied by nuclear reactors or special neutron emitters. These systems have to be operated for a certain time period to reduce the amount of nuclear waste. Nuclear energy production has to be economically competitive with other means of energy production, and therefore transmutation should not induce a strong increase of the energy price.

Another possibility might be that one strives to reduce the absolute amount of nuclear waste even if cost are very high. Some environmental protection societies may favor this option. Then, transmutation might be used to reduce a certain amount of waste assuming that nuclear energy production will be stopped. In this PhD-thesis, both options will be studied.

Recently, the nuclear waste problem received new attention. Both the U.S. and the former Soviet Union have agreed upon the destruction of a large part of their nuclear arsenal. About 150,000 kg plutonium and 1,000,000 kg of highly-enriched uranium are to be decommissioned. Both countries are studying the possibilities to use this material in nuclear energy production. Especially the former Soviet Union expresses its need for "cheap" energy to be obtained from this source¹. The highly-enriched uranium can be used in current reactors, but this is more difficult for plutonium. The amount of transuranics produced by commercial nuclear energy production until now is approximately 1,000,000 kg¹. Yearly, about 80,000 kg transuranics are produced by commercial nuclear power plants all around the world^{2,3}. Together with the weapons grade plutonium, we speak about a huge amount of hazardous materials with a large energy content.

1.2 Motivation to Perform this Work

Already in the seventies, many studies on transmutation were conducted. Probably, all arguments against nuclear transmutation for environmental and safety reasons were already presented by Johnson⁴:

1. It does not make a significant addition to our energy resources,
2. separation of the actinides from the lanthanides, fission products which are chemically similar to the actinides, is difficult,
3. multiple recycling is required, which is not feasible for current technologies,
4. it is impossible to proof the same safety for fuel designs containing higher actinides,

5. it will be very expensive to develop and operate special fuel in existing designs of power reactors, or to design special incinerator reactors,
6. the actinide recycle strategy should be adopted world wide,
7. the more conventional way of waste management: conditioning, encapsulating, and disposing in deep geological barriers is more reliable and better verified.

Croff et al presented an overall assessment of the feasibility and the incentives for transmutation^{5,6}. According to these reports, the transmutation and partitioning of actinides is feasible at reasonable costs. Their conclusions about incentives are:

1. The short term risks from partitioning and transmutation are substantial if the non-radiological impacts from fuel reprocessing and fabrication are taken into account, but small for the radiological risks.
2. The long term benefits are small.

According to Croff et al^{5,6}, no incentives for partitioning and transmutation remain. So, why is transmutation studied again, after these negative conclusions? We will answer this question by commenting on each single argument mentioned by these two reports and by overviewing developments after these reports.

First, Johnson states that transmutation does not make a significant addition to the energy resources⁴. This can only be true if he means transmutation of minor actinides instead of all actinides. Minor actinides are the transuranics, excluding plutonium. About 10% of the transuranics discharged from current nuclear reactors are minor actinides. Johnson considers this 10% not a significant amount, which is true compared to the potential energy available in plutonium.

Second, the technical argument of separating the actinides from the lanthanides is partly resolved at least on laboratory scale for some special reprocessing techniques.

The third argument to the multiple recycling requirement of Johnson is not true anymore. Breeder reactors can operate on recycled plutonium until the resources of uranium are exhausted. The fuel design of these breeders has proven to be safe.

Johnson argues that the option should be adopted world wide to be worthwhile, which he considers impossible. This argument is not valid because the possible effects of leakage from storage facilities occur locally at the storage site. Therefore, adoption of a nuclear waste reduction program by one nation can reduce the effects of the nuclear waste for that particular country.

Croff et al and Johnson compare partitioning and transmutation to disposal in geological barriers. Of course, these repositories are extremely suitable for storing

waste and the releases to the environment will be negligible, especially when the waste is vitrified in glass^{7,8,9}. However, the public opinion is against storage of waste which will be potentially dangerous for so many years even if calculations show low risks. Not one final waste repository is in operation.

Both Johnson and Croff et al reason that the costs of safety, fuel fabrication, and reliability will be too high. At the same time, Johnson believes that all these problems can be solved for plutonium recycling. It depends on the techniques used if the incremental costs (radiological and economical) of recycling the minor portion of minor actinides are much higher. In the US, a new technique is currently being developed which includes the minor actinides with plutonium automatically¹⁰. Nuclear energy without the re-use of plutonium will be able to produce energy to the world for about one century based on currently known uranium reserves. When all uranium is transmuted into plutonium in breeder reactors, the nuclear energy resources will increase by a factor of 100 at least¹¹. If plutonium is not going to be used, recycling of other actinides is useless. However, if plutonium is recycled, the recycling of minor actinides might pose only minor extra problems. Therefore, the study to reduce both the plutonium and minor actinides is useful. On the other hand, the study of transmutation of minor actinides without transmutation of plutonium is useless, because plutonium is the major contributor to the long-term radiotoxicity of nuclear waste¹².

Many new techniques have been introduced after the studies of Croff et al and Johnson. Especially, reprocessing techniques have been improved substantially. Not only plutonium can be reprocessed with small losses, also the process to extract the minor actinides has been developed. New reactors have been designed for which fuel fabrication and reprocessing is simplified. Even reactors which operate in symbiosis with accelerators are studied to improve the safety characteristics. Also, the public acceptance of disposing nuclear waste in geological repositories is low. In the U.S., stringent regulations on repositories leads to new incentives for transmutation, also admitted by Croff et al¹³.

1.3 What this Thesis Covers

The main object of this PhD-study is to determine the possibilities in terms of physics and technology of nuclear transmutation in fission reactors to reduce the actinide component of nuclear waste. Two approaches are considered: one is the absolute reduction of waste, and the other is the reduction of waste per unit of energy production.

In the next chapter, the parameters to describe the hazard of nuclear waste are discussed. Factors are introduced to evaluate waste reduction scenarios. Then,

using these factors, recycling actinides in Light Water Reactors is studied, because this type is the most common reactor in the world. Several energy scenarios are studied, and the influence of special burner reactor operation on the reduction factors is determined.

The last two chapters deal with special burner systems which burn as much transuranics as possible. In this way, we overcome the problem that the benefits of transmutation are small and the risks due to increased inventories in the fuel cycle are large.

Chapter 2

Nuclear Waste and Nuclear Waste Reduction

2.1 Introduction

In the evaluation of reactor systems for waste transmutation, several factors are of interest. Suppose that a certain amount of waste should be diminished; what should one know to make a choice between several options? First, the time necessary to reduce this waste is important: will it take years, decades, or centuries? Second, to what extent can a certain machine reduce this amount of waste? Furthermore, risks to the population and the costs of the system should be considered. A certain transmutation system can be evaluated in this way. However, suppose that one wants to develop a nuclear energy production system which generates as little waste as possible, how do we evaluate that?

The ideal energy production system produces energy at no costs, safely, without waste, and with little or no resource usage. All energy production systems can be compared to this ideal based on these characteristics. In the evaluation of a nuclear energy production system, the waste, the resources used, the risk to the population, and the cost should all be considered per unit of produced energy. Only factors involved with waste and potential waste streams will be developed in this thesis. The costs and the risks should also be taken into account, but this is beyond the scope of this study.

2.2 Waste Parameters

Nuclear waste is defined as the material to be deposited in final storage. *Inventory* is defined as the material which remains in the nuclear fuel cycle and which is to be reused as fuel. This inventory is considered as potential waste, because at the end of nuclear reactor operation the inventory will have to be disposed of unless special incinerators are built to reduce this inventory. Nuclear waste and inventory can be characterized by quantities called *waste parameters*. Several waste parameters are of interest in the study of nuclear transmutation of waste and inventory:

1. The mass (kg)
2. The radioactive inventory (Bq)
3. The radiotoxicity (ALI)
4. The mass of specific nuclides in kg(HM) e.g. the mass of transuranics, which are nuclides with a atomic number higher than uranium, the mass of minor actinides, which are all transuranics except for the plutonium isotopes ^{14,15,16,17}, or the mass of all radiotoxic actinides except Th-232, U-235, and U-238 (ARA = Artificial Radiotoxic Actinides)

5. The possible dose to the future populations due to leakage from underground storage facilities.

In case of disposal in granite or rock salt, the possible dose is determined by the long-lived mobile isotopes in the deposited waste, especially Np-237, Tc-99, and I-129^{9,18}. So, the mass of Np-237 plus the mass of all precursors of Np-237, which will eventually decay to Np-237, is a measure for the contribution of the actinides to this dose.

6. The space needed in underground storage facilities for disposal.

This space is determined either by the heat production of the material or by limitations on the maximum possible dose, which could result from a release from the repository. The calculated distance between bore holes in a German salt repository design is 57 meters determined by the maximum temperature allowed in the salt (200 °C)⁹, which could have been reduced by removing heat producing elements from the stored waste. The maximum temperature is reached within the first one hundred years after storage in the repository. The heat produced during the first 100 years is mainly due to two fission products: Cs-137 and Sr-90. These fission products have a half life of about 30 years. When these two fission products are separated from the waste to be deposited, the actinides are responsible for the main part of the heat production¹⁹.

7. The time during which the radiotoxicity is significant (y).

This time is defined as the elapsed time between the time of disposal and the time at which the radiotoxicity for ingestion becomes equal to a low reference value, e.g. the radiotoxicity of uranium ore necessary to produce the same amount of energy by once-through LWRs. At this time, the radiotoxicity produced by the system is equal to the radiotoxicity of the ore used for once-through reactors. Once-through reactors, in which the fuel is not recycled, are used as reference to assure that good resource utilization by recycling would not have a negative impact on the time of significant radiotoxicity.

In the study of transmutation of waste, three waste parameters are important: the possible dose to the population, the time during which the radiotoxicity of the waste is significant, and the space needed for underground disposal. These three waste parameters are difficult to determine and are dependent on a number of quantities which are uncertain. The possible dose to the population depends on the mobility of the various isotopes, which is not well known for many isotopes and which differs per repository site. The time of significant radiotoxicity is dependent on the dose conversion factors of the isotopes, which are still the subjects of research. For instance, the dose conversion factor of Np-237 was significantly adjusted twice during the last fifteen years^{20,21}. The space needed for disposal can vary significantly from one site to the other.

Transuranics mass is a suitable waste parameter in the study on waste transmutation, because this quantity can be calculated directly. The mass of the artificial radioactive actinides should be considered when the thorium/uranium fuel cycle is studied, in which case also the actinides built up by neutron capture in Th-232 should be accounted for.

Of course, the transuranics mass, or the mass of the artificial radioactive actinides will never be exactly proportional to the possible dose to the population due to actinides, or proportional to the time of significant radiotoxicity, or proportional to the number of repositories needed to store the actinide component of the waste. To establish a relationship between these quantities, the actinide decay chains need to be studied. Also, the important isotopes for each waste parameter have to be identified.

In the range of actinide isotopes which are present in the reactor, six alpha decay chains can be identified. Three chains end with one of the "stable" isotopes (half life larger than 10^8 years): Th-232, U-235, or U-238. The other chains belong to one of three uranium isotopes: U-232, U-233, or U-234. All members of the U-232 chain are short-lived (< 100 years). All other chains consist of a mixture of long-lived and short-lived isotopes. Furthermore, the dose conversion factors of most alpha decaying isotopes do not differ very much from each other; only the

dose conversion factors of some of the decay products of the thorium isotopes and of the uranium isotopes are smaller by approximately a factor of 20.

The number of storage facilities is dominated by the heat production of the fission products. Chang¹⁹ and Baetsle²² concluded that mainly the strontium and cesium isotopes are responsible for the decay heat. The presence of large amounts of these fission products leads to the conclusion that final storage of this part of the nuclear waste is necessary²². However, after 100 years, the actinides produce 75% of the heat¹⁹. The heat production after about 100 years of decay will be determined by alpha decaying actinides with approximately a half life of 100 years. Only a few actinides need to be considered: U-232 and Pu-238, of which U-232 is hardly present in the discharge of a uranium fueled reactor. So, the number of storage facilities can only be affected by transmutation of actinides when temporary storage for about 100 years is considered, combined with a reduction of U-232 and Pu-238 unless there is a way to separately store the strontium and cesium isotopes. The total transuranics mass is not a very good representation of the amount of these short-lived isotopes.

The possible dose to the population is determined by some long-lived fission products and Np-237. Reduction is achieved by transmuting these fission products and the Np-237 and its precursors Pu-241, Am-241, and Cm-245^{23,24}. Isotopic separation is considered too expensive. Therefore, one should consider all neptunium, plutonium, americium, and curium isotopes.

In figure 2.1, the radiotoxicity of plutonium isotopes, the minor actinides, and the fission products of an LWR discharge at a burnup of 33 MWd/kg(HM) is presented relative to the radiotoxicity of the initial uranium ore to produce the fuel. The first 250 years after discharge, the radiotoxicity of nuclear waste is due to the fission products and the actinides. Thereafter, mainly the plutonium isotopes determine the radiotoxicity. Reduction of the transuranics mass will accomplish a reduction of the time of significant radiotoxicity.

An important aspect in the determination of the waste parameter to be studied in waste reduction studies is the public opinion. Our society believes that the present generation should not put a burden in terms of nuclear waste on future generations. The desire for the complete annihilation of the long-lived component of nuclear waste results from this philosophy. A large reduction of the transuranics component of nuclear waste is the best the nuclear industry can do.

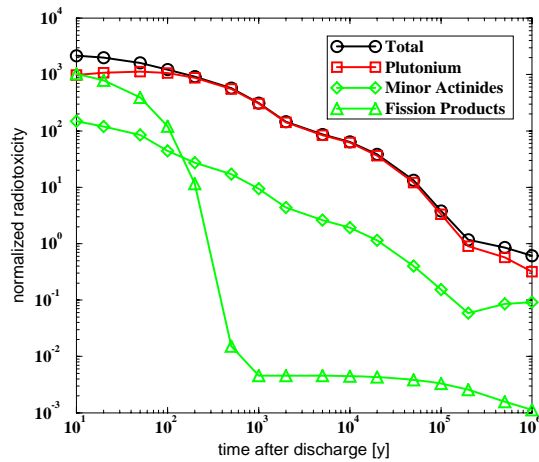


Figure 2.1: *Normalized radiotoxicity for ingestion for the plutonium isotopes, the minor actinides, and the fission products as a function of time after discharge for a once-through LWR normalized to the radiotoxicity of the initial uranium ore, mined to produce fuel.*

2.3 Waste Production and Reduction Factors

2.3.1 Fuel and Waste Amounts and Flows

First, the system for which waste production and reduction will be studied has to be defined. This system is part of the nuclear fuel cycle which describes the whole process of mining, milling, conversion, enrichment, fuel fabrication, energy production, reprocessing, and waste management. In this thesis, we will consider only the fuel and waste flows and amounts in two types of reactors: 1) LWRs and 2) Advanced Reactors (ARs) which are called burners when they are able to transmute LWR discharges.

In figure 2.2, the fuel, energy and waste amounts for the combined system are given.

The LWRs operate on mined uranium and produce energy as well as potential waste. This potential waste is reprocessed, and part of it is used in advanced reactors, which might need mined uranium and some fuel (B_i) from other advanced reactors. The discharged fuel of the advanced reactors is recycled, producing waste

and possibly some fuel (B_o) for other reactors.

All amounts of fuel and waste given in figure 2.2 are quantities integrated over the whole reactor life (except for the inventories) and have parameter values associated with them. In the next section, useful factors to evaluate the effectiveness of this system will be defined; the quantities introduced in this section have the meaning of "value of the particular waste parameter considered corresponding to the material flow or amount".

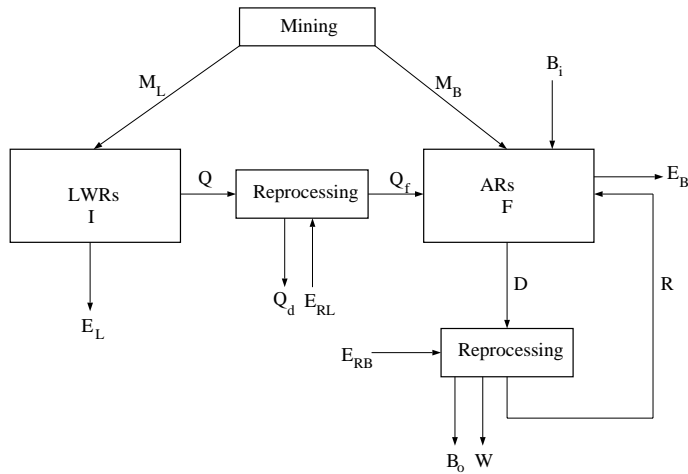


Figure 2.2: Flow sheet of waste, energy and fuel amounts for the combination of Advanced Reactors and LWRs.

parameter definition for LWR

E_L = energy produced by LWRs I = inventory of LWRs Q = amount discharged by LWRs Q_f = part of LWR discharges which will be fed to the ARs Q_d = part of LWR discharges which will be disposed of as waste

parameter definition for Advanced Reactor (AR)

E_B = energy produced by Advanced Reactors R = amount of fuel at BOC produced by reprocessing Advanced Reactors fuel B_i = amount of fuel at BOC bred in other reactors B_o = the bred quantity of fuel D = amount of fuel discharged from Advanced Reactors at the end of cycle (EOC) F = in-core and out-of-core fuel inventory of Advanced Reactors W = amount of waste produced by Advanced Reactors
--

2.3.2 Definitions to Evaluate Waste Production and Reduction

First, we introduce factors which enable us to express effectiveness of a reactor in reducing waste. These factors are expressed in terms of the waste parameters which were described in section 2.2. Three questions are of interest: how much waste can be reduced, to what extent, and in what time period.

The *BURned amount*, BU , represents the burned amount in terms of a certain waste parameter per unit of energy produced and is used to describe how much waste a reactor burns. It is defined by:

$$BU = \frac{F^{BOC} - F^{EOC}}{E_B}, \quad (2.1)$$

with $F^{BOC} - F^{EOC}$ the parameter value of the amount burned per cycle, E_B the energy produced per cycle by the burner.

The *Waste Ratio* WR of a burner system for an arbitrary waste parameter is the ratio of the parameter value of the material fed to the burner system, Q_f , and the parameter value of the waste produced by the burner system, W . So:

$$WR = \frac{Q_f}{W}. \quad (2.2)$$

W represents the parameter value of the waste produced by the burner which is disposed of after reprocessing. This definition is clarified by the flow schedule in figure 2.2. Some potential waste is loaded to the burners represented by the Advanced Reactors, which reduces this potential waste to a final waste quantity W . Assumed is that the amounts B_i and B_o are zero. The Waste Ratio is introduced to determine how effective a burner or a set of burners is in reducing material fed to the burner, independent of the energy produced.

The *Inventory Transmutation Time* ITT of a burner for an arbitrary waste parameter is defined as the time to transmute an amount equal to the parameter value of the inventory of this burner. Then, the Inventory Transmutation Time equals:

$$ITT = \frac{F^{BOC}}{P_B \cdot BU}, \quad (2.3)$$

where P_B is the power of the reactor system considered. For a large number $N(t)$ of burners operated asynchronously (not started and stopped at the same time), the burnup of an amount of potential waste $I(t)$ equal to the inventory of the whole set of burners can be described by:

$$\frac{dI}{dt} = -N(t) \cdot P_B \cdot BU = \frac{-I(t) \cdot P_B \cdot BU}{F^{BOC}} = \frac{-I(t)}{ITT} \quad (2.4)$$

The time to halve the initial inventory is $\ln 2 \cdot ITT$. Once in a while, not enough fuel material is available to operate all current burners. Then, a burner is stopped and its fuel inventory is used in the remaining burners. The burnup of the initial inventory is an exponential curve given by $\exp(-t/ITT)$. This relationship holds until the number of burners is small.

The Waste Production Ratio WPR is introduced to determine how much waste a reactor or a system of reactors produces per unit of energy produced. It takes into account the energy production and all waste flows. The *Waste Production Ratio WPR of a certain system of reactors for an arbitrary waste parameter is the ratio of the parameter value of the waste produced per unit of energy by once-through LWRs and the parameter value of the waste produced per unit of energy by the system considered.*

This definition is translated into equation 2.5 with the flow sheet of figure 2.2:

$$WPR = \frac{Q/E_L}{(W + Q_d)/E_{net}}, \quad (2.5)$$

where Q is the waste produced by LWRs during the time period considered, E_L is the energy produced by these LWRs, W is the waste produced by the Advanced Reactors, assuming that B_o is zero, and E_{net} is the net energy produced by the system.

Now, four factors to evaluate waste production and reduction have been introduced. A burner system is evaluated by the Waste Ratio, the Inventory Transmutation Time, and burned amount per unit of time. An energy producing system is evaluated by the Waste Production Ratio.

2.4 On Reducing LWR Waste by Recycling in LWRs

2.4.1 Introduction

Currently, almost all nuclear waste is produced by Light Water Reactors (LWRs), the most common nuclear reactor type. Therefore, we try to reduce the waste output of this reactor type. Two methods can be applied to accomplish this improvement in terms of reduced waste production:

- to reduce the amount of U-238 in the reactor for instance by using inert matrices of non-actinide materials,
- to recycle the actinides produced by the reactor itself.

The first way is beyond the scope of this thesis. It is noted that by reducing the U-238 inventory the efficiency of the use of uranium as an energy source will decrease. More U-235 replacing the fissile plutonium produced by neutron capture in U-238 is required for energy production. This limits the prospects of nuclear energy considerably.

The second way is studied by looking at the best way LWRs can be used in terms of energy versus waste production. This is the case when actinides are recycled to the reactor for many cycles. Recycling of these actinides will induce an increase in the amount of transuranics in the reactor. When the concentration of transuranics in the reactor is so high that the production of these actinides equals their destruction by fission, the concentration will be constant from cycle to cycle. This situation is referred to as *equilibrium*; production and destruction rates are in equilibrium. When a reactor is operated this way, the discharged fuel has to be reprocessed each cycle in order to remove the fission products and the actinides not to be recycled. Then, U-238 and U-235 are added to complete the fuel mass and accomplish the reactivity needed to operate the reactor. During reprocessing and fuel fabrication, a certain loss of actinides occurs. So, the net growth in disposed waste will never be zero, but will be equal to the losses in reprocessing.

Recycling of transuranics in LWRs has been studied for several years. The recycling of mixed oxide fuel, in which uranium and plutonium are used as fuel in LWRs is already performed. In the literature available, it is not clear what the benefits and restrictions are of recycling in LWRs. According to Lancaster²⁵, recycling all actinides in LWRs appears feasible for many cycles, but during the same conference, Wiese argued that recycling for more than one or two cycles in LWRs is not possible due to the high plutonium content, which makes reprocessing based on current technologies impossible²⁶.

In this section, we calculate the composition of the inventory of LWRs which operate in equilibrium, and determine for that composition the feasibility of the design. The feasibility is determined by calculation of the fissile requirement for the fuel to start up and operate to the same burnup as for the once-through system. Furthermore, the change in reactivity during a cycle is determined, as well as the amount of isotopes, which will emit neutrons by spontaneous fission and the produced heat due to alpha decay. These determine whether reprocessing and fuel fabrication is feasible. The current limit of Pu-238 in plutonium is 2.5%, based on heat production and neutron emission^{22,27}. Above this limit, heat production leads to problems with fuel fabrication, and neutron emission makes automated remote fuel fabrication and reprocessing necessary. For the near future, 5% is seen as possible to handle in fuel reprocessing^{28,29}. This process is carried out for three sets of actinides included in reprocessing: plutonium, transuranics, and uranium. For these nuclides, no losses in reprocessing were assumed. With the calculated

compositions, the reduction in growth of transuranics compared to once-through LWRs is calculated assuming 1% loss in reprocessing. This factor is represented by the Waste Production Ratio.

2.4.2 Calculational Method

A special code EQUI was developed for this study in order to calculate the fuel composition in equilibrium for any reactor type, when the spectrum-weighted cross section data are known. This code is discussed in Appendix B. The most important assumption made in deriving the basic equations used in this code is that the cross sections are problem-independent. One-group cross-section data for EQUI were obtained from Croff et al for the Pressurized Water Reactor fueled with uranium³⁰.

EQUI has been verified for a non-recycling scheme and for a total recycling scheme in which all actinides are recycled without losses in reprocessing (see appendix B). For the non-recycling case, results are different from values calculated with the ORIGEN-S code^{30,31}, especially for Pu-239 and higher curium isotopes with higher atomic numbers due to the linearizations used in the code. However, these linearizations are valid for recycling cases. For the simple total recycling scheme, good agreement is obtained with values calculated with the ORIGEN-S code.

Calculations were performed for a one year cycle length. A core consists of three batches, and assumed was that a discharged batch will be in cooling for three years. So, the in-core residence time was three years. A constant flux was chosen to obtain a burnup of 33 MWd/kg(HM) at the end of the in-core residence time of three years. The limit for the infinite multiplication factor k_{∞} after an in-core residence time of three years without fission products was chosen to be 1.2. The infinite multiplication factor is the ratio of neutron production rate and neutron absorption rate. The value of 1.2 is based on isotopic composition of the actinides after an in-core residence time of three years for the once-through LWR. The concentration of U-235 at the beginning of cycle was adjusted to obtain this k_{∞} and the average flux was adjusted to obtain a burnup of 33 MWd/kg(HM).

The uncertainties in the results will be rather large due to the uncertainties in the one-group cross sections, which is due to the assumptions made. As the density increases cross sections of the transuranics will decrease due to selfshielding effects. Moreover, a higher plutonium content will cause a spectrum hardening due to the higher thermal cross sections of plutonium than of uranium. Spectrum hardening will lead to a decrease in the one-group cross sections³². The density of the short-lived actinides at the end of cycle will be underestimated because average densities are calculated. This will lead to an underestimation of the absorption in the short-lived isotopes. The influence of these effects on the transuranics content

and on k_{∞} are unclear. k_{∞} is important because it determines the U-235 content. Nevertheless, the EQUI calculations can be used to show qualitatively the effect of recycling in LWRs.

2.4.3 Plutonium Recycling in LWRs

The radiotoxicity of the waste produced by a once-through LWR is mainly due to plutonium. So, when recycling is considered in LWRs, the first option is to reduce the net plutonium production by recycling plutonium. In figure 2.3, the radiotoxicity for ingestion of the equilibrium fuel and the waste produced when all plutonium is recycled for many cycles is compared to the radiotoxicity of the waste produced by the once-through LWR as calculated by EQUI, normalized to an energy production of 1 MW_e for one year, assuming that one batch is discharged per year and a thermal efficiency of 33% and a capacity factor of 70%. An assumption was made that no losses of plutonium occurred during reprocessing.

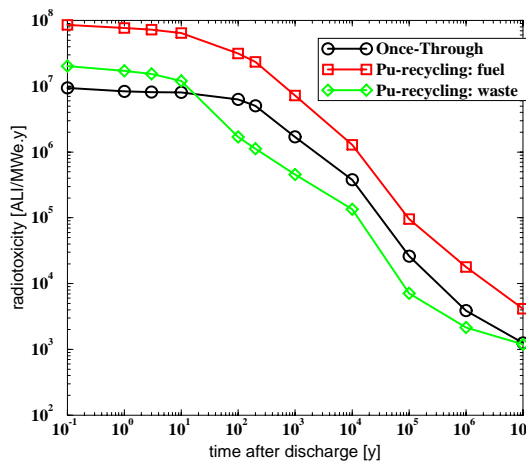


Figure 2.3: Radiotoxicity for ingestion as a function of time after discharge for a once-through LWR and the fuel and waste for an LWR with plutonium recycling, normalized to an energy production of 1 MW_e during one year, assuming that one batch per year is discharged.

The first ten years of decay, the radiotoxicity of the waste when plutonium is recycled is higher, and after ten years of decay, the radiotoxicity of the waste for

plutonium recycling is lower by approximately a factor of three than the waste of the once-through LWR. For the fuel, the radiotoxicity for ingestion is always higher than the radiotoxicity of the waste of the once-through LWR, due to the buildup of plutonium and the higher production of americium and curium. Also, one batch per year of the LWRs is discharged, which means that the fuel radiotoxicity is higher by an extra factor.

In table 2.1, the mass fractions for transuranics, minor actinides, and the artificial radioactive actinides are presented for the waste of a once-through LWR and the fuel and waste for plutonium recycling at the end of cycle. The transuranics mass, the minor actinides mass, and the mass of the artificial radioactive actinides (ARA) are relative to the total mass of all actinides (HM).

Table 2.1: *Mass Fractions of important isotopes, transuranics (TRU), minor actinides (MA), and the artificial radioactive actinides of Fuel and Waste for Plutonium Recycling compared to Once-Through Discharge at the end of cycle.*

Parameter	mass fractions [%HM]		
	Once-Through	Pu Recycling	
		fuel	waste
U-235	0.92	1.5	1.5
U-238	97.5	96.8	96.8
Np-237	0.04	0.04	0.04
Pu-238	0.02	0.03	0.0
Pu-239	0.64	0.46	0.0
Pu-240	0.15	0.14	0.0
Pu-241	0.13	0.18	0.0
Pu-242	0.04	0.23	0.0
TRU	1.06	1.23	0.19
MA	0.08	0.19	0.19
ARA	1.55	1.71	0.67

The waste parameters of the fuel increase due to the recycling of plutonium, but the waste parameters of waste decrease by more than a factor five, when reprocessing losses are assumed to be zero for plutonium. For minor actinides, the parameter value of the waste increases by more than a factor of two due to the buildup of americium and curium, whereas the amount of neptunium is almost the same. The relative fissile content, the mass of all fissile isotopes relative to the total mass of all actinides, is higher when plutonium is recycled, because of the higher content of fissile transuranics at the beginning of cycle and the higher content of U-235. The U-235 enrichment when plutonium is recycled is 3.9% at the beginning of cycle compared to 3.6% for the once-through reference LWR. This is due to the

fact that the capture cross sections of the fissionable transuranics compared to the capture cross section of U-238 are higher and that relatively less U-238 is present when plutonium is recycled. *Fissionable isotopes are the actinides which will not be fissioned by thermal neutrons, whereas fissile isotopes, like U-235, may be fissioned by thermal neutrons.* Examples of fissionable isotopes are U-238 and Pu-240. The flux is 28% lower due to the higher macroscopic fission cross sections resulting from the higher fissile content. The change in reactivity due to the actinides during a cycle is 0.26 when plutonium is recycled compared to 0.25 for the once-through reference case.

The amount of spontaneously fissioning isotopes is important to estimate the increase of spontaneous fission neutrons. The amount of Pu-238 in plutonium is 3% when plutonium is recycled, compared to 1.5% for the once-through LWR. The curium isotopes increase strongly, which will increase the amount of spontaneous fission neutrons. The heat production by the actinides in the discharged fuel is mainly determined by the alpha decay of actinides in the fuel. After ten years of decay, the specific alpha activity is $1.0 \cdot 10^{12}$ Bq/kg(HM), compared to $3.0 \cdot 10^{11}$ Bq/kg(HM) for a once-through discharge.

When plutonium is recycled in LWRs, the concentration of plutonium isotopes will increase, but only slightly due to the fact that some isotopes of plutonium, like Pu-239 and Pu-240, are almost in saturation in the once-through LWR at EOC (see appendix B). Because the increase in plutonium concentration is small, the effects on safety and reactivity coefficients will be small. The problem with plutonium recycling is the increased neutron and heat production during fuel reprocessing and fabrication, due to the increased content of Pu-238, Cm-242 and Cm-244.

2.4.4 Transuranics Recycling in LWRs

Plutonium recycling can reduce the growth in transuranics by maximally a factor of five compared to once-through operation of LWRs. To obtain higher reductions, the recycling of all transuranics is considered in this section. In figure 2.4, the radiotoxicity for ingestion of the fuel and the waste when all transuranics are recycled and for a discharge of a once-through LWR are presented. The radiotoxicity of the equilibrium fuel is much higher especially for the first 100 years of decay compared to the radiotoxicity of a once-through LWR. The radiotoxicity of the waste is fully due to uranium isotopes and is much lower than the radiotoxicity of a once-through LWR because no losses of transuranics occurs.

In table 2.2, the mass fractions for transuranics, minor actinides, and the artificial radioactive actinides are presented for the waste of a once-through LWR and the fuel and waste for transuranics recycling. For the fuel, the parameter values increase strongly due to the recycling. For the waste, these values are zero except

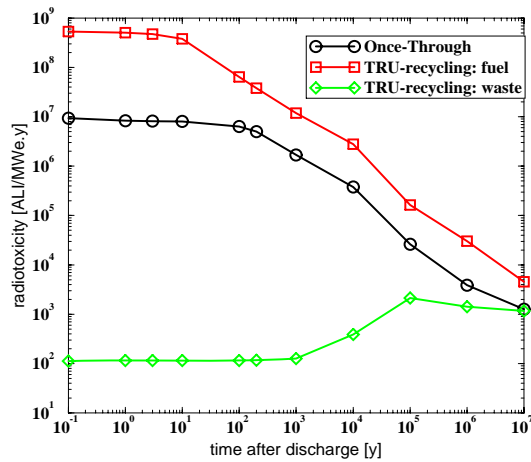


Figure 2.4: Radiotoxicity for ingestion as a function of time after discharge for a once-through LWR and the fuel and waste for an LWR with transuranics recycling, normalized to an energy production of 1 MW_e during one year, assuming that one batch per year is discharged.

for the mass of the artificial radioactive actinides because reprocessing losses of the transuranics are assumed to be zero.

The amounts of americium and curium in the equilibrium fuel increase by approximately a factor of 10 and 80 compared to the discharge of a once-through LWR. These amounts are higher than for plutonium recycling, because now americium and curium are recycled as well. The relative fissile content is higher when all transuranics are recycled than when only plutonium is recycled, because the amount of fissionable transuranics is higher. The content of U-235 at the beginning of cycle is increased from 3.6% for the once-through reference case to 4.1% when all transuranics are recycled. The change in reactivity due to the actinides during a cycle is 0.22 when transuranics are recycled compared to 0.25 for the once-through reference case. The smaller reactivity change is due to the fact that the concentration of the transuranics is assumed to be constant during the in-core residence time.

The Pu-238 fraction in plutonium is 10% when transuranics are recycled, compared to 1.5% for the once-through LWR and 3% when plutonium is recycled. This strong increase compared to the plutonium recycling case is induced by the much higher

Np-237 content, when transuranics are recycled. The relative masses of curium isotopes increase strongly, especially Cm-244, which will increase the amount of spontaneous fission neutrons further. After ten years of decay, the specific α -activity is $7.5 \cdot 10^{12}$ Bq/kg(HM), compared to $3.0 \cdot 10^{11}$ Bq/kg(HM) for a once-through discharge. When transuranics are recycled in LWRs, the concentration of minor actinides increases strongly, almost by a factor of 100, which will present considerable problems, especially for reprocessing and fuel fabrication.

Table 2.2: *Mass Fractions of important isotopes, transuranics (TRU), minor actinides (MA), and the artificial radioactive actinides for once-through LWRs and for LWRs with recycling of all transuranics.*

Parameter	mass fractions [%HM]		
	Once-Through	TRU Recycling	
		fuel	waste
U-235	0.92	1.7	1.7
U-238	97.5	95.8	95.8
Np-237	0.04	0.07	0.0
Pu-238	0.02	0.11	0.0
Pu-239	0.64	0.47	0.0
Pu-240	0.15	0.17	0.0
Pu-241	0.13	0.20	0.0
Pu-242	0.04	0.28	0.0
Am-241	0.007	0.03	0.0
Am-243	0.012	0.18	0.0
TRU	1.06	2.08	0.0
MA	0.08	0.85	0.0
ARA	1.55	2.55	0.47

2.4.5 Uranium Recycling in LWRs

Recycling of plutonium and of transuranics are ways to reduce the net production of actinide waste, but because of the higher fissile requirement, the need for uranium is not decreased, but is even somewhat increased. In this section, the possibility of reducing the uranium ore need by recycling uranium in LWRs will be studied.

In table 2.3, the mass fractions for transuranics, minor actinides, and the artificial radioactive actinides are presented for the waste of a once-through LWR and the fuel and waste for an LWR with uranium recycling. The waste parameters for the fuel and the waste increase strongly due to the uranium recycling.

The relative fissile content is much higher when uranium is recycled, because of the high U-235 need. The enrichment of the uranium in U-235 at the beginning of cycle is increased from 3.6% for the once-through reference case to 6.6% when all uranium is recycled. This need is so high due to the buildup of the fissionable isotopes U-236, Np-237, and Pu-238 with higher capture cross sections than U-238. The U-235 requirement is about 4.2 kg/MW_e.y compared to 4.3 kg/MW_e.y for a once-through LWR. At the end of cycle, 41% of the U-235 is discharged for the uranium recycling LWR compared to 24% for the once-through LWR. The amount of neptunium increases by approximately a factor of 10 compared to the discharge of a once-through LWR. The relative amount of the transneptunium elements decreases due to a lower average flux, which leads to a reduced plutonium production by capture in U-238. The flux is lower because the macroscopic fission cross section is higher due to the relative higher fissile content.

Table 2.3: *Mass Fractions of important isotopes, transuranics (TRU), minor actinides (MA), and the artificial radioactive actinides for once-through LWRs and for LWRs with recycling of uranium.*

	mass fractions [%HM]		
	Once-Through	U Recycling fuel	waste
U-235	0.92	2.5	0
U-236	0.5	5.1	0
U-238	97.5	91.0	0
Np-237	0.04	0.53	0.53
Pu-238	0.02	0.11	0.11
Pu-239	0.64	0.52	0.52
Pu-240	0.15	0.10	0.10
Pu-241	0.13	0.07	0.07
TRU	1.06	1.37	1.37
MA	0.08	0.54	0.54
ARA	1.55	6.50	1.37

The amount of Pu-238 in plutonium is 13% when uranium is recycled compared to 1.5% for the once-through LWR. This is due to the higher Np-237 content and the lower production of Pu-239 by neutron capture in U-238.

The burnup reactivity loss δk is 0.29 for the LWR with uranium recycling compared to 0.25 for the once-through case because Pu-239 production decreases due to the higher content of U-235 and the lower flux for the uranium recycling case. Therefore, less Pu-239 will buildup during a cycle to replace burned U-235 and the relative amount of U-235 fissioned will increase compared to the once-through

LWR.

When uranium is recycled in LWRs, the uranium ore need will not drop due to the higher fissile requirement, mainly due to the strong buildup of U-236 and Np-237. All waste parameters for fuel and waste increase strongly, and the Pu-238 contents are too high to allow for reprocessing.

2.4.6 Transuranics Waste Produced by Equilibrium LWRs

In the previous sections, the fuel inventories when actinides are recycled have been studied. In this section, an estimate of the transuranics waste will be presented assuming a loss fraction of 1%. The Waste Production Ratio for the equilibrium systems introduced in the previous section will be determined. The assumption is made that at the start of the operation of the equilibrium LWRs, enough material is present to start with the equilibrium fuel content. During operation of the LWRs, 1% loss of the discharged fuel per cycle is assumed. The cycle length is one year, and one batch is discharged per cycle. The core consists of three batches. It is assumed that the out-of-core inventory consists of one-batch. At the end of operation, the fuel inventory is supposed to be disposed of as waste. Only the cases for plutonium and transuranics recycling were studied.

In figure 2.5, the Waste Production Ratio *WPR* for transuranics mass is presented for equilibrium LWRs with plutonium recycling and with transuranics recycling.

The Waste Production Ratio for transuranics mass increases to a limit of approximately five for the plutonium recycling. However for transuranics recycling, the Waste Production Ratio does not reach a limit within 100 cycles. This is due to the large difference between inventory and waste produced per cycle; the latter is only 0.3% of the inventory for the case with transuranics recycling. So, after 300 cycles, the amount of waste equals the inventory, which is taken into account in the Waste Production Ratio as potential waste. So, when the reactor is stopped after 100 cycles, the Waste Production Ratio is about 25, which means that compared to once-through operation, the transuranics waste production is reduced by a factor of 25. Presently, it is assumed that plutonium recycling is only technically feasible for five cycles at maximum. Then, the reduction in transuranics production is reduced by maximally a factor of two²⁶.

2.5 Energy Scenarios and Waste Production

In this section, we will return to our system of LWRs and Advanced Reactors to determine if it is possible to achieve a higher reduction in growth of transuranics or even achieve an actual decrease of transuranics. For the Advanced Reactors, we

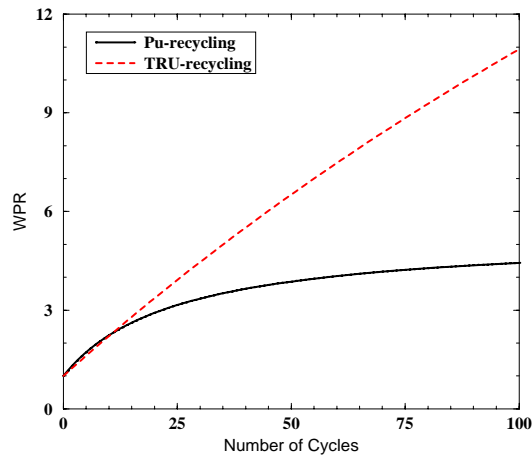


Figure 2.5: Waste Production Ratio for transuranics mass as a function of the number of cycles for Equilibrium LWRs with plutonium recycling and transuranics recycling.

used the advanced liquid metal reactor (ALMR), developed by General Electric Company, in cooperation with Argonne National Laboratory.

Thompson explains the way the ALMR designs might be used to reduce the amount of nuclear waste³³. First of all, reference breeder ALMR reactors might be started up with LWR discharges as fuel. Secondly, in symbiosis with LWRs, ALMR burner cores might be operated to consume the waste produced by LWRs. Unfortunately, Thompson did not make clear what reduction in LWR waste will be achieved in which time period, when ALMRs are introduced to produce nuclear energy³³. The main emphasis of the ALMR designs developed in reference 33 for actinide burning was to maintain the same safety characteristics when the ALMRs are fueled with LWR waste.

Cockey et al present more details on consumption rates of transuranics and minor actinides^{34,35}. The changing concentrations of actinides during 50 years of operation in some specific burner designs are discussed. In the ALMR, 66 percent of the transuranics mass introduced may be consumed in that period, which is an amount of 3.3 tonne (MT) per reactor of 471 MW_t. However, details on total reduction of LWR waste per unit of energy produced are not presented.

Pigford et al present some calculations on the symbiotic combination of LWRs

and ALMRs^{36,37}. From these calculations, one might conclude that it may take thousands to ten thousands of years to get a large reduction (i.e. an inventory reduction factor > 100) of the total amount of waste compared to the waste produced when only once-through LWRs would have been used to generate the same amount of energy. One may argue that this factor is of little interest because LWRs are not able to produce energy for such a long time period.

The aim of this work is to study the potential of ALMRs to reduce the amount of nuclear waste in terms of transuranics mass considerably and to see if this can be done in a shorter time period than was obtained by Pigford. Shorter time scales have been considered because one cannot expect acceptance of scenarios where waste reduction takes thousands of years of nuclear power plant operation.

Three energy scenarios are considered in which ALMRs are used to reduce LWR waste: one scenario, called the fast decline scenario, is based on a fast decline in the use of nuclear energy after fifty years of constant power production and is using burner ALMRs, and the second, called low increase scenario, is based on a small increase of nuclear power production during a longer time period using low breeding and burner ALMRs. The third scenario, called the high increase scenario, considers a strong increase in nuclear power production during 100 years using high breeding and burner ALMRs.

2.5.1 Energy Scenarios

We assume that all LWR reactors presently operating in the world take part in our system. According to reference 2, 323 GWe electricity is produced by LWRs in the world. Also, we assume that all transuranics waste takes part in the system: about 10^6 kg transuranics¹. Part of this amount is still present in the operating LWRs (about 175,000 kg). The power of the LWRs is assumed to be 1400 MW_e.

In the fast decline scenario, the nuclear power production is kept constant during 50 years. Thereafter, all remaining LWRs are stopped. The number of burner ALMRs started up is determined by the initial amount of transuranics waste and the amount of transuranics waste produced by once-through LWRs during these 50 years. 335 ALMRs of 155 MW_e (thermal power is 471 MW_t assuming a thermal efficiency of 33%) will be started and 37 out of 231 LWRs will be stopped at the beginning of this scenario. The goal is to use all LWR discharges in ALMRs for at least one cycle during the 50 years considered, which determines the above mentioned numbers. All ALMRs are operated in a burner mode and need to be fed with fuel made of LWR discharges every cycle³⁴.

In the low increase and high increase scenarios, all initial transuranics waste is used to start up breeder ALMRs. Because the operating LWRs and ALMRs produce

fuel material for other ALMRs, once in a while a new ALMR is started up. After 50 years, the number of LWRs is gradually reduced until all LWRs are shutdown at 100 years from the start of these scenarios. After the first 100 years, the ALMRs are changed to be completely self supporting and each reactor produces just enough new fuel material for itself during the following 100 years producing constant power. The number of low breeding ALMRs of 155 MW_e started is about 248 and about 27 out of 231 LWRs will be stopped at the beginning of the low increase scenario. For the high increase scenario, 162 high breeding ALMRs of 280 MW_e are started and 32 LWRs are stopped at the start of this scenario.

At the end of all three scenarios, i.e. 50, 200, and 200 years for, respectively, the fast decline, the low increase, and the high increase scenarios, only reactor operation to reduce the nuclear waste will be considered and reactor operation will be focused on nuclear waste reduction instead of maximization of energy production. Then, the fuel inventory will be used in ALMR burners to reduce this inventory. The number of burners decreases in time, because each burner needs a certain amount of new fuel every cycle, which will be made of fuel of the stopped ALMRs. This ALMR stand-alone operation may continue until the last ALMR requires shutdown due to lack of fuel material. In this study, a maximum stand-alone burner operation time of 200 years is considered.

In figure 2.6, the power production is shown for the three scenarios as a function of operating time. For the fast decline scenario, the produced power decreases after 50 years because all LWRs are shutdown at once. For the low increase scenario, the gradual reduction of LWRs after 50 years can be seen to be larger than the increase of the number of new ALMRs. For the high increase scenario, the influence of shutdown of LWRs on the power is not strong due to the high breeding ratio of the ALMR design used in this scenario, which leads to start-up of new ALMRs.

Every cycle, the number of operating reactors is calculated by using some basic equations which are dependent on the energy scenario. The amount of transuranics waste produced in processing is subtracted from the total amount of transuranics mass in the fuel and the amount of transuranics waste produced by LWRs is added to the total amount of transuranics mass in the fuel available for ALMRs. This total amount of fuel is used to calculate a new discrete number of ALMR cores. Also, the total amount of transuranics waste produced by LWRs is calculated for the same energy production with once-through LWRs.

2.5.2 Reactor Designs

The reference design in 1992 of the ALMR is a 471 MW_t (155 MW_e) modular breeder reactor fueled with a ternary metal fuel, and this core design is labeled

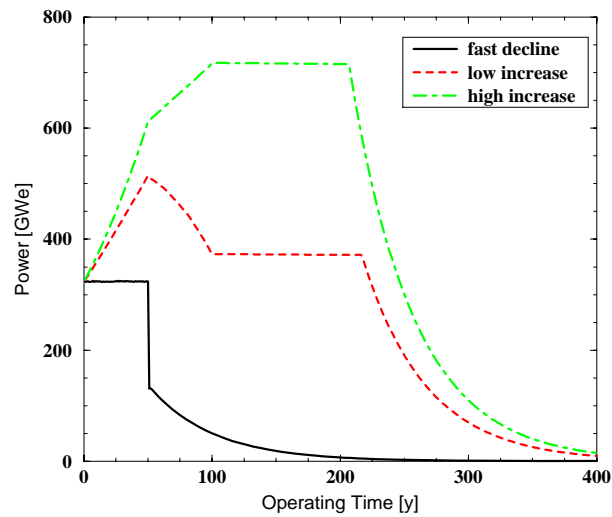


Figure 2.6: Power production level as a function of operating time for the three energy scenarios.

ALMR-92Q6³⁸. Several metal fueled burner cores have been developed in the ALMR program and studied for their actinide burning capabilities^{33,35}. In this study, the burner design with the highest transuranics consumption rate has been used, labeled ALMR-92I³⁴. An alternative, larger ALMR design developed in 1993 is a 840 MW_t (280 MW_e) modular breeder reactor. By adding more axial blanket material, this design becomes a high breeder design, labeled ALMR-93M5, with a breeding ratio 1.23 instead of 1.06 for the 92Q6 design. This high breeder reactor is used in the third scenario.

In table 2.4, data on mass inventories and flows of the 1992 and 1993 metallic fueled ALMR reference and burner designs are presented and are normalized to an electric power production of 155 MW_e. Also, the amount of transuranics produced by a once-through LWR normalized to 155 MW_e is presented. The smaller inventory of the burner (ALMR-92I) represents the fact that no blankets are present. A higher amount is discharged for this case because the number of batches in-core is three, whereas this is higher for the blankets of the breeders. The inventory of the large breeder (ALMR-93M5) is smaller than of the small breeder (ALMR-92Q6), because it is normalized to the same power. The data for

Table 2.4: Mass inventory and flows for a once-through LWR, the ALMR reference core 92Q6, the ALMR burner core 92I, and for the ALMR high breeder core 93M5. All reactors are normalized to operate at 155 MW_e with a thermal efficiency of 33% and a capacity factor of 85%.

Reactor	Parameter	TRU Mass
LWR	discharged	41.6 kg/y
ALMR 92Q6 Low Breeder	inventory	3442.7 kg
	discharged	329.6 kg/y
	bred	10.7 kg/y
ALMR 92I Burner	inventory	2583.8 kg
	discharged	380.4 kg/y
	burned	51.0 kg/y
ALMR 93M5 High Breeder	inventory	2931.5 kg
	discharged	307.1 kg/y
	bred	31.3 kg/y

the burner 92I is used in the fast decline scenario, and for the stand-alone burner operation to end all three scenarios. The data for the 92Q6 reference breeder is used in the low increase scenario, and the data for the 93M5 breeder is used in the high increase scenario. For the self supporting reactor operation, data for the breeders is used except for the amount bred which is changed to zero.

2.5.3 Waste and Energy Production

In figure 2.7, the integrated amount of transuranics waste for the fast decline scenario is presented for processing loss fractions of 0.1% compared to the waste produced when only once-through LWRs would have been used to produce the same amount of energy.

The integrated amount of transuranics waste for the fast decline scenario using ALMR burners is much lower due to the recycling of the actinides. The sharp increase at the end of operation is due to the fuel inventories of the remaining 16 ALMRs, which have to be disposed of. It would take another 166 years to reduce the remaining inventories to the inventory of one ALMR. For the low increase scenario, the number of remaining ALMRs after 400 years of operation is 60, and it would take another 232 years to reduce the remaining inventories to that of one ALMR. For the high increase scenario, the number of remaining ALMRs is 65, producing 280 MW_e each, and it would take another 236 years to reduce the remaining inventories to that of one ALMR, producing 280 MW_e.

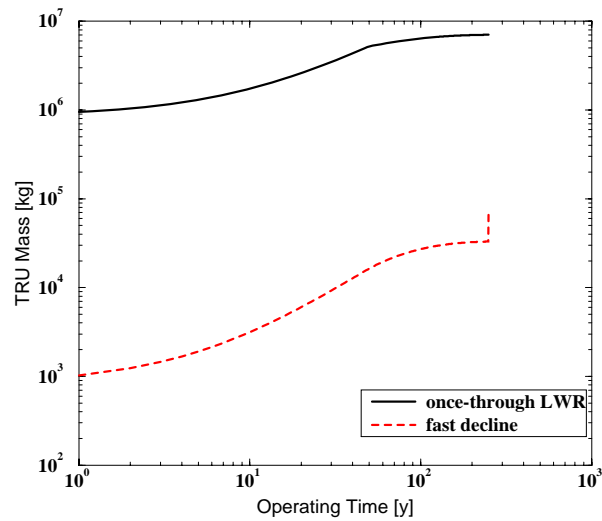


Figure 2.7: *Integrated transuranics waste as a function of operating time for the fast decline scenario.*

In figures 2.8 and 2.9, the Waste Production Ratio WPR and the Waste Ratio WR for transuranics mass for the three energy scenarios are presented for processing loss fractions of 0.1% as a function of Operating Time. For each Operating Time, we assume that the scenario is stopped, which means that the inventory of the fuel cycle is assumed to be disposed of as waste.

In table 2.5, these ratios are presented for three Stand-Alone Burner Operation Times (SABOT = 0, 100, and 200 years), which are measured from the end of each scenario: 50, 200 and 200 years for the fast decline, the low increase, and the high increase scenario, respectively.

The Waste Production Ratios for the three scenarios are almost the same for equal Stand-Alone Burner Operation Times. The ratios are small when the Stand-Alone Burner Operation Time is zero at 50, 200, and 200 years after the beginning of the scenarios for the fast decline, the low increase, and the high increase scenarios, respectively. The Inventory and Waste Ratios increase strongly when the Stand-Alone Burner Operation Time increases. The maximal Waste Production Ratios will be obtained when only one ALMR remains. Then, the Waste Production Ratios are 265, 141, and 137 for the fast decline scenario, the low increase scenario,

and the high increase scenario, respectively.

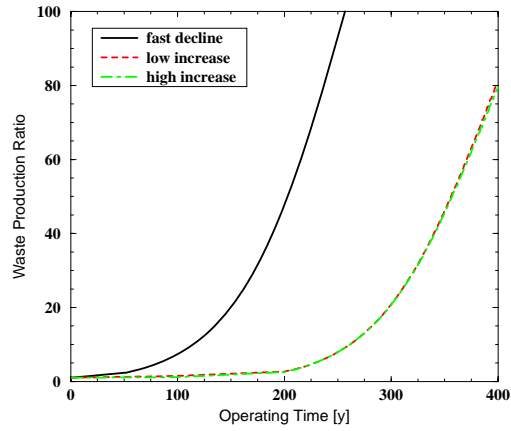


Figure 2.8: *Waste Production Ratio as a function of operating time for transuranics mass for the three energy scenarios.*

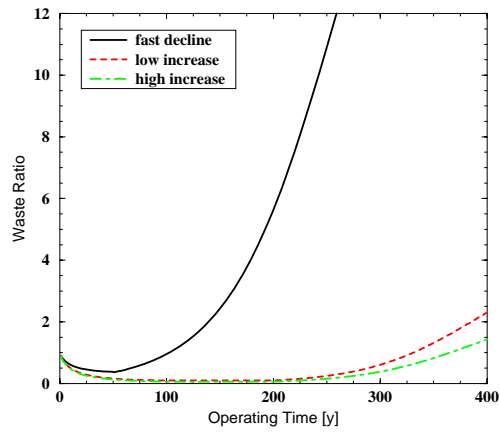


Figure 2.9: *Waste Ratio as a function of operating time for transuranics mass for the three energy scenarios.*

The amount of transuranics waste including the potential waste in the fuel cycle will increase compared to the initial amount of transuranics waste ($WR < 1.0$), if no stand-alone burner operation is considered, especially for the low and high increase scenarios. However for long burner operation, the initial amount of transuranics waste can be reduced substantially, even for the low and high increase scenarios.

Table 2.5: *Waste Production Ratios WPR and Waste Ratios WR for three energy scenarios using the ALMR burner for three Stand-Alone Burner Operation Times (SABOT) and a processing loss fraction of 0.1%.*

Scenario	WPR			WR		
	SABOT [y]	0	100	200	0	100
fast decline	2.4	20	93	0.4	3.7	19
low increase	2.7	21	81	0.1	0.6	2.3
high increase	2.6	21	79	0.06	0.4	1.1

The Inventory and Waste Ratios are not only sensitive to the operation time, but also to the processing loss fraction. Processing losses in the range from 1% down to 0.1% are likely in the future for the pyroprocess to be used for metallic fuel³⁹. In this study a range up to 4% is considered. In figure 2.10, the Inventory and Waste Ratios are presented for the fast decline scenario as a function of the reprocessing loss fractions.

For higher loss fractions, the Inventory and Waste Ratios are much smaller due to the higher integrated amount of transuranics waste. Then, long stand-alone burner operation to reduce the fuel inventory of the ALMRs is not helpful. To obtain substantial ratios, the loss fraction has to be at least less than 0.5%.

We have seen that the Waste Production Ratio is very dependent on the loss fraction and only slightly dependent on the energy scenario as long as stand-alone burners are operated to end each scenario. The question arises in which situation the operation of the stand alone burners is still significant. Let's say that a significant change in the Waste Production Ratio is by a factor of 10 in 200 years. This is, of course, an arbitrary choice. We calculate the loss fraction and the energy production which will obtain this factor of 10 for the high increase scenario. The amount of energy is represented by the time of operation of the break-even ALMR. So, the start-up level achieved after 100 years of operation of breeder ALMRs is not changed. The minimum amount of energy produced is equal to 61 $TW_e y$, for which significant burner operation can be obtained for loss fractions smaller than 1.8%. The results are presented in figure 2.11.

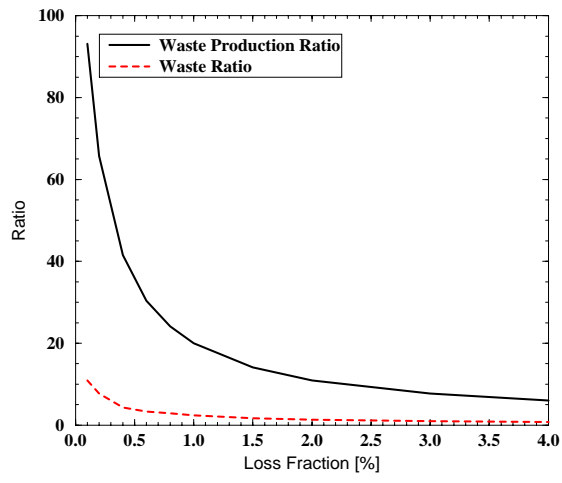


Figure 2.10: *Waste Production Ratio and Waste Ratio as a function of reprocessing losses for transuranics mass for the fast decline scenario.*

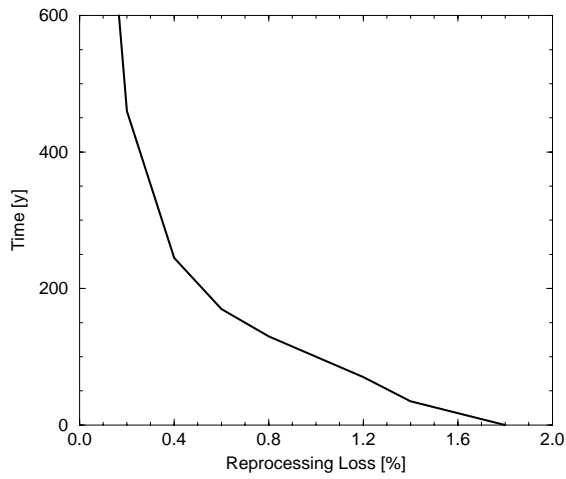


Figure 2.11: *Relation between loss fraction and number of years of break-even operation for which significant burner operation in 200 years is possible.*

For every point to the left side of the graph, significant burner operation is possible. So, for a small loss fraction (i.g. 0.2%), it is almost always significant to operate a burner for a period of time.

Another possibility is that one operates LWRs and burns all the potential waste produced after LWRs have been stopped. We calculated the Waste Production Ratio assuming that the burners are ALMR burners. In 50 years, the amount of potential waste from LWRs is six times more than 10^6 kg assumed before. So, many more ALMR burners have to be started up; in fact, 1955 ALMRs of 155 MW_e have to be started, which is almost six times more than for the fast decline scenario. Of course, one might start up less ALMRs, but this will mean an increase in time to achieve the same waste reduction. The Waste Production Ratio is similar to the one calculated for the fast decline scenario, it reaches the same value 50 years later.

The Waste Production Ratio for transuranics waste is not very dependent on the energy scenario, but mainly on the stand-alone burner operation time and the loss fraction in fuel processing. Stand-alone burner operation times of several hundreds of years and loss fractions less than 0.5% are needed to obtain an Waste Production Ratio of 100. If ALMR burner reactors are not used in stand-alone mode after the symbiosis with LWRs, a small Waste Production Ratio of three is obtained. So, one should always operate ALMRs in stand-alone burner operation mode, if ALMRs are considered for transuranics inventory reduction. This is the main reason for the difference between the operation times mentioned in this study and the operation times mentioned by Pigford in references 36 and 37.

This study shows the possibility for nuclear energy production using ALMRs without an increase of the initial amount of transuranics waste. This is true even for large loss fractions of 4% and operation times of about 200 years.

Finally, we conclude that the development and operation of special burners is only significant when the reprocessing losses are small and the energy production is limited. In this thesis, we assume that this will be the case.

2.6 Physics Aspects of Burner Design

2.6.1 Burner Design Objective

In the previous section, we have shown that for low loss fractions in reprocessing, low waste production can be achieved by operating special burners, which reduce the inventory of the systems at the end of the nuclear era. In this PhD-study, the optimization of the loss fraction is not studied, but in the last section we showed that for larger loss fractions, waste reduction compared to once-through LWRs is

small. We assume that sufficiently low loss fractions can be obtained.

In this section, the transmutation potential of a reactor system will be studied. Two parameter dependencies will be considered: dependence on uranium content, and dependence on flux spectrum. This section provides the knowledge to decide which reactor types have favorable characteristics for burning transuranics.

Slessarev and Salvatores express the transmutation potential of nuclear systems by the neutron excess available for transmutation of actinides and long-lived fission products^{40,41}. The neutron excess is important to be able to transmute long-lived fission products. The conclusion of that paper is that one either needs fast reactors or hybrids of a reactor and accelerator. In a fast reactor spectrum, more actinides have a positive neutron balance compared to thermal systems, because the fission cross sections of fissionable isotopes relative to the capture cross section increase for higher energies. In a thermal spectrum, the fissionable isotopes have a negative neutron balance, because the ratio of fission and capture cross section is low. For high fluxes, however, this balance is positive for some specific fissionable isotopes^{40,41}. Furthermore, the extra neutrons produced by an accelerator can be used to load extra fission products compared to a critical system operated without accelerator.

In this study, we only deal with actinides, and the neutron excess is not important, assuming that critical operation on the actinides is possible. However, neutron excess is very important when transmutation of fission products is the objective, because this determines the amount of fission products which can be transmuted. The burning capabilities are expressed in the three factors defined at the beginning of this chapter: time (Inventory Transmutation Time), amount (burned amount of transuranics), and reduction (Waste Ratio). These factors will be studied as a function of transuranics enrichment and flux spectrum. Another important physics parameter is the flux level. This level is dependent on material constraints and is therefore considered in the next chapters as an outcome of the design.

2.6.2 Waste and Enrichment

To optimize a burner, the fewest possible neutron captures in Th-232, U-235, and U-238 and as many as possible fissions in the artificial radioactive actinides should be accomplished. So, the ratio

$$\frac{\Sigma_{ARA}^f}{(\Sigma_2^c + \Sigma_5^c + \Sigma_8^c)} = (N^{ARA} \sigma_{ARA}^f) / (N^2 \sigma_2^c + N^5 \sigma_5^c + N^8 \sigma_8^c)$$

should be maximized. This will be the case for a high enrichment of the artificial radioactive actinides. Also, the ratio of microscopic fission cross section of the

artificial radioactive actinides to the microscopic capture cross sections of Th-232, U-235, and U-238 should be high.

Some data for typical reactor spectra are presented in table 2.6. Pu-239 is used, because this isotope is directly produced by neutron capture in U-238. Neutron capture in U-238 is the main production path of transuranics for most reactor types. The transuranics of a once-through LWR discharge consist of about 54% of Pu-239³⁰. The transuranics in the fuel of a fast reactor consist of about 56% of Pu-239⁴².

The cross section data of the following reactor types were used:

- CANDU: The thermal flux is half of the total flux⁴³.
- LWR: Approximately one seventh of the flux is thermal³⁰.
- FR: The thermal component is almost zero, the flux in the resonance energy range is about 20% of the total flux⁴².
- Fission spectrum reactor: The thermal and resonance flux are almost zero.

Table 2.6: *Spectrum-weighted one-group fission cross sections for Pu-239 and capture cross sections for U-238.*

spectrum	cross section [b]		$\frac{\sigma_f^{Pu-239}}{\sigma_c^{U-238}}$
	fission Pu-239	capture U-238	
CANDU	267.0	1.16	230.0
LWR	121.0	0.9	134.0
FR	1.85	0.3	6.2
Fission	1.75	0.1	17.5

The ratio of the fission cross section of Pu-239 and the capture cross section of U-238 is highest for the CANDU reactor, which has the most thermalized spectrum. This is due to the strong decrease in fission cross section of Pu-239 with energy. For fissionable isotopes like Pu-240, the fission cross section will increase with energy, mostly to a value of about 1 to 2 barn. For a typical fuel with more than 50% Pu-239 in the transuranics, the fission cross section of the transuranics will mainly be determined by the fission cross section of Pu-239. Therefore, the most thermalized spectrum will have the lowest net production of transuranics for a certain transuranics enrichment.

When no U-238 is present, the net burned amount of radioactive actinides is completely determined by the energy production, which is proportional to the power

of the burner. Assuming an average mass number of 240, a thermal efficiency of 33%, and thermal energy produced per fission of 200 MeV, the burned amount of transuranics per MW_e annually is $1.2 \text{ kg}/MW_e \cdot y$.

For a burner without U-238, the Waste Ratio is proportional to the ratio of the burned amount and the inventory of the reactor, assuming that the losses in reprocessing are proportional by the inventory, and thus the Waste Ratio is proportional to the specific power of the reactor. The Inventory Transmutation Time is inversely proportional to the specific power.

2.6.3 Transmutation Efficiency of a Transuranics Fueled Reactor

The best transmutation system will not contain any uranium or thorium. In this section, the relation between flux spectrum and transmutation efficiency for a transuranics system is studied. In the previous section, it was shown that the burned amount of transuranics per unit of time is completely determined by the power of the burner when only transuranics are present:

$$BU(t) = \frac{1}{T_{cyc}} \int_0^{T_{cyc}} \int \Sigma_f(t, E) \phi(t, E) dE dt \cdot V. \quad (2.6)$$

When both the power and the specific power of a design are fixed, the transuranics inventory and thus the burner capability is fixed, and the choice of flux spectrum will make no difference, except on the isotopic composition of the fuel. The dependence of isotopic composition on flux spectrum is studied in this paragraph.

The following system has been considered: A continuous load of LWR discharges is fed to the burner. Assumed is that no reprocessing is carried out and no fission products are present in the system. So, it is a system in which mass is loaded and energy is produced. Then, after a while, the nuclei fed to the system will be equal to the nuclei fissioned. Furthermore, it is assumed that only transuranics will be present in the system. So, the number of fissions in the system is equal to the amount of transuranics burned. The produced energy is completely determined by the amount of material fed to the system. The flux level is determined by the specific power and the flux spectrum.

The program EQUI is used to calculate the inventory of the burner system with a continuous feeding of LWR discharges and fixed specific power. In EQUI, it is possible to calculate the influence of feeding a mixture of actinides into the reactor. EQUI determines the equilibrium concentration of that reactor with that feed vector. The actinide burning capability is determined by comparing the inventory vector and the feed vector of a reactor type for a specific power, which is equal to $0.4 \text{ MW}_t / \text{kg(HM)}$. This specific power is based on a typical flux level for an LWR, but

is about a factor 10 higher than for normal LWRs. So, the transuranics should be diluted, for instance in an inert matrix of MgO. In these calculations, selfshielding effects were not accounted for leading to overestimated cross sections, especially for the thermal spectrum reactors. This leads to overestimated transmutation rates, which leads for a fixed power and flux to a smaller inventory and an overestimated specific power.

The neutron spectra of the CANDU, LWR, Fast Reactor, and the fission spectrum reactor were used. The LWR cross sections were obtained from reference 30, the cross section for CANDU were obtained from reference 43, the cross sections for Fast Reactors were obtained from reference 42, and the cross sections for a fission spectrum were calculated by collapsing the JEF-1 data file with a fission spectrum.

In three years, an amount of 10 kg of LWR discharges is fed to the burner, which is equal to the amount of transuranics mass produced by a 13 MW_e once-through LWR in three years. In these three years, the 10 kg of transuranics fed to the burner is transmuted, when the reactor is in equilibrium. This 10 kg of transuranics fissioned is equal to an energy production of 8.5 MW_t for three years.

In table 2.7, the relative element masses of the transuranics inventory of the four burner types are presented. Also, the numbers for an LWR discharge are presented.

Table 2.7: Relative element masses for the four flux spectra.

case	flux [10 ¹⁴ cm ⁻² s ⁻¹]	elements				k _∞
		Np	Pu	Am	Cm	
discharge	.	4.6	89.2	6.0	0.2	1.2
LWR	2.0	3.2	41.1	11.1	44.4	1.09
CANDU	1.7	2.2	40.7	7.8	49.1	1.14
FR	57.0	3.5	80.6	11.0	4.9	1.9
FISSION	35.0	4.7	86.5	7.8	0.9	2.7

The transuranics discharge of LWRs for a burnup of 33 MWd/kg(HM) consist mainly of plutonium (90%). In thermal spectrum reactors, this plutonium is partly transmuted to Minor Actinides (MA), and the relative content of plutonium is about 40%, while the content of curium is almost 45%. For the fast spectrum reactors, the relative content of plutonium is only slightly lower than for the LWR discharge. This is explained by the change in ratio of capture to absorption cross sections, which is extremely large for the fissionable isotopes like Pu-240. For instance, the ratio of capture and absorption cross section for Pu-240 is 0.997 and 0.45 for the LWR and the fast reactor, respectively. Therefore, the production of higher actinides is much lower for the fast reactor. The infinite multiplication factor k_∞

for the LWR is 1.09, which is considerably lower than the k_{∞} of once-through LWRs (not including fission products) at the end of cycle (≈ 1.2). The k_{∞} of the transuranics mixture is higher for the other flux spectra: 1.14 for the CANDU spectrum, 1.9 for the fast reactor spectrum, and 2.7 for the fission spectrum.

In conclusion, to optimize a burner fueled with transuranics only, the power and specific power should be as high as possible. For the thermal spectra, the reprocessing and fuel fabrication will be extremely difficult due to the buildup of short-lived and spontaneously fissioning actinides. The low infinite multiplication factor for thermal systems shows that neutron losses by leakage and parasitic absorptions should be kept as low as possible.

2.7 Conclusions

We started this section with a discussion of the properties of nuclear waste. Several quantities can be considered describing the risks and costs of nuclear waste to society, but most of these are sensitive to changes in basic data. Therefore, the waste parameter transuranics mass is used, because it is a fixed quantity and it is a good representation of the long term radiotoxicity of the actinide waste.

For low loss fractions during reprocessing, the waste produced per unit of produced energy can be reduced by using special burner systems to reduce the inventory at the end of the nuclear era. Using burner systems, nuclear energy can be produced for a long time period without increasing the actinide waste currently present. High reductions can be obtained compared to producing energy with once-through LWRs.

Also, the physics aspects of designing a burner were considered. One system emerged: The one with the highest power and specific power and without any of the basic isotopes: Th-232, U-235, and U-238. In this system, the amount of transuranics burned per unit of time and electric power is $1.2 \text{ kg/MW}_e \cdot \text{y}$, which is the maximum value to be achieved. Other parameters are of no importance considering the physics of burners, unless the basic isotopes are present. Then, for a fixed enrichment, the reactor with the most thermalized spectrum will produce the lowest amount of transuranics by neutron capture in U-238. In the next chapters, technological aspects of burner design are considered. These aspects concern material constraints, safety, and reliability.

Chapter 3

LWR Waste Reduction with ALMR Burners

3.1 Introduction

The influence of the neutron spectrum on burner characteristics has been studied in chapter two. It was shown that for a fast reactor, higher actinides are being built up at a lower rate than for thermal reactors. These higher actinides cause problems in reprocessing because of the neutrons from spontaneous fission of higher actinides and the high α -activity. Therefore, the fast reactor technology is currently best equipped to handle actinide waste.

Almost all literature on the application of fast reactors for transmutation of actinides can be divided into two subjects:

1. Operation of a purely transuranics or minor actinides burner containing no U-238
2. Adding minor actinides in the fast reactor core

The first approach, a fast spectrum burner without U-238, is studied by Mukaiyama and by Hill^{14,44}. Mostly, these studies include no or little information on safety characteristics. Mukaiyama presents a sodium void worth of 2.5 % $\delta k/k$ (16\$, where 1\$ is equal to β , the fraction of delayed neutrons per fission, equal to 0.0016 according to Mukaiyama), which is almost a tripling of the effect compared to fast reactors containing U-238. This reflects the very hard flux spectrum due to the presence of only minor actinides¹⁴. Furthermore, the absence of Doppler

broadening of the U-238 resonances will reduce the negative Doppler feedback. Currently, fast reactor burners without U-238 are only considered as part of a hybrid system, in which a subcritical fission reactor is operated with an external source, for instance an accelerator. Then, reactivity coefficients are not as important, because of the subcritical operation of the reactor.

Addition of minor actinides to an oxide fueled fast reactor and to a metallic fueled fast reactor was studied by Strömich et al²⁹ and by Timm et al⁴⁵. The influence of addition of minor actinides on quantities like sodium void worth, Doppler coefficient, burnup reactivity loss, and the control rod worth were studied. Also, the influence of core size on transmutation rate was studied. It was concluded that the addition of minor actinides reduces the burnup reactivity loss per cycle, but that the sodium void effect, which is a negative characteristic of a fast reactor, is increased. The Doppler coefficient is decreased due to the addition of minor actinides. It was concluded that reduction of core size leads to a reduction in the amount of minor actinides burned. For addition of 15% (HM) minor actinides, the amount of minor actinides burned is about 0.33 kg/MW_e·y, whereas the amount of transuranics burned is maximally 0.36 kg/MW_e·y, which is achieved in a smaller core.

Timm et al compare addition of minor actinides to an oxide fueled design with addition of minor actinides to a metallic fueled design, with the same core layout⁴⁵. The only change in the core design was a longer in-core residence time for the oxide fueled core to achieve the same burnup. It was concluded that the burning capabilities of minor actinides in these cores are about the same, but that the safety characteristics are better for the oxide fueled core.

Many of these studies consider only minor actinides, and the plutonium isotopes are considered as "fuel." As already argued in chapter 1, a proper recycling scheme should include plutonium¹². Very few studies consider recycling of all actinides for fast reactors. Cockey et al present three Advanced Liquid Metal Reactor burner designs operating on metallic fuel³⁴. These reactors consume transuranics from LWR discharges. The designs differ in core height and cycle length. Although these designs are optimized on neutronics behavior, little is known on the systematic optimization of such a design for both neutronics and TRU burning.

In this chapter, relations between reactor parameters like core height and cycle length, and the burning capabilities of ALMR burners operating on LWR discharges are studied to optimize burners in a systematic way. With the developed approach, an oxide and metallic fueled burner are optimized for burning actinide waste. In the next section, the Advanced Liquid Metal Reactor is introduced. Then, the design process and the calculational methods are explained.

3.2 The ALMR system

In 1982, General Electric started the development of an oxide fueled small fast reactor, with a thermal power of 300 MW_t. This reactor was called the Power Reactor Inherently Safe Module (PRISM). At the same time, Argonne National Laboratory (ANL) started the Integral Fast Reactor (IFR) project. In this project, the knowledge of metal fuel processing developed in the military industry was used in the development of a metal fueled fast reactor in which the fuel would be produced and reprocessed on-site. In 1985, GE started work on metallic fuel, and raised the thermal power to 425 MW_t. By that time, GE concluded that the name inherently safe reactor was too ambitious and changed the name to Power Reactor Innovative Small Module.

The ALMR program started in 1987 as the Department of Energy (DoE) funded long term nuclear program, in which the design of the PRISM and the fuel cycle development of IFR are combined. In 1990, the power of the ALMR was increased to 471 MW_t, because of the better performance of the metal fuel compared to the oxide fuel and the use of the ferritic stainless steel alloy HT-9 as a structural material, which has low swelling in high radiation levels.

Because of economics of scale and the difficulty in designing an oxide fueled alternative, the thermal power of the ALMR module was increased in 1993 to 840 MW_t. Oxide fuel is maintained as an alternative to the reference metallic fuel, because of some uncertainties involved in the cost and development of the reprocessing technique for metallic fuel called pyroprocessing.

The development program of the ALMR focuses on the design certification by the Nuclear Regulatory Commission in 2008. One of the major steps in the process is the construction of a prototype, whose anticipated operation will start in 2004.

The ALMR design goals are a safe, reliable, and economically competitive liquid metal fast reactor power plant. The ALMR is designed with the following key features⁴⁶:

1. The capability to utilize long-lived radioactive actinide material from LWR spent fuel.
2. Passive reactivity control to a safe, stable state during undercooling and overpower transients with failure to scram, with abundant time for ultimate shutdown to cold conditions by operator initiated action.
3. Protection against severe accidents by a combination of simple and passive design features.
4. Passive shutdown heat removal for loss-of-cooling accidents.

5. Self-sustaining fissile supply with capability for breeding more fuel than is consumed.
6. Compact modules to enable factory fabrication

In figure 3.1, an overview of an ALMR module is shown.

Figure 3.1: *Overview of an ALMR module.*

The reactor module is about nine meters in diameter and about 18 meters high. Full containment is provided by the containment vessel, which surrounds the reactor vessel, and the containment dome, which encloses the head access area above the reactor closure. The reactor module, the intermediate heat transport system (IHTS), and the major portion of the steam generator are underground⁴⁶.

Primary sodium is circulated in the reactor by four electromagnetic pumps during normal operation. Important for safety is that the primary sodium circulates in the reactor vessel. Both the pumps and the intermediate heat exchangers are located in the vessel.

A feature of the ALMR module is the passive backup decay heat removal provided by the radiant vessel auxiliary cooling system (RVACS). This passive system can remove the reactor's decay heat without damage to the reactor. Another alternative design feature is the 30% lower specific power than earlier designed fast reactors and a heterogeneous core layout to enhance breeding and reduce the burnup reactivity loss⁴⁷. As a consequence, the control rod worth was limited such that if any single control assembly were inadvertently withdrawn from the core, the resulting transient would be limited by the core with no fuel melting and no pin failures⁴⁷.

To increase the negative reactivity feedback during a loss of flow without scram transient, gas expansion modules (GEM) are placed in-core. The GEM is a hollow assembly duct, placed in the reactor core which is sealed at the top and open at the bottom. A helium gas bubble trapped inside the assembly expands when the core inlet pressure decreases and expels sodium from the assembly. When the GEM is positioned at the periphery of the core, the drop in the sodium level increases the core neutron leakage and reducing reactivity. Six GEMs were incorporated in the ALMR design for this approach⁴⁷.

The reprocessing technique for metallic fuel is based on pyroprocessing. In this process, spent fuel from ALMRs is fed to an electrorefiner, in which the actinides and some rare earths fission products are collected at a liquid cadmium cathode. The cathode deposits are recovered and sent to a cathode processor, which is a high temperature vacuum furnace. The metal ingots resulting from the cathode processing are free of impurities. The next operational step is injection casting; uranium, plutonium, minor actinides, and zirconium are blended and casted into slugs suitable for loading into new fuel rods. The whole process will be carried out remotely, which is possible due to the simplicity of all operations⁴⁸. This is the main advantage of this process compared to the process used for oxide fuel. It is called PUREX and TRUOX for plutonium and minor actinides recovery, respectively. This process is an aqueous process, in which the fission products and the actinides are separated because of a difference in solubility. Wichers presents an overview of these two reprocessing techniques focussed on the proliferation resistance^{49,50}. It was concluded that a definite advantage of one or the other system does not exist, although material control in pyroprocessing will be difficult, because of the continuous process of dissolving and extraction.

Claims have been made that pyroprocessing can attain losses smaller than 0.02%⁵¹. Other publications give more conservative estimates of 1%^{10,39}. Thompson et al

estimate the reprocessing losses for the aqueous process to be a factor of at least ten times smaller³⁹.

3.3 Design Approach

The primary goal of the design of a reactor core is to determine that set of system parameters which will yield reliable, safe, and economical operation at the rated power level over the desired core lifetime. All these goals will impose several constraints on reactor performance. This design process for an ALMR core is presented in figure 3.2 in which the left side gives all the necessary steps in evaluation of the design, the system parameters are represented by the right block in the figure, and all constraints are represented by the middle block.

The ALMR design is described by seven design parameters: The thermal power, fuel pin design, the assembly design, the core zoning, the core height, the cycle length, and the number of batches. The thermal power will be prefixed in this study. The actual thermal power requested is chosen for economical reasons, which are partly influenced by the reactor physics characteristics of the design. Furthermore, we will not change the assembly design, because this will influence the thermal hydraulics of the design, which will not be the subject of this study. Also, the pin design will be changed only by assuming no changes in the thermal hydraulics. The core zoning for the burners is not changed because a quantitative optimization method including zoning will be very difficult. Each of the other parameters can be changed during the design process. So, in this study, four design parameters will be considered: the pin design (represented by the fuel volume fraction), the core height, the cycle length, and the number of batches.

The design process can be described by a number of steps:

1. ALMR design parameters are chosen on the basis of preliminary thermal hydraulic analysis and experience (first guess).
2. ALMR design parameters are optimized to fulfill all neutronics constraints (burnup reactivity loss, peak fuel burnup, peak fast fluence, peak linear power, and TRU enrichment) imposed on the ALMR. The value of the quantities on which constraints are imposed is calculated in the neutronics calculation, in which mass balances, fluxes, and depletion are calculated.
3. Determined next is the reactivity control requirement comprising burnup reactivity loss, temperature defect, fuel axial growth, overpower margin, shutdown margin, and uncertainties in all these.

4. Calculation of the control rod worth. If the control worth is too low to accommodate the burnup reactivity loss, the limit on the burnup reactivity loss should be adjusted; the ALMR design should be changed, and the optimization should be redone.
5. Calculation of thermal hydraulic behavior. The assumptions to determine the pin and assembly design should be confirmed, especially concerning peak fuel, cladding, and moderator temperatures, cladding thickness and duct dilation. A restatement of some constraints, especially peak linear power and fast fluence, is possible. In this study, this step was not considered, because for most designs the constraints are stringent enough to keep the chance of pin failure low.
6. Calculation of the reactivity coefficients, which determine the behavior of the reactor in transients: temperature coefficients, expansion coefficients, and sodium density coefficient.
7. Calculation of the safety characteristics of the design in several reactivity accidents. Especially cladding attack and cladding failure should be determined. A restatement of some constraints is possible.

These steps are repeated until all parameters are within the constraints. The design is optimized economically when the average linear power density and the average burnup are maximized. The linear power density is directly related to the power density, which is maximized to minimize core volume, and the average burnup is equal to the energy per unit of mass produced in the fuel before it will be reprocessed. So, a higher burnup means that fuel has to be reprocessed at a later time, and that per unit of energy, less fuel is reprocessed, which increases the economic efficiency of the design. High average linear power density and burnup can be obtained when the peak values are equal to the limits imposed on them, and when the power distribution is as flat as possible.

In the design process, the results are compared with constraints imposed on performance parameters of the design. These constraints are:

1. The burnup reactivity loss should be kept below 12\$ for burner cores to ensure proper reactivity control. The use of control rod stops to control reactivity insertion to a maximum of 0.3\$ is feasible for this limit. A lower limit could result when the control rod worth is too low.
2. The peak fuel burnup should be limited to about 150 MWd/kg(HM) to limit the cladding strain from the fission gas buildup in the upper plenum region and to assure proper fuel performance and fuel pin integrity.

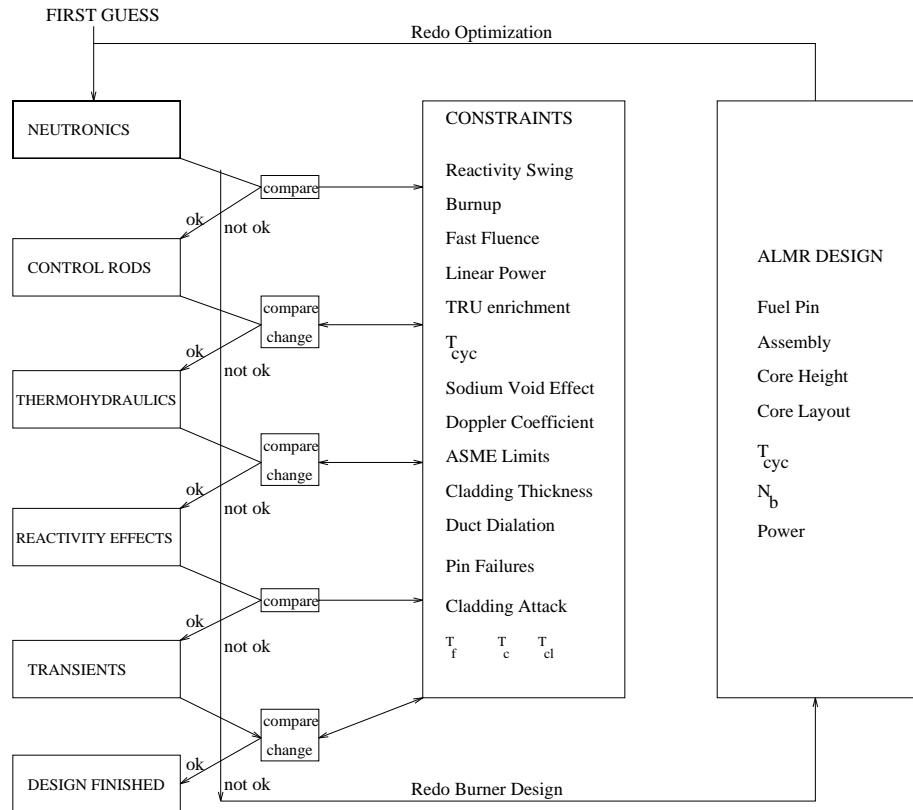


Figure 3.2: Flow diagram for the design process of an ALMR core.

3. The peak fast neutron fluence should be limited to about $3.6 \cdot 10^{23} \text{ n/cm}^2$. This limit is based on constraints imposed by the use of HT9 ferritic steel as the core structural material, which might swell appreciably above this fluence.
4. The peak linear power should be below 32.8 kW/m to exclude fuel melting in steady state and transient conditions.
5. The transuranic enrichment should be limited. For the oxide fuel, the TRU enrichment should be less than about 33 w/o, to ensure proper fuel fabrication. The solubility of plutonium in HNO_3 is reduced when the enrichment is above this limit and hydrogen-fluoride has to be used in fuel-processing. This will lead to a strong increase of the fuel fabrication costs⁵².

The TRU enrichment for metal fuel should be less than 30 w/o of the ternary alloy to remain in the range of the current metallic fuels database⁵³.

6. The cycle length should not be shorter than 12 months, because of plant availability, which should be as high as possible for economical reasons.

Furthermore, some constraints are imposed on the design for safety. These constraints can not be quantified that easily, and should be determined for every design by a safety analysis:

1. The sodium void effect should be sufficiently small.
2. The Doppler coefficient should be sufficiently negative.
3. The code limits proposed by the American Society of Structural Mechanical Engineers (ASME) should be maintained for all reactor structures.
4. The cladding attack by fuel/clad eutectic should be less than 10% of the cladding wall thickness.
5. The centerline fuel melting should be very limited.
6. The number of unrelated pin cladding failures should be small, and no pin failure propagation should occur.

However, this study aims for a burner which burns as much transuranics as possible. Still, the design should be safe, reliable, and cost effective. In this study, we assume that this will be accomplished when the design falls within the constraints on the burnup reactivity loss, the burnup, the fast fluence, the linear power, the transuranics enrichment, and the cycle length. Some cost implications of the burning of transuranics will be discussed.

3.4 Calculational Methods

The calculational methods can be separated roughly into cross section generation, core calculations, and transient calculations. The calculational methods and computer programs are presented in figure 3.3.

In this study, transient calculations were not performed. Instead, some calculations on the basis of some empirical equations were performed to assess the behavior of the cores designed. The next paragraphs will present the calculational methods in more detail.

3.4.1 Multigroup Cross Section Generation

The basic cross section data used for the nuclear design evaluations are contained in the Evaluated Nuclear Data File, Version V.2 (ENDF/B-V.2)⁵⁴. The NJOY data processing code system⁵⁵ was used to process the ENDF/B-V.2 data into a 80-group cross section library containing infinite diluted cross sections for various temperatures and lists of Bondarenko self-shielding f-factors. This library was prepared by the Los Alamos National Laboratory (LANL).

Regionwise microscopic cross sections were generated by utilizing the TDOWN pin cell data processing code and the preprocessed 80-group data library. The TDOWN pin-cell code was developed by General Electric to perform the data processing calculations and to generate multigroup cross section libraries in a format that can directly be applied to whole core calculations. The data processing in TDOWN includes resonance selfshielding, spatial selfshielding, elastic removal correction, reactor and cell flux solutions, and cross section condensation to few groups.

A cylindrical cell model for typical fuel and blanket pins was used in the TDOWN calculations. The heterogeneous cell configuration consists of four regions: a smeared fuel pellet/gap region (for the metallic fuel, the gap is filled with sodium), a cladding region, a sodium coolant region, and a smeared fuel assembly region (i.e., smeared fuel, coolant, cladding and duct material). Resonance selfshielding calculations for each region are based on the Bondarenko f-factor approach using narrow resonance approximation. Heterogeneous selfshielding is based upon the multi-region equivalence theory, which is an extension of the Wigner rational approximation⁵⁶. Finally, cell homogenization over the fuel pellet/gap, cladding, and sodium regions is performed to obtain the cross section data for a typical homogenized pin mixture. For every typical region and for a typical enrichment, a cross section set is generated and combined to one working library. A typical fuel pin has a fuel volume fraction of 37% for the metallic fuel library and 42.1% for the oxide fuel library.

One-dimensional reactor flux solution calculations with the transport code TDOWN were also performed to obtain neutron spectra for collapsing the cross section data to 12-group libraries for both metallic and oxide fuel. These calculations are typically carried out for several radial and axial models. It is noted that the preprocessed 80-group library was generated using a fixed neutron spectrum typical of a fast reactor. To account for the difference in neutron spectra between the base library and the reactor of interest, elastic removal correction is applied to correct the slowing down of neutrons and improve the accuracy of the predicted neutron spectra.

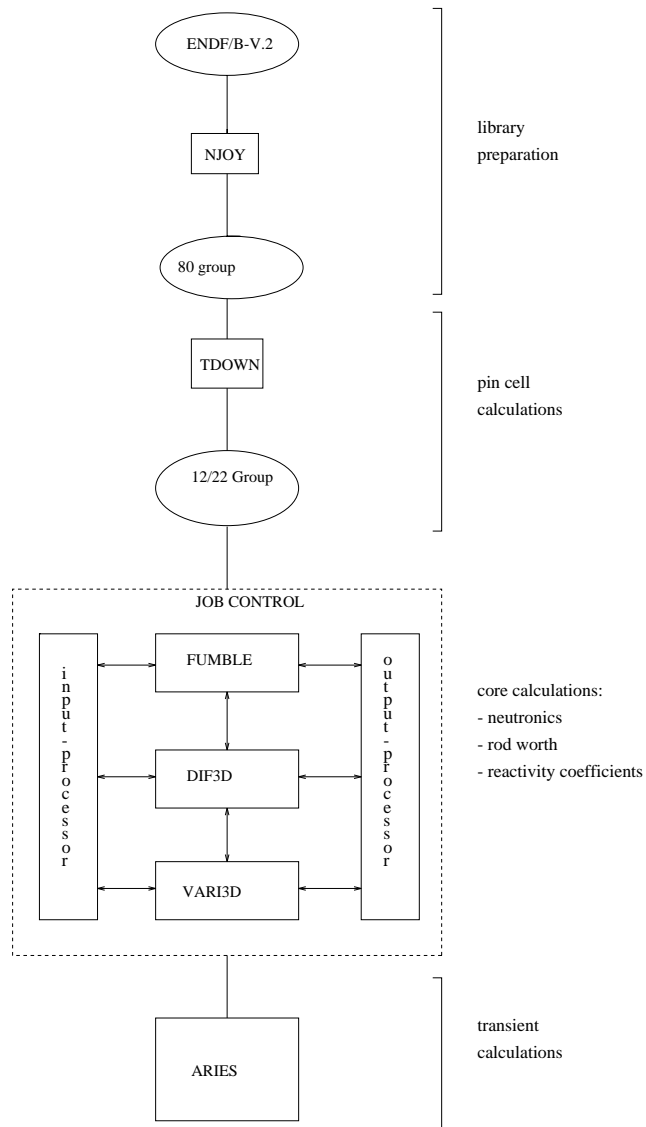


Figure 3.3: Representation of calculational methods and computer codes used in the design of an ALMR core.

The reference regionwise temperatures used in the data processing calculations are taken from thermal hydraulic analysis for steady-state full-power operating conditions.

3.4.2 Flux Solution and Burnup Calculations

For all cores investigated in this study, the same fuel cycle calculation procedure was used to provide a consistent comparison. All fuel cycle calculations were carried out with the three-dimensional flux solution code DIF3D⁵⁷ and the fuel management and burnup code FUMBLE, developed by General Electric. Flux solution calculations were performed using three-dimensional (3-D) hexagonal-z geometry, and the coarse-meshed nodal diffusion theory approximation to neutron transport. The 12-group cross section library for the specific fuel type under consideration was used for all basic neutronics computations.

The fuel cycle computations for the specified effective-full-power-day (EFPD) operating interval were performed by a burnup calculation in which the regionwise fluxes and fuel cross sections were taken from converged beginning-of-cycle and end-of-cycle flux solutions and interpolated for several burnup substeps (normally 10) within the cycle. A well converged fuel cycle mass balance solution was obtained by successive iterations of the flux solution and fuel management calculations, in which the initial enrichment was adjusted to obtain the EOC reactivity requested by the user. With this set of programs, it is not possible to do a calculation including the reprocessed burner waste in the external feed of transuranics like for a true burner scenario. Instead, it is assumed that, at the beginning of each cycle, the loaded assemblies are fresh fuel, made of, for instance, LWR waste. In these calculations, the positions of the assemblies are fixed from the beginning of life to the end of life. Assembly shuffling after each cycle would reduce power peaking, but is not applied.

For the sake of simplicity in the flux solution calculations, all control rods were assumed to be parked at a fixed position at both the beginning of the equilibrium cycle (BOEC) and the end of equilibrium cycle (EOEC). In reality, the control rod insertion depths at BOEC are highly dependent upon the burnup reactivity loss that requires excess reactivity in the fuel for burnup compensation. However, the simplification utilized is not expected to have a significant impact on the calculated performance parameters.

3.4.3 Reactivity Control Requirement and Control Rod Worth Calculation

Reactivity control requirement is determined by the burnup reactivity loss, temperature defect, fuel axial growth, overpower margin, shutdown margin, and uncertainties in all these.

Here, the temperature defect is defined as the reactivity change from hot full power to zero power at refueling temperature. This positive reactivity comprises the Doppler effect, radial and axial core contraction, and sodium density change and will be calculated using calculated reactivity coefficients.

The fuel axial growth term currently only pertains to the metallic fuel, which expands with fuel burnup from the accumulation of fission products. For this assessment, a 5% axial growth is assumed.

The overpower margin is allocated to permit the reactor to operate at 103% of the rated power, and is equivalent to 3% of the temperature defect. The shutdown margin is required for the assurance of subcriticality and is assumed to be 1\$.

The uncertainties consist of 15% of the total burnup reactivity, 20% of the total temperature defect, 20% of the fuel axial growth, and is assumed 1\$ each for criticality prediction, refueling, and fissile loading (tolerance for manufacture uncertainty in fissile enrichment). The total uncertainty is obtained by statistically combining all uncertainties.

The control rod worth is calculated by determination of the reactivity of the core with one rod in and with all rods in. The influence of the rod interaction is estimated and accounted for.

3.4.4 Void Worth and Reactivity Parameters

Calculations of reactivity feedback parameters and neutron kinetics parameters were carried out by utilizing the DIF3D and VARI3D computer codes. The DIF3D code is utilized to perform the neutron flux and adjoint solution calculations, using the 22-group cross section libraries, in the finite difference solution with fine-meshed triangular-z geometry. The VARI3D code was utilized for the perturbation computations to generate neutron kinetics parameters as well as mesh-dependent reactivity parameters.

Global reactivity parameters were computed and utilized to normalize the results of mesh-dependent reactivity parameters from the perturbation calculations. The global feedback coefficients are determined by the results from direct flux computations for the unperturbed and perturbed systems. These coefficients include the total density coefficients, uniform radial expansion, and uniform axial expansion.

For the calculation of the Doppler coefficient, libraries are generated with two average temperatures: 551 K and 829 K for both oxide and metal fuel. These temperatures are too low, especially for the oxide fueled core with an operating fuel temperature of 1200 K. The calculated Doppler coefficients are extrapolated to the operating region. This should lead to approximately correct results because the factor $T_f dk/dT_f$ is expected to be constant⁵⁸.

Sodium void reactivity can be computed in several ways. The first method is to perform a direct flux calculation by voiding the sodium in the core regions of interest using the sodium-voided cross sections. This method is the most accurate method of predicting the void worth. However, it is prohibitively expensive in computational costs to obtain a spatial distribution of void worth since each voided region would require a separate direct k-effective calculation.

The second method is to use the sodium density coefficients from the first-order perturbation calculations and then estimate the effect of sodium voiding. This approach generally does not accurately predict the sodium void reactivity because:

1. it does not take into account the changes in few-group cross sections that are affected by the spectral hardening when the sodium is voided, and
2. the first-order perturbation theory is not applicable to a 100% removal of sodium.

The third method is the exact perturbation method to obtain the spatial distribution of void worth. The exact perturbation approach requires a perturbed adjoint flux solution in addition to the reference (unperturbed) forward flux solution. It has the advantage above the first method that it gives the contribution to the reactivity effect by component (axial and radial leakage, absorption, scattering, and fission).

For this study, the exact perturbation approach based on 22-group cross sections and fine-meshed triangular-z geometry is used for the evaluation of the reference ALMR to obtain the void worth distribution. On the other hand, the direct flux solution approach based on 22-group cross sections and coarse-meshed hexagonal-z geometry is used to compute the sodium void worth for all cores analyzed to obtain a rapid estimation of the void worth.

Sodium void worths indicated in this report represent the estimated reactivity effect of voiding whole assemblies from top to bottom. This is perceived to be the most likely event if core voiding is to occur and therefore was chosen as the reference scenario for void worth calculations. Partial assembly voiding of only the active fuel region or positive worth sections would increase the positive void reactivity worth somewhat, depending on the core height and the presence of axial blankets. On the other hand, voiding of non-fuel assemblies, especially the interior control rods, adds substantial negative reactivity from the increased neutron leakage.

3.5 Influence of Design Parameters on Actinide Burning

3.5.1 Introduction

To optimize an ALMR design, design parameters have to be adjusted to increase linear power and burnup, while remaining within the limits imposed on several other performance parameters. These limits are set to obtain a safe and reliable design. In this study, we are interested how to design a reactor which consumes as much transuranics as possible, within the limits set for safety, reliability, and cost.

The influence of the core design parameters on how much the ALMR burns is examined. At first, no constraints on any performance parameters were taken into account. Then, these limits were considered, and it was determined how design parameters have to be chosen to optimize the design for burning within the constraints.

The design of a reference breeder ALMR consists of a heterogeneous core layout of fuel and blanket assemblies. The blanket assemblies are used to produce fuel for future fuel cycles and to flatten the power profile. For a burner, the fuel for future fuel cycles is assumed to be available from other sources, for instance a stockpile produced by once-through LWRs. So, blanket assemblies, normally used to produce fuel for use in the future, will not be used. The internal blanket assemblies will be exchanged for fuel assemblies. The radial blanket assemblies will be used for reflector assemblies and the reflector assemblies will be exchanged for extra shielding assemblies, which are necessary because the radial blanket is removed.

Important design parameters are core height, fuel volume fraction, cycle length and the number of batches. Other design parameters are reactor power, core layout, fuel pin and assembly design. These parameters can all be varied to obtain an ALMR design, all other quantities are a result of these parameters, and are called "performance parameters". The core layout is kept constant in this section, and the fuel pin and assembly design are represented by the fuel volume fraction, which is varied by the pin radius. The reactor power is kept constant too.

The core layout consists of a two region core. In the center of the core, 84 low-enriched fuel assemblies are present, and surrounding these assemblies, 108 high-enriched assemblies are positioned, with a 20% relatively higher enrichment than in the center. This enrichment split is applied to improve the performance of the burner by the reduction of power peaking. The determination of the magnitude of the enrichment split is not studied, because a systematic approach of this process is hard to give. The split is kept constant in the calculations described in

this chapter. In this report, only the high enrichment value is given.

The burning capability is measured in terms of the amount of transuranics burned per year. Five other performance parameters are considered in this study: the burnup reactivity loss, peak burnup, peak linear power, peak fast fluence, and transuranics enrichment. These parameters are used, because constraints are imposed on each of them. These constraints will limit the range of the design parameters. Assumed was that the four design parameters are independent variables for all these performance parameters and that the performance parameters are linearly dependent on changes in the design parameters:

$$b_j(\vec{x}) = \sum_{i=1}^4 \frac{\partial b_j}{\partial x_i} \cdot \Delta x_i + c_j, \quad (3.1)$$

where b_j is a performance parameter, x_i is a design parameter, and c_j are constants.

An oxide fueled ALMR with a thermal power of 840 MW_t will be studied. First, the partial derivatives of the six performance parameters to the design parameters will be discussed. The data were collected by varying these parameters, while no constraints were considered. All calculations were carried out with the DIF3D/FUMBLE interpolation scheme. The partial derivatives to the design parameters were determined by linear regression using the FIT routine of reference 59. The baseline case is the design of GE, which is presented in table 3.3. The design parameters are: Core height of 81.3 cm, fuel volume fraction of 39.5%, a cycle length of 12 months, and five batches. All partial derivatives were determined from data calculated by varying only one design parameter at a time. So, we assume that the design parameters are independent for all performance parameters. This assumption will be examined for the design parameters cycle length and number of batches, because these are expected to be correlated and because the number of batches is always varied by a large fraction due to its small value.

Third, the partial derivatives are used to optimize a burner with oxide fuel for the thermal power of 840 MW_t. The experience with this process is translated into general rules on how to optimize a burner when these relations are not known in detail.

3.5.2 Partial Derivatives of the Performance Parameters to the Design Parameters

The partial derivatives of the performance parameters to the design parameters were determined. The design parameters are the core height, which was varied between 58 cm and 91 cm, the fuel volume fraction, which was varied between

36.5% and 42.5%, the number of batches, which was varied between two and six, and the cycle length, which was varied between 10 months and 14 months. For some of these cases, the limits set on performance parameters were exceeded. For each design parameter, five cases were calculated.

Table 3.1: *Partial Derivatives of the Performance Parameters to the Design Parameters.*

$\partial b_j / \partial x_i$	Design Parameter			
	Core Height [cm]	Volume Fraction [%]	Number of Batches	cycle length [months]
burning capability [kg/y]	-1.9 ± 0.1	-5.11 ± 0.05	5. ± 1.	3.01 ± 0.02
Reactivity loss - δk [\$]	-0.18 ± 0.02	-0.533 ± 0.001	0.30 ± 0.01	0.90 ± 0.01
peak burnup [MWd/kg(HM)]	-1.8 ± 0.2	-3.5 ± 0.4	31.1 ± 0.4	12.5 ± 0.1
peak Linear Power [kW/m]	-0.49 ± 0.03	-0.096 ± 0.001	0.52 ± 0.07	0.22 ± 0.01
peak Fast Fluence [10^{22} n/cm ²]	-0.20 ± 0.01	-0.10 ± 0.01	6.31 ± 0.05	2.49 ± 0.02
TRU enrich. [%HM]	-0.30 ± 0.03	-0.79 ± 0.02	0.9 ± 0.1	0.47 ± 0.01

In table 3.1, the partial derivatives for the performance parameters to the design parameters are presented. The partial derivatives for the burning capability to the number of batches and the cycle length are of opposite sign compared to the derivatives to the core height and the fuel volume fraction. A decrease in fuel inventory increases the burning capability while a decrease in in-core residence time reduces burning capability. To explain this, the influence on reactor performance should be clear, which will be studied in more detail in the next three sections.

The partial derivatives for the core height and fuel volume fraction are both of opposite sign compared to the partial derivatives for the number of batches and the cycle length. For instance, a reduction in core height will increase the peak burnup (because less fuel inventory produces the same power), but a reduction in cycle length will reduce the peak burnup.

The assumed linearization of the relation between the performance parameters and

the design parameters is only valid for a limited range of the design parameters. For instance, the linear power is inversely proportional to the core height, which can be approximated by a linear relation for small deviations from the baseline value, which is 81.3 cm. A decrease in core height with 50% will double the peak linear power, whereas the linearization leads to an increase in linear power with approximately 60%,

One relation is remarkable and that is the relation between the number of batches and the peak linear power. The use of more batches results in an increase in the peak linear power. One would expect a decrease: The larger spread in burnup of the batches can be used to flatten the power distribution. This is not the case for these calculations because the assemblies are not reshuffled after each reload. So, a large spread in burnup will lead to larger differences in the power production of some elements, which will increase the peak linear power.

In figure 3.4, the burned amount of transuranics per year as calculated by the DIF3D/FUMBLE scheme is plotted as a function of the transuranics enrichment. This figure shows that the relation between these two parameters is quite linear in the parameter range considered. So, to maximize the burning rate of transuranics, one should aim for a high transuranics enrichment as explained in chapter two.

One can go to a higher enrichment by wasting more neutrons. More neutrons are wasted by adding absorber material to the fuel and by reducing the fuel inventory, which is proportional to the product of fuel volume fraction and core height. One can increase the enrichment also by increasing the burnup of the fuel, for instance by an increase of the in-core residence time. The range in which these parameters can be varied is set by the constraints on the design. The use of extra absorber material is not considered in this thesis. The questions to be answered in the next sections are:

1. Is reduction of fuel inventory more efficient than the increase of in-core residence time?
2. Should an increase of in-core residence time be accomplished by the number of batches or by the cycle length?
3. Should a reduction of fuel inventory be accomplished by the core height or the fuel volume fraction?

However, before answering these questions, we will first study the correlation between the linear relations for the design parameters cycle length and number of batches.

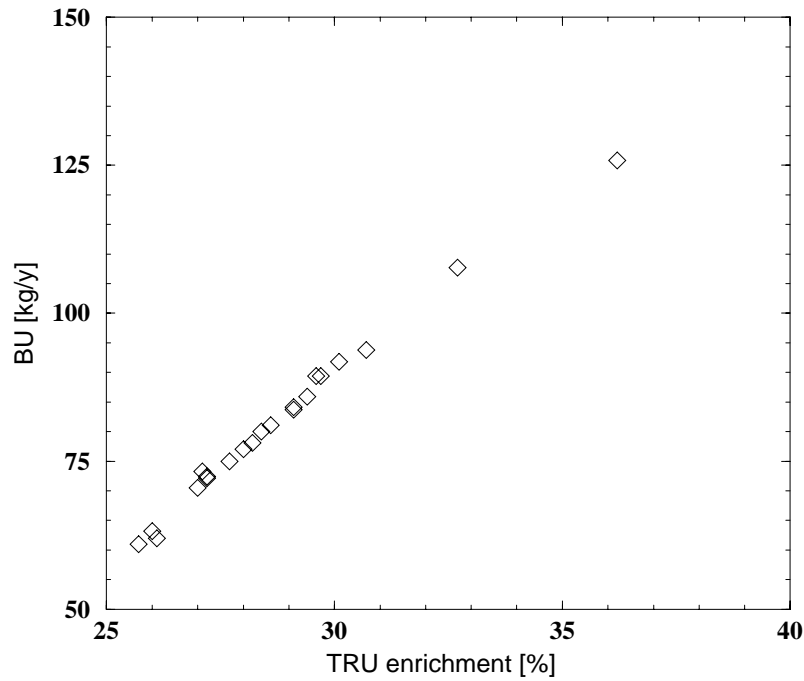


Figure 3.4: *The amount of transuranics burned per year as a function of the transuranics enrichment of the fuel.*

3.5.3 Correlations between the Coefficients for Cycle Length and Number of Batches

In this section, the correlations between the coefficients for cycle length and number of batches are studied. The in-core residence time is the product of cycle length and the number of batches. For instance, one would expect the average burnup to be constant for constant in-core residence time. The performance parameters were calculated for a constant in-core residence time while the number of batches and the cycle length were varied. This was done with the DIF3D/FUMBLE scheme as well as with the linear relations determined in section 3.3. In table 3.2, the maximum deviations between the two approaches are presented, in the range of

three batches and 20 months to six batches and 10 months.

For the peak burnup and the peak fast fluence, the deviations between the two approaches is high, showing the correlation between the cycle length and the number of batches for these parameters. Both parameters are almost constant for the range of batches and cycle lengths considered. This shows that both are linear with the **product** of number of batches and cycle length. Therefore, the peak burnup and the peak fluence will be linearized to the in-core residence time.

These results show that the assumed non-correlation between the linear relations might lead to large discrepancies between the results obtained by the direct calculation and by the linear relations. This could also be the case for the linear relations for core height and fuel volume fraction. The results presented in this paragraph were obtained by varying the number of batches and the cycle length by a factor of two. However, the fuel volume fraction and the core height are varied on a much smaller scale.

Table 3.2: *Maximum deviations between direct calculations and calculations with the linear relations.*

Performance Parameter	Deviation [%]
reactivity loss	1.3
peak burnup	24
peak linear power	1.0
peak fast fluence	24
TRU enrich.	-2.0
burned TRU	-5.1

3.5.4 Burner Optimization within Performance Constraints

Optimization Method

In the previous sections, relations between design parameters, burning capability, and performance parameters have been calculated. An increase of in-core residence time, by adjusting cycle length and/or the number of batches, and a decrease in fuel volume, by adjusting the core height and/or the fuel volume fraction, will increase the transuranics enrichment need and thus the burning capability. However, due to several constraints imposed on the performance parameters of the reactor design, the design parameters are restricted to a certain range. In this paragraph, the way to choose these design parameters will be explained. The linear relations

will be used to maximize the burning rate of transuranics while complying with the constraints on the performance parameters. It is almost impossible to do this without an optimization model, because of the amount of information involved.

In reference 59, a computer code to solve a linear maximization problem is presented. This code maximizes the function :

$$z = a_{01}x_1 + a_{02}x_2 + \dots + a_{0N}x_N \quad (3.2)$$

subject to the primary constraints

$$x_1 \geq 0, x_2 \geq 0, \dots, x_N \geq 0 \quad (3.3)$$

and simultaneously subject to $M = m_1 + m_2 + m_3$ additional constraints, m_1 of the form

$$a_{i1}x_1 + a_{i2}x_2 + \dots + a_{iN}x_N \leq b_i \quad (b_i \geq 0) \quad (3.4)$$

$$i = 1, \dots, m_1$$

m_2 of the form

$$a_{j1}x_1 + a_{j2}x_2 + \dots + a_{jN}x_N \geq b_j \geq 0 \quad (3.5)$$

$$j = m_1 + 1, \dots, m_1 + m_2$$

and m_3 of the form

$$a_{k1}x_1 + a_{k2}x_2 + \dots + a_{kN}x_N = b_k \geq 0 \quad (3.6)$$

$$k = m_1 + m_2 + 1, \dots, m_1 + m_2 + m_3$$

The x_i are the four design parameters and the a_{ij} are the linear coefficients calculated in the previous sections. The b 's are the constraints imposed on the design parameters (cycle length and number of batches) and the five performance parameters. N is four, m_1 is five (for burnup reactivity loss, burnup, linear power, fast fluence, and transuranics enrichment), and m_2 is 1 (for the cycle length), and m_3 is 1 (for the number of batches). The number of batches is fixed to an integer number (in this study three, four, or five) to be able to use linear relations between in-core residence time and peak burnup and peak fast fluence. So, the number of batches is not present in the optimization problem. Absolute values are needed for the performance parameters to check whether these are within their limits. So, we need also the constants calculated by the linear regression code. These are also used to obtain absolute values for the burning capability. The absolute values are all the same as for the baseline case calculated with the DIF3D/FUMBLE scheme and presented in table 3.4. Only the values for peak burnup, enrichment, and burning capability deviate slightly: the peak burnup is 161.7 MWd/kg(HM), the transuranics enrichment is 28.3%, and the burning capability is 78.7 kg/y.

Table 3.3: Design parameters, performance parameters, and burning capability for baseline case, and for optimal cases for three, four, and five batch operation.

design parameters				
parameters	baseline	$N_B = 3$	$N_B = 4$	$N_B = 5$
Core Height [cm]	81.3	76.3	77.3	110.7
Volume Fraction [%]	39.5	37.8	38.1	27.7
Cycle Length	12	12	12	12
performance parameters				
parameters	baseline	$N_B = 3$	$N_B = 4$	$N_B = 5$
React. Loss $-\delta k$ [\$]	8.8	10	10	10
Peak Burnup [MWd/kg(HM)]	160.6	114.2	142.7	150
Peak Linear Power [kW/m]	31.2	32.8	32.8	18.4
Peak Fast Fluence [10^{23} n/cm ²]	3.2	2.1	2.7	2.8
TRU Enrichment [%HM]	28.2	29.4	29.8	28.8
Burning Capability				
parameters	baseline	$N_B = 3$	$N_B = 4$	$N_B = 5$
BU [kg/y]	78.1	86.7	88.6	82.5

Results of Optimization

In table 3.3, the results of the optimization for three, four, and five batch operation are shown. These results are obtained with the optimization program discussed, and with the following constraints: peak burnup at 150 MWd/kg(HM), a maximum burnup reactivity loss of 10\$, peak linear power at 32.8 kW/m, peak fast fluence at $3.6 \cdot 10^{23}$ cm⁻², and a maximum transuranics enrichment of 33%. The burnup reactivity loss of 10\$ was taken because the control rod worth for the 840 MW_t ALMR is less than for the 471 MW_t which is due to the larger core size of the 840 MW_t ALMR. Furthermore, the cycle length had to be at least 12 months to have a plant capacity factor of 85%, which is important for the economics of the design. These calculations have been done at separate number of batches to include the linear relation between in-core residence time and burnup and fast fluence.

Let's take a look at what happens in going from three to four batches. The in-core residence time is increased, which will increase the enrichment need. Also, the reactivity loss and the peak linear power increase, and will be higher than their limits. Therefore, the fuel inventory is increased to reduce the reactivity loss and the peak linear power. That causes the transuranics enrichment to drop. Finally, a small transuranics enrichment increase remains, and the transuranics burning capability is only slightly increased.

Table 3.4: Design parameters, performance parameters, and burning capability for optimal cases for three, four, and five batch operation at a fixed fuel volume fraction of 39.5%.

design parameters			
parameters	$N_B = 3$	$N_B = 4$	$N_B = 5$
Core Height [cm]	76.4	77.4	87.8
Volume Fraction [%]	39.5	39.5	39.5
Cycle Length	13.0	12.9	12.0
performance parameters			
parameters	$N_B = 3$	$N_B = 4$	$N_B = 5$
React. Loss $-\delta k$ [\$]	10	10	7.7
Peak Burnup [MWd/kg(HM)]	116.8	146.6	150
Peak Linear Power [kW/m]	32.8	32.8	28.2
Peak Fast Fluence [10^{23} n/cm ²]	2.2	2.8	3.1
TRU Enrichment [%HM]	28.6	29.1	26.4
Burning Capabilities			
parameters	$N_B = 3$	$N_B = 4$	$N_B = 5$
BU [kg/y]	81.0	83.6	66.1

In going from four to five batches, not only the limits on reactivity loss and peak linear power are violated, also the peak burnup will be higher than its limit. So, again the fuel inventory should be increased to reduce these performance parameters. The fuel inventory is proportional to the product of fuel volume fraction and the core height, and indeed this product increases in going from four to five batches. One would expect the peak burnup to be about 178 MWd/kg(HM) for five batches in case that the fuel inventory is not increased. The average burnup is inversely proportional to the fuel inventory. So, one would expect the fuel inventory to be increased by approximately a factor of 1.2, but it only increases with 4%. This is because the burnup is inversely proportional to the **product** of the fuel volume fraction and the core height, which leads to a large deviation from the baseline values for this case. Therefore, this result falls outside the validity range of this model.

In the design practice as operated by GE, one takes a certain fuel volume fraction, which gives the best performance in fuel temperatures and pin failure. In this case, the fuel volume fraction is fixed to 39.5%. The results of optimization with this fixed fuel volume fraction are presented in table 3.4.

The burning capabilities are somewhat less than for the cases with a free choice of fuel volume fraction. The core height is approximately the same as for the free

choice cases, except for the five batch case. For the three and four batch cases, the peak linear power and the burnup reactivity loss are equal to their limits. The cycle length is longer for the three and four batch cases to increase the transuranics enrichment. This is possible because the burnup reactivity loss and the peak burnup are lower than their limits, due to the fact that the limit on the peak linear power prohibits a smaller core height.

The difference between the baseline case presented in table 3.3 and the five batch case of table 3.4 is the peak burnup, which is 7% lower for the latter case. Therefore, the core height is increased with 8%. This results in a strongly reduced transuranics enrichment, burning capability, peak linear power, and burnup reactivity loss.

In going from five to four batches, the peak burnup, peak fast fluence, and the peak linear power will decrease as is shown in table 3.4. Therefore, the core height can be reduced and the cycle length can be increased. The highest transuranics enrichment is obtained when both the reactivity loss and the peak linear power are equal to their limits. In going from four to three batches, again the core height can be reduced slightly and the cycle length can be increased slightly.

The conclusion is that there is no definite answer to the question whether the fuel inventory should be decreased instead of an increase in in-core residence time. It depends on which performance parameters are limiting the choice of the design parameters. The same holds for the choice between core height and fuel volume fraction, and between cycle length and number of batches.

The way to reduce a certain performance parameter with the smallest reduction in burning capability can be determined by comparing the ratios of the partial derivatives for that particular performance parameter and the burning capability as is presented by:

$$ratio = \frac{\partial b_j}{\partial x_i} / \frac{\partial BU}{\partial x_i} = \left[\frac{\partial b_j}{\partial BU} \right]_{x_k=C, k \neq i} \quad (3.7)$$

These ratios are presented in table 3.5. Such a ratio represents the change in a performance parameter to obtain an increase in the burning capability by 1 kg/y by variation of only one design parameter.

The highest ratio represents the highest change in that performance parameter with the smallest change in the burning capability accomplished by a change in one design parameter. For instance, suppose that your design has a burnup reactivity loss, which is higher than the limit. So, you want to decrease the burnup reactivity loss at the lowest change in burning rate. You can do that by increasing the cycle length. The cycle length is the most effective design parameter to reduce the reactivity loss. The number of batches is the most effective factor to reduce the peak burnup and the fast fluence. The core height is the most effective factor to reduce the peak linear power.

Also, these ratios present the way to increase the burning capability with the smallest change in a certain performance parameter. The lowest ratio represents the lowest change in that performance parameter with the highest change in the burning capability accomplished by a change in one design parameter. Increase of the number of batches is the most effective way to increase the burning capability when the reactivity loss is lower than its limit. Decrease of the fuel volume fraction is the most effective way to increase the burning capability when the peak burnup, the peak linear power, the peak fast fluence, and the transuranics enrichment are lower than their limits.

Table 3.5: *Ratio of the Partial Derivatives to the Design Parameters for the Performance Parameters to the Partial Derivative of the Burning Capability.*

Performance Parameters	Ratio of Linear Coefficients			
	Core Height	Volume Fraction	Number of Batches	cycle length
Reactivity loss	0.095	0.104	0.06	0.3
peak burnup	0.9	0.7	6.2	4.2
peak Linear Power	0.3	0.02	0.1	0.07
peak Fast Fluence	0.1	0.02	1.3	0.8
TRU enrich.	0.16	0.15	0.18	0.16

From these observations, several generalizations can be obtained:

1. In practice, only three performance parameters reach their limits in designing an ALMR burner: the burnup reactivity loss, the peak linear power, and the peak burnup.
2. The cycle length should be equal to its minimum unless the fuel volume fraction is fixed.
3. One should increase the cycle length when the burnup reactivity loss and the peak burnup are lower than their limits and when the fuel volume fraction is fixed.
4. One should reduce the number of batches and the cycle length when the peak burnup is equal to its limit and the peak linear power and/or the burnup reactivity loss are not equal to their limits.

5. The core height and the fuel volume fraction should be chosen in such a way that both the burnup reactivity loss and the peak linear power are equal to their limits. When the burnup reactivity loss is lower than its limit, and the peak linear power is equal to its limit, the core height should be increased and the fuel volume fraction should be decreased. When the peak linear power is lower than its limit, and the burnup reactivity loss is equal to its limit, the core height should be reduced and the fuel volume fraction should be increased. The reason for this rule is that the ratio of the linear coefficients of the peak linear power and the burning capability for the core height is much higher than this ratio for the fuel volume fraction while these ratios of the burnup reactivity loss are almost equal. Therefore, any change involving the peak linear power leads to a small change in core height and a larger change in another design parameter.

Optimization Scheme

The observations and conclusion of the optimizations lead to the following scheme to maximize the burning rate of transuranics:

1. Choose a core layout and enrichment split,
2. Take the lowest cycle length and the smallest number of batches,
3. Calculate the core height from the limit on the peak linear power using an estimated peaking factor,
4. Calculate core performance with DIF3D/FUMBLE,
5. Adjust the fuel volume fraction and the core height according to the rules presented in this section, adjust the number of batches only when the estimated peak burnup remains below its limit. If the fuel volume fraction is fixed, adjust the cycle length until the limit on burnup reactivity loss is reached,
6. Redo DIF3D/FUMBLE calculation,
7. Repeat until result is satisfactory.

Discussion of Optimization of Burners

The central question of this chapter is to optimize an ALMR for burning transuranics. To optimize a reactor economically, the fuel inventory should be as small as possible, and the in-core residence time should be as high as possible. We have

seen that to increase burning of transuranics, these parameters should be maximized too. So, the optimizations of burning capability and costs seem not to be conflicting. However, the optimization on burning leads to a short cycle length, which might not be the most cost effective way of plant operation.

In the optimization process developed in this chapter, several factors were not accounted for:

- shuffling of fuel assemblies, which could lead to a considerable reduction in power peaking increasing the average linear power and burnup. Higher average linear power and burnup lead to a higher transuranics enrichment and burning capability.
- optimization of enrichment split, which could also lead to a reduction in power peaking.
- application of burnable absorber rods, which could lead to a strong reduction in burnup reactivity loss and power peaking, both allowing for reduced fuel inventory and increased in-core residence time.
- optimization of reactor power leading to lower average burnup and linear power. In this way, an increase of burned amount of transuranics per unit of energy might be achieved.
- optimization of assembly and pin design, leading to lower peak burnup and linear power.

3.6 Metallic and Oxide Fueled ALMR Burners

3.6.1 Optimization Process and Core Description

For the metallic fueled core, the burner was designed by GE to operate with the core layout as shown in figure 3.5 at a thermal power of 471 MW_t .

To control power peaking, the core was divided in a central low-enriched fuel region and a high-enriched surrounding fuel region of 30 and 66 fuel assemblies, respectively. The number of shielding assemblies of a burner is increased compared to a break-even core by exchanging the radial blanket for reflector material, and by exchanging reflector material for shielding material. Cockey et al discussed the characteristics of the metallic fueled burner design³⁴. The burnup reactivity loss is near its limit of 12\$, but the peak burnup is much lower than its limit, while the cycle time is 15 months and the number of batches is three.

ALMR Metal Burner Core, case 92i

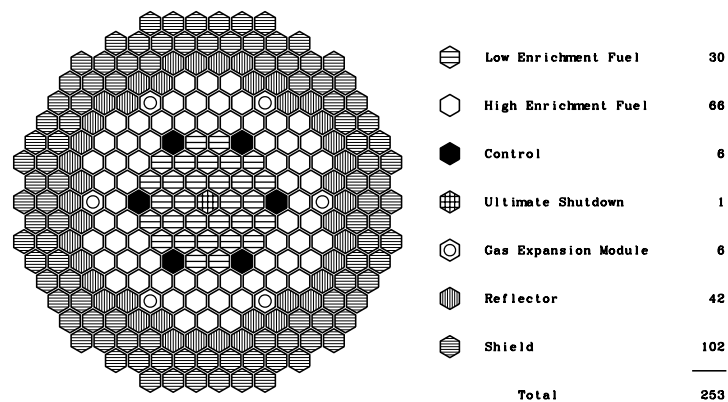


Figure 3.5: Core layout for the burner cores.

To optimize this metallic fueled design according to the scheme presented in section 3.5.4, the cycle time has to be minimal, so equal to 12 months to allow for the smallest possible core. Then, the burnup reactivity loss was lower than the limit. First, the core height was decreased, but only 4 cm could be achieved due to the limit on peak linear power. To obtain the largest benefit of the reduction in cycle length, the burnup reactivity loss has to be equal to the limit, so the fuel pin diameter was changed to lower the fuel volume fraction. The fuel volume fraction was decreased from 35.8% to 31.8% by reducing the pellet diameter from 0.53 cm to 0.50 cm and increasing the cladding thickness from 5.5 mm to 6.4 mm, which leads to an increase in sodium volume fraction from 38% to 40%. In this way, the burnup reactivity loss was near its limit. Still, the peak burnup is low, but more batches increased the peak burnup above the limit. The peak burnup could be

lowered by increasing core height and fuel volume fraction, but that will decrease the burning capability substantially, as is shown in section 3.5. Therefore, the optimized design operates with three batches in-core.

For the oxide fueled burner design, the metallic fueled design as presented by Cockey was used as a start with the oxide fuel characteristics³⁴. Then, the burnup reactivity loss and the transuranics enrichment were too high. By taking a cycle length of 12 months, the transuranics enrichment and the burnup reactivity loss dropped below their limits. The peak burnup is much lower than the limit, but not low enough to increase the number of batches.

3.6.2 Comparison of the Metallic and Oxide Fueled Burners

In this paragraph, some of the specific aspects of the metallic and oxide fueled burners will be discussed. The oxide and metallic fueled designs operate similarly, as can be seen in table 3.6.

Table 3.6: *Specifics of the metallic and oxide fueled ALMR burners.*

parameter	metallic	oxide
Core Height [cm]	107	107
Fuel Volume fraction [%]	31.8	35.8
Cladding Volume Fraction [%]	28.1	26.5
Sodium Volume Fraction [%]	40.1	37.7
burnup reactivity loss [%]	11.5	12
Average fuel burnup [MWd/kg(HM)]	72.6	78.2
Peak fuel burnup [MWd/kg(HM)]	114.4	128.9
TRU enrichment [%]		
low	23.5	25.8
high	28.4	31.2
Average linear power [kW/m]	20.7	20.7
Peak linear power [kW/m]	35.1	37.1
Peak Fast Fluence [10^{23} cm^{-2}]	2.8	2.3
Total Flux [$10^{15} \text{ cm}^{-2} \text{ s}^{-1}$]	2.80	2.62
Median Energy [keV]	220	165

Still, the results are not completely satisfactory as can be seen by the peak linear power, which is too high. An important difference between the two burners is the transuranics enrichment. For the metallic fueled core, the transuranics enrichment is 23.5% and 28.4% for the inner and outer fuel region, respectively, and for the oxide fueled core, the transuranics enrichment is 25.8% and 31.2% for the

inner and outer fuel region, respectively. This difference reflects the difference in utilization of the neutrons between the two cores. For the metallic core, 72% of the source neutrons is absorbed in the core, and 28% leaks out of the core region. For the oxide fueled core, these numbers are 76% and 24%, respectively. Of the absorbed neutrons, 49% causes fission in the metallic fuel, and 46% causes fission in the oxide fuel. So, the infinite multiplication factor k_{∞} of the metallic fuel is larger than of the oxide fuel. This is due to the absence of moderating oxygen atoms. When the enrichment of the oxide fuel would be used for the metallic fueled burner, the multiplication factor would be too high. Therefore, the enrichment of the metal fuel is lower.

In table 3.7, the important data on the fuel mass inventories are tabulated.

Table 3.7: Uranium mass and transuranics mass for the metallic fueled ALMR and the oxide fueled ALMR at BOC, for loading and discharge per cycle.

quantity	mass [kg]	
	Metal	Oxide
In-core Inventory at BOC		
U-235	7.3	6.5
U-238	4214.8	3768.4
TRU	1516.4	1556.1
Out-core Inventory at BOC		
U-235	4.9	4.3
U-238	2809.9	2512.3
TRU	1010.9	1037.4
Loaded		
U-235	2.8	2.5
U-238	1434.2	1285.7
TRU	526.9	539.9
Discharged		
U-235	1.8	1.5
U-238	1347.8	1198.5
TRU	466.3	480.1
Burned		
U-235	1.0	1.0
U-238	87.3	88.1
TRU	60.6	59.8

The total amount of actinides fissioned is 148 kg and the amount of transuranics burned is about 60 kg. This is about 1.5 times the amount discharged yearly by an ordinary Light Water Reactor operated at the same power level³. The difference in

burned transuranics between the metal and oxide fueled design can be explained by the difference in transmutation of U-238. This is explained in chapter two: The amount of transuranics burned is equal to the amount of atoms fissioned minus the amount of U-238 atoms transmuted. The initial inventory of U-238 is higher for the metal core than for the oxide core. The transmutation of U-238 is almost equal for the metal and oxide fuel, so the microscopic absorption cross section for metal fuel should be smaller than for oxide fuel. This is to be expected due to the softer spectrum for the oxide fuel.

The amount of transuranics burned for these 471 MW_t reactors is about 0.39 kg/MW_e·y, assuming a capacity factor of 85% and a thermal efficiency of 33%. For the 840 MW_t reactor studied in paragraph 3.5, the amount of transuranics burned is about 0.32 kg/MW_e·y, assuming a capacity factor of 85% and a thermal efficiency of 33%. A smaller core will lead to a higher transuranics enrichment due to the higher neutron leakage. In general, a smaller core will lead to higher cost.

The time to halve the inventory, the Inventory Transmutation Time, is calculated by dividing the inventory by the burned amount. The Inventory Transmutation Time is 42 years and 43 years for the metallic fueled and oxide fueled ALMR, respectively. The Inventory Transmutation Time of the oxide fueled ALMR is higher due to the higher inventory.

3.6.3 Reactivity Control

In this section, the reactivity requirement and actual worth of the control rods are determined for the optimized oxide and metallic fueled burner cores. The control system reactivity is required to have sufficient worth to bring the reactor from hot full power operation to cold subcritical at refueling temperature. This requirement can be categorized into several components: temperature defect, burnup reactivity loss, fuel axial growth, overpower margin, shutdown margin, and uncertainties in all these.

Temperature defect is the reactivity change from hot full power to zero power at refueling temperature, which is 477 K according to General Electric. This positive reactivity comprises the Doppler effect, radial and axial core contraction, and sodium density change. This reactivity component is calculated from the reactivity coefficients calculated and listed in table 3.9. The results are 1.1\$ for metallic fuel and 2.1\$ for the oxide fuel, which is higher due to the higher operating fuel temperature. At 300 K, the temperature defect would have been 2\$ and 3\$ for the metallic and oxide fueled burner, respectively.

Burnup reactivity loss is the excess reactivity built for the compensation of fuel burnup. For the metallic fueled core, the burnup reactivity loss is 11.5\$, compared

to 12\$ for the oxide core.

The fuel axial growth term for the metallic fuel is caused by a fuel expansion with 5%. Only one-third of the axial expansion factor listed in table 3.8 is included because axial expansion occurs only in the fresh elements, which is one-third for a three batch core. So, this term is 1.10\$ for the metallic fueled core.

The overpower margin is allocated to permit the reactor to operate at 103% of the rated power and is equivalent to 3% of the temperature defect. The shutdown margin is 1\$.

The total shutdown requirement is estimated to be 17.5\$ for the metallic fueled core and 17.7\$ for the oxide fueled core, including all uncertainties.

The primary control system for these cores consists of six control rods in row four, with natural B₄C. The worth of these rods at BOEC is computed to be 23.9\$ for the metallic fueled core and 24\$ for the oxide fueled core. The total worth for six rods in these cores is enough to shutdown the reactor. However, the feature of shutdown with only one rod, as was accomplished in the reference cores, is not maintained in the burner designs, unless boron enriched in ¹⁰B is used. For instance, the control worth will be increased by a factor of 1.5 for an enrichment of 50%.

3.6.4 Void Worth and Reactivity Parameters of the Optimized Burner Designs

Sodium void worths, reactivity parameters and neutron kinetics parameters were calculated with DIF3D/VARI3D with the 22 neutron group libraries in a fine-meshed triangular-z geometry model. The results of these calculations are summarized in table 3.8 for BOEC and EOEC for the metallic and oxide fueled cores.

The effective delayed neutron fractions (β_{eff}) are 0.003 for metallic and oxide fueled cores. These fractions are much lower than the delayed neutron fraction in a light water reactor (0.007), due to the large content of Pu-239 and higher actinides with a relatively low delayed neutron yield compared to the delayed neutron yield of U-235¹¹. The average neutron lifetime based on the 6-group delayed neutron data is about 35 ms for both the metallic and oxide fueled burner. The average neutron lifetime $\langle l \rangle$ equals¹¹:

$$\langle l \rangle = (1 - \beta) \cdot l + \sum_{i=1}^6 \beta_i \left(\frac{1}{\lambda_i} + l \right) \approx \sum_{i=1}^6 \frac{\beta_i}{\lambda_i}, \quad (3.8)$$

where l is the prompt neutron lifetime, β_i is the delayed neutron fraction of

precursor group i with decay constant λ_i . For Pu-239, this average neutron lifetime is equal to 31 ms, whereas for a reactor operated on U-235, the average neutron lifetime is 84 ms^{11,60}.

Table 3.8: *Sodium void worths, reactivity parameters and kinetic parameters of the metallic and oxide fueled ALMR burners.*

label	Metallic Fueled		Oxide Fueled	
	BOC	EOC	BOC	EOC
Uniform Axial Expansion (Hdk/dH)				
Net Effect	-0.263	-0.265	-0.227	-0.229
Geometry Effect	0.193	0.193	0.166	0.166
Uniform Radial Expansion (Rdk/dR)				
Net Effect	-0.656	-0.658	-0.568	-0.569
Geometry Effect	0.256	0.258	0.219	0.220
Doppler Parameters (Tdk/dT)				
Inner Fuel	-0.0013	-0.0013	-0.0023	-0.0041
Outer Fuel	-0.0015	-0.0016	-0.0023	-0.0024
Total	-0.0028	-0.0029	-0.0046	-0.0047
Sodium Density Parameters ($\rho_{Na} dk/d\rho_{Na}$)				
Inner Fuel	-0.0099	-0.0112	-0.0069	-0.0078
Outer Fuel	0.0007	-0.0001	0.0010	0.0004
Others	0.0070	0.0071	0.0067	0.0069
Total	-0.0021	-0.0041	0.0008	-0.0006
Sodium Void Reactivity (β)				
Inner Fuel	2.37	2.75	1.72	2.00
Outer Fuel	-0.80	-0.60	-0.70	-0.56
Others	-4.84	-5.03	-4.37	-4.55
Total	-3.27	-2.88	-3.35	-3.11
Kinetics Parameters				
Total Beta-effective	0.0031	0.0031	0.0031	0.0030
Average Neutron Lifetime [s]	0.036	0.035	0.035	0.035
Prompt Neutron Lifetime [10^{-7} s]	3.4	3.5	3.9	4.1

The prompt neutron life time is 337 ns for the metallic fueled core and 391 ns for the oxide fueled core. The prompt neutron lifetime for a critical core equals¹¹:

$$l = \frac{1}{\nu v \Sigma_f}, \quad (3.9)$$

where v is the average neutron velocity. For the oxide fuel, the ratio of scattering cross section and the absorption cross section is relatively higher than for the metallic fuel due to the presence of the oxygen atoms. Furthermore, the energy decrement per scattering is higher for the oxygen atoms than for the sodium atoms, which are the thermalizing atoms for the metallic fuel. Therefore, the mean free path of neutrons in the oxide fuel will be higher, and the average speed of the neutrons will be lower. Therefore, the prompt neutron lifetime for the oxide fuel is higher than for metallic fuel. Both are much smaller than the prompt neutron lifetime for an LWR which is between 10^{-6} and 10^{-4} s¹¹.

The calculated reactivity effects are explained with a three factor formula:

$$k = \eta f P_{NL}, \quad (3.10)$$

where k is the effective neutron multiplication factor, η is the number of fission neutrons produced per absorption in the fuel, f is the probability that if a neutron is absorbed it will be absorbed in the fuel, and P_{NL} is the non-leakage probability. η equals $\bar{\nu}(\Sigma_f^F/\Sigma_a^F)$, with $\bar{\nu}$ the average number of fission neutrons per fission, Σ_f^F is the macroscopic fission cross section of the fuel, and Σ_a^F is the macroscopic absorption cross section of the fuel. f equals Σ_a^F/Σ_a , with Σ_a is the total macroscopic absorption cross section in the core. P_{NL} is given by:

$$P_{NL} = \frac{1}{1 + M^2 \cdot B_g^2} \quad (3.11)$$

where M^2 is the migration area and B_g^2 is the geometric buckling, which for a cylindrical core equals $(\nu_0/R)^2 + (\pi/H)^2$, with H and R the extrapolated dimensions of the core and where ν_0 , equal to 2.405, is the smallest zero of the zeroth order Bessel function¹¹.

The uniform axial expansion parameter contributes to the axial fuel expansion feedback during transient events. As fuel temperature rises, axial fuel expansion increases the core height and provides a negative reactivity. For uniform axial expansion, the parameter (measured as Hdk/dH) at BOEC is -0.263 for metallic fueled and -0.227 for the oxide fueled core. The reactivity effect of expanding core size consists of two parts:

$$\frac{dk}{dH} = \left[\frac{\partial k}{\partial \rho_f} \right]_{H=c} \cdot \left[\frac{\partial \rho_f}{\partial H} \right]_{M_f=c} + \left[\frac{\partial k}{\partial H} \right]_{\rho_f=c}, \quad (3.12)$$

where the partial derivative of the fuel density to the core height is determined for a constant fuel mass. The first term is due to reduced fuel density and the second

term is from the enlargement of the core leading to a reduced neutron leakage. For a constant fuel mass, the fuel density ρ_f is inversely proportional to the core height H . Then, the reactivity effect of expanding core height is given by:

$$H \frac{dk}{dH} = -\rho_f \left[\frac{\partial k}{\partial \rho_f} \right] + H \cdot \left[\frac{\partial k}{\partial H} \right]_{\rho_f=c}. \quad (3.13)$$

The fuel density coefficient is positive because f and the non-leakage probability increase with fuel density due to the increased chance of absorption in the fuel. The fuel density coefficient for the metallic fueled burner is 16% larger than for the oxide fueled burner. This can be explained by the dependence of the non-leakage probability on fuel density ρ_f . Using equation 3.10, the derivative of k with respect to the fuel density can be written as:

$$\frac{1}{k} \frac{\partial k}{\partial \rho_f} = \frac{1}{\eta} \frac{\partial \eta}{\partial \rho_f} + \frac{1}{f} \frac{\partial f}{\partial \rho_f} + \frac{1}{P_{NL}} \frac{\partial P_{NL}}{\partial \rho_f} \quad (3.14)$$

The derivative of the non-leakage probability to the fuel density becomes

$$\frac{1}{P_{NL}} \frac{\partial P_{NL}}{\partial \rho_f} = \frac{2}{P_{NL}} \cdot \left(\frac{1}{1 + M^2 B_g^2} \right)^2 \cdot M^2 B_g^2 \cdot 1/\rho_f, \quad (3.15)$$

assuming that the migration area M^2 is inversely proportional to the square of the fuel density¹¹. Then, the ratio of $\frac{\partial P_{NL}}{\partial \rho_f}$ for metal to oxide equals

$$\frac{\left[\frac{\partial P_{NL}}{\partial \rho_f} \right]_{metal}}{\left[\frac{\partial P_{NL}}{\partial \rho_f} \right]_{oxide}} = \frac{[P_{NL} M^2 B_g^2]_{metal}}{[P_{NL} M^2 B_g^2]_{oxide}} \quad (3.16)$$

The data to calculate this ratio is:

quantity	metal	oxide
leakage	27.5%	23.9%
P_{NL}	0.725	0.761
$M^2 B_g^2$	0.38	0.31

which leads to a ratio of 1.17, a difference somewhat larger than that between the fuel density coefficient of metal and oxide fuel. The difference comes from changes in f , which are determined by the difference in spectrum, construction materials, and fuel enrichment. An estimate of the influence of these on f in going from metallic to oxide fuel is difficult to make.

The geometry effect is smaller in the oxide core, because of the lower leakage in the oxide core. Therefore, the influence of a change in core size is less for the oxide core. This can be illustrated using the same method as to explain the fuel

density effect:

$$\frac{1}{P_{NL}} \frac{\partial P_{NL}}{\partial H} = \frac{2}{P_{NL}} \cdot \left(\frac{1}{1 + M^2 B_g^2} \right)^2 \cdot M^2 \cdot \frac{\pi^2}{H^3}, \quad (3.17)$$

Then, the ratio of $\frac{H}{P_{NL}} \partial P_{NL} / \partial H$ for metal to oxide equals

$$\frac{\left[\frac{H}{P_{NL}} \partial P_{NL} / \partial H \right]_{metal}}{\left[\frac{H}{P_{NL}} \partial P_{NL} / \partial H \right]_{oxide}} = [P_{NL} M^2 H^{-2}]_{metal} / [P_{NL}^2 M^2 H^{-2}]_{oxide}. \quad (3.18)$$

which leads approximately to 1.17, assuming that the geometric buckling and the core height are the same for the metallic and oxide fueled cores. The geometry effect is 16% higher for the metallic fuel. The effect of core height on the fuel utilization and η are negligible.

The uniform radial expansion is controlled by two important inherent reactivity feedback mechanisms: the radial thermal expansion of the grid plate which is governed by the coolant inlet temperature, and the radial thermal expansion of core load pads. For uniform radial expansion, the parameters (measured as Rdk/dR) at BOEC are -0.656 and -0.568 for metal and oxide fuel, respectively. The effect for oxide fuel is smaller than for metal fuel for the same reasons as mentioned above for the axial leakage. The radial expansion effect is about two times larger than the axial effect, because the volume changes with the square of the radius.

The Doppler parameters given by as Tdk/dT at BOEC for the metallic and oxide fueled core are calculated to be -0.0028 and -0.0046. These parameters are assumed to be temperature independent for fast reactors⁵⁸. The Doppler coefficient (dk/dT) is about equal for metal and oxide fuel at operational temperature, which is about 800 K for metal fuel and 1300 K for oxide fuel. According to Wade et al in reference 61, the Doppler coefficient is about a factor of 1.5 larger for the oxide fuel. Here, the Doppler coefficient for the oxide fuel is almost the same as the one for the metal fuel because of three reasons. First, the TRU enrichment is smaller for the metal fuel. A higher TRU enrichment decreases the influence of the absorptions in U-238 and increases the average energy of the neutron spectrum⁵⁸. Second, the fuel volume fraction for the metal fueled core is lowered by decreasing the fuel pin diameter and increasing the cladding thickness. So, selfshielding is reduced and resonances are more effective. Third, the difference in average neutron energy between the oxide and metallic fueled burner will be lower than for the reactors studied by Okrent et al due to the larger amount of moderating cladding material for the metallic fueled burner⁵⁸. These reasons explain why the Doppler coefficients of the metal and oxide fueled core are not as different from each other compared to what can be found in literature. The Doppler coefficient for a break-even design is approximately a factor of two larger than for the burners⁵³. This is

due to the large content of U-238 in the blankets of such a break-even core; these blankets have been removed in the burners.

The reactivity effect of sodium voiding consists of three principal effects⁵⁸:

1. a negative reactivity effect due to increased neutron leakage,
2. a positive reactivity effect due to hardening of the neutron energy spectrum,
3. a positive reactivity effect due to reduced neutron capture in sodium.

The exact perturbation method has been used to obtain the spatial distribution of the sodium void worth for the burner cores. This shows that sodium void worths of the metallic fueled core are 2.15\$ for the fuel and -2.88\$ for the whole core. For the oxide fueled core, the sodium void worth is 1.44\$ for the fuel and -3.11\$ for the whole core. The values for the fuel are less for the oxide core, because the spectral hardening, which results from the sodium removal, is less for oxide fuel. In the metal core, sodium and cladding are the only thermalizing materials, but for the oxide fuel, the oxygen atoms are important for the thermalization of neutrons, which results in a much lower median energy for the oxide core than for the metal core. These oxygen atoms remain in the fuel during voiding, and the absence of thermalizing sodium atoms is of less importance.

On the other hand, the absolute influence of voiding on leakage is higher for the metal core. This can be seen by the difference between whole core voiding and fuel voiding. This difference is -5.0\$ for the metal core, and -4.6\$ for the oxide core. This difference represents the influence of voiding of non-fuel elements, which will have mainly effect on leakage. The leakage increases due to voiding are relatively the same for the oxide and metallic fueled core, but the absolute value of this effect and the influence on reactivity are higher for the metal core because leakage is higher for the metal core.

The results for sodium density parameters can be explained by similar arguments. Cockey et al present the sodium density parameter of a break-even reactor⁵³. The sodium density parameter for fuel and blanket for this 840 MW_t core is -0.0205, and for the whole core -0.0186. For the metal burner of 471 MW_t, the sodium density parameters are -0.0112 and -0.0041 for the fuel and the whole core, respectively. So, the sodium density effect in the fuel is reduced by a factor of two compared to break-even designs. The total sodium density effect is reduced by more than a factor four. This reduction is partly due to the smaller reactor power, but mainly due to the removal of the radial blankets.

3.6.5 Safety Parameters

Any safety predictions on the basis of only the reactivity calculations discussed in the previous section will be highly inaccurate. However, a safety study with complete transient calculations falls outside the scope of this section. The ALMR

group has defined some anticipated transients without scram (ATWS). Wade et al introduce a quasi-static approach to evaluate the consequences of these events^{61,62}. These transients will in general be sufficiently slow to be studied with a quasi-static approach. Here, we will use the asymptotic outlet temperature to determine if a transient remains within safety bounds. The sodium temperature should remain below the boiling temperature of about 940 °C, but also below a temperature of 700 °C which is the ASME limit above which strong fuel-clad interaction occurs resulting in high pin failure rates⁶³. Of course, in a more general safety analysis, other parameters, like peak fuel temperature and cladding temperatures, should be considered too.

The quasi-static reactivity balance is given by^{61,64}:

$$0 = \delta\rho = (P - 1)A + \left(\frac{P}{F} - 1\right)B + \delta T_{in}C + \delta\rho_{ext} \quad (3.19)$$

where P and F are power and flow normalized to nominal power and flow, δT_{in} is the change from nominal coolant inlet temperature, $\delta\rho_{ext}$ the externally imposed reactivity, A is the net power reactivity increment given by $(\partial\delta\rho/\partial P)_{(P/F, T_{in} constant)}$, B the power flow coefficient given by $(\partial\delta\rho/\partial(P/F))_{(P, T_{in} constant)}$, and C is the inlet temperature coefficient of reactivity. (A+B) is the reactivity increment experienced in going to full power and flow from zero-power at constant coolant inlet temperature.

A, B, and C are calculated from the reactivity coefficients by:

$$A = \left[\frac{\partial\delta\rho}{\partial P}\right]_{(P/F, T_{in} constant)} = (\alpha_D + \alpha_H) \cdot \Delta T_f, \quad (3.20)$$

$$B = \left[\frac{\partial\delta\rho}{\partial(P/F)}\right]_{(P, T_{in} constant)} = (\alpha_D + \alpha_H + \alpha_{Na} + \alpha_R) \cdot \Delta T_c/2, \quad (3.21)$$

$$C = \left[\frac{\partial\delta\rho}{\partial T_{in}}\right]_{(P, F constant)} = \alpha_D + \alpha_H + \alpha_{Na} + \alpha_R, \quad (3.22)$$

where ΔT_f is the average fuel temperature increase over the fuel pin, and ΔT_c is the average coolant temperature increase from inlet to outlet. In going from zero to full power, at a constant ratio of power and flow, and thus at a constant coolant T_c , and at a constant inlet temperature, the fuel temperature increases by ΔT_f . So, A includes the Doppler coefficient, represented by α_D , and the axial fuel expansion, represented by α_H . At full power, the outlet coolant temperature is $T_{in} + \Delta T_c$, where ΔT_c is the coolant temperature rise from inlet to outlet. B represents the reactivity change due to the increase in coolant temperature in going from zero to full power at nominal full flow. So, B includes the Doppler coefficient, the axial fuel expansion, the sodium density effect, represented by α_{Na} , and the radial expansion, represented by α_R . A change in inlet temperature causes a change in average coolant temperature. So, for C, all effects have to be included also.

The reactivity coefficients in $\$/K$ are given by

$$\alpha_D = \frac{1}{\beta} [T_f \frac{dk}{dT_f}] \frac{1}{T_f}, \quad (3.23)$$

$$\alpha_H = \frac{1}{\beta} [H \frac{dk}{dH}] \gamma_f, \quad (3.24)$$

$$\alpha_{Na} = \frac{1}{\beta} [\rho_{Na} \frac{dk}{d\rho_{Na}}] [\frac{1}{\rho_{Na}} \frac{d\rho_{Na}}{dT}], \quad (3.25)$$

$$\alpha_R = \frac{1}{\beta} [R \frac{dk}{dR}] \gamma_g, \quad (3.26)$$

where γ_f is the linear expansion coefficient of the fuel, ρ_{Na} is the sodium density, $[\frac{-1}{\rho_{Na}} \frac{d\rho_{Na}}{dT}]$ is the volumetric expansion coefficient of Sodium (equal to $0.28 \cdot 10^{-3} K^{-1}$), R is the equivalent core radius, and γ_g is the linear expansion coefficient of the grid plates made of HT9⁶¹. For the linear fuel expansion coefficient, the fuel expansion and the cladding expansion have to be considered. For metal fuel, the linear expansion coefficient is $17.6 \cdot 10^{-6} K^{-1}$, for oxide fuel, it is $12.8 \cdot 10^{-6} K^{-1}$, and for cladding made of HT9, it is $13.9 \cdot 10^{-6} K^{-1}$ ⁶¹. For the metal fuel, it is assumed that the fuel is attached to the cladding even for low burnup. Therefore, the fuel expansion of the metallic fueled reactors is controlled by the cladding, which is determined by the coolant temperature. Therefore, the coefficient A for the metallic fuel does not contain the axial expansion coefficient. For oxide fuel, the fuel is assumed to be free to expand from the cladding. The axial expansion coefficient for metallic fuel is calculated with the expansion coefficient of HT9.

With the reactivity parameters calculated in section 3.6.4, the reactivity coefficients are calculated and presented in table 3.9. Also, the design temperatures, and the coefficients A, B, and C are presented. These data are compared to data abstracted from reference 61 for the IFR reactor with a higher total power of 900 MW_t and an average linear power of 39-43 kW/m. To show the influence of reactivity coefficients only, the A, B, and C for the IFR have been calculated for the temperatures of the burner also. These are indicated by IFR*.

A few differences are noticeable, especially between the burners and the IFR breeder designs. First, the fuel temperature T_f and fuel temperature rise ΔT_f is much higher for the IFR breeder designs than for the burners due to two times higher average linear power for the IFR designs. The influence of temperatures is on A and B, which are smaller for lower temperatures. Second, the sodium density coefficients of the burners are much lower than those of the IFR designs due to the smaller burner core size which leads to higher leakage.

Table 3.9: *Parameters and temperatures to evaluate asymptotic behavior for ATWS events (100 c = 1\$).*

parameter	Burner		IFR		IFR*	
	metal	oxide	metal	oxide	metal	oxide
T_f [K]	774	1239	848	1448	774	1239
ΔT_f [K]	80	542	150	750	80	542
ΔT_c [K]	129	129	150	150	129	129
T_{in} [K]	629	629	623	623	629	629
T_{out} [K]	758	758	773	773	758	758
α_D [c/K]	-0.114	-0.121	-0.10	-0.16	-0.10	-0.16
α_H [c/K]	-0.117	-0.0947	-0.12	-0.10	-0.12	-0.10
α_R [c/K]	-0.291	-0.237	-0.25	-0.20	-0.25	-0.20
α_{Na} [c/K]	+0.0363	+0.0052	+0.18	+0.11	+0.18	+0.11
A [c]	-9.1	-117	-15	-195	-8.0	-141
B [c]	-31.3	-28.9	-21.8	-26.3	-18.7	-22.6
C [c/K]	-0.486	-0.448	-0.29	-0.35	-0.29	-0.35

Five ATWS are postulated in three categories:

1. Events induced by changes in flow due to the primary pumps:

- (a) Loss of Flow without scram (LOFWS) in which the pumps stop and the circulation reduces to the level of natural circulation. P/F is larger than one, and the average temperature in the core will increase. This causes a negative reactivity effect which leads to reduced power. Finally, the power will be small ($P \ll 1$) and the reactivity equation gives

$$\frac{P}{F} = 1 + \frac{A}{B}, \quad (3.27)$$

$$\delta T_{out} = \Delta T_c \delta\left(\frac{P}{F}\right) = \frac{A}{B} \Delta T_c. \quad (3.28)$$

- (b) Pump overspeed, which causes the flow to increase. At first, the temperature in the core will decrease, which will cause an increase in power according to:

$$P = \frac{A + B}{A + B/F} > 1, \quad (3.29)$$

$$\delta T_{out} = \Delta T_c \delta\left(\frac{P}{F}\right) = \Delta T_c \frac{A(1 - F)}{AF + B} < 0. \quad (3.30)$$

So, the outlet temperature is lower, even with higher power. The higher power will eventually result in a temperature rise of the inlet coolant temperature because the balance of plant system is not capable of handling a higher power for a longer time period. So, the power will return to its initial value (1). Then:

$$\delta T_{in} = \left(1 - \frac{1}{F}\right) \cdot \frac{B}{C}, \quad (3.31)$$

$$\delta T_{out} = \delta T_{in} + \Delta T_c \delta \left(\frac{P}{F}\right) = \left(1 - \frac{1}{F}\right) \cdot \left(\frac{B}{C} - \Delta T_c\right). \quad (3.32)$$

2. Events induced by changes in external reactivity (control-rod induced)

- (a) Transient Over Power (TOP) event, in which a control rod is withdrawn slowly, which causes a positive reactivity insertion $\delta \rho_{ext}$. F and T_{in} remain unchanged. At first, reactivity is compensated by a power rise (higher fuel temperatures). So, the quasi-static balance equation gives:

$$P = 1 - \frac{\delta \rho_{ext}}{A + B} \quad (3.33)$$

$$\delta T_{out} = \left(\frac{P}{F} - 1\right) \Delta T_c = -\frac{\delta \rho_{ext} \Delta T_c}{A + B}. \quad (3.34)$$

Eventually, the increase in power will result in an increase of the inlet coolant temperature and the power will decrease to the initial level (1). The outlet coolant temperature will increase according to the increase in inlet temperature:

$$\delta T_{in} = \delta T_{out} = -\frac{\delta \rho_{ext}}{C}. \quad (3.35)$$

3. Events induced by changes in inlet temperature (Balance of Plant induced)

- (a) Loss of Heat Sink (LOHS) in which the inlet temperature of the coolant rises due to the loss of cooling by the secondary circuit. The increase in inlet-temperature causes a decrease in power. Asymptotically, the power will be effectively zero and the outlet and inlet temperature of the coolant will be the same. Then:

$$\delta T_{in} = \frac{A + B}{C} \quad (3.36)$$

$$\delta T_{out} = \delta T_{in} - \Delta T_c = \Delta T_c \cdot \left[\frac{A + B}{C \Delta T_c} - 1\right]. \quad (3.37)$$

- (b) Chilled inlet temperature, in which the inlet temperature is too low, for instance due to a steam pipe break in the tertiary system. The decrease in inlet temperature will lead to a positive reactivity insertion, which is compensated by the reactivity decrease due to the increase in power. So:

$$P = 1 - \frac{\delta T_{in} C}{A + B} \quad (3.38)$$

$$\delta T_{out} = \left[\frac{C \Delta T_c}{A + B} - 1 \right] \cdot -\delta T_{in} \quad (3.39)$$

The minimum inlet temperature is equal to the sodium melting temperature equal to 98 °C. This event will turn into a LOHS event after dry-out of the steam generator⁶⁴.

For the LOFWS event, it is possible that the asymptotic results underestimate the event due to short term dynamics effects. Then, the net reactivity departs from equilibrium, which invalidates the quasi-static balance equation. Without special design measures, the pump flow coastdown time constant τ is shorter than the delayed neutron time constant. Due to the continuing high delayed neutron production, P/F will be even larger, and the outlet coolant temperature overshoots the asymptotic result given by equation 3.28. According to Wade et al in reference 62, the overshoot is reduced when

$$\tau \gg \left(\lambda \cdot \left(1 + \frac{A}{B} \right)^2 |B| \right)^{-1} = \tau_o, \quad (3.40)$$

where $1/\lambda$ is the delayed neutron time constant with $\lambda = \beta / \langle l \rangle$ and A and B are in \$'s.

In this quasi-static analysis, the influence of afterheat and passive heat removal were not considered. These effects will play an important role for the events leading to passive shutdown of the reactor, i.e. the LOFWS and the LOHS events. Assumed is that the afterheat will be removed by the passive heat removal system (RVACS). In that case, the in-core temperatures will be similar, because the temperatures are set to compensate for the reactivity change.

With these data, the average outlet coolant temperatures for the five ATWS events are calculated and are presented in table 3.10. The results for the pump overspeed event are obtained by assuming an increase in flow of 50%, and the results of the transient overpower event are obtained by assuming a reactivity insertion of 0.3\$.

Above 970 K fuel cladding interaction is much stronger leading to a higher pin failure rate. The outlet temperatures for these events are lower for the metal cores

Table 3.10: Average outlet temperature for five ATWS accidents.

accident	equation	T_{out} [K]					
		Burner		IFR		IFR*	
		metal	oxide	metal	oxide	metal	oxide
normal		758	758	773	773	758	758
LOFWS	3.28	796	1280	876	1885	813	1563
Pump Overspeed	3.30	745	721	748	727	741	719
Pump Overspeed	3.32	736	737	748	748	737	737
TOP	3.34	854	785	895	793	903	782
TOP	3.35	820	825	876	859	861	844
LOHS	3.37	712	955	750	1255	721	1096
Chilled Inlet	3.39	900	602	819	581	861	571
LOFWS	3.40	τ_o [s]					
		22	1.6	19	0.6	30.4	1.0

than the oxide fueled cores except for the Transient Over Power event and the chilled inlet event. Especially for the Loss of Flow event, the temperature rise is much higher for the oxide core. The higher asymptotic outlet temperature for the oxide fuel is due to the larger ratio A/B due to the much higher ΔT_f for the oxide core. The minimum pump flow coastdown time constant τ_o is almost a factor 10 smaller for the oxide fueled cores due to the larger ratio of A/B . For the Transient Over Power event, the coolant outlet temperatures of the metallic fueled cores are higher due to the smaller Doppler effect caused by the smaller ΔT_f . This event has been calculated for a slow withdrawal of the control rods for a small reactivity insertion of 0.3\$, which is particular small considering the 12\$ burnup reactivity loss for the burner cores. For the burner cores, the control rods have a large worth and have to be kept inserted deeply at startup to make a large burnup reactivity loss possible. Therefore, this event is very important, and the oxide fueled burner core has a smaller temperature increase than the metallic fueled burner. For the chilled inlet event, the outlet coolant temperatures for the metallic fueled cores are higher due to the smaller value of $A + B$. This event will turn into a LOHS event for which the outlet coolant temperatures of the oxide fueled cores are much higher than the outlet coolant temperatures of the metallic fueled cores for either event.

The coolant outlet temperatures for the burner designs are less than for the IFR breeder design, which is due to the smaller sodium density coefficient and the lower linear power. For the metal burner, the outlet temperature is always much less than 970 K, but outlet temperature for the Transient Over Power event is much higher than for the oxide fueled burner. For the oxide burner, three ATWS events cause a high outlet temperature: the LOFWS event, the LOHS event, and the

chilled inlet temperature event leading to a LOHS event.

3.7 Conclusions

The process to maximize the transuranics burning rate of ALMRs has been studied. It is concluded that the transuranics enrichment should be maximized to reduce the amount of transuranics formed by neutron capture in U-238. The transuranics enrichment can be maximized by reducing the fuel inventory and by increasing the in-core residence time. A different approach is necessary due to constraints on core performance parameters. The way to proceed in this optimization process is to choose both the smallest cycle length and number of batches, and then to reduce the core height and the fuel volume fraction. The reduction in fuel inventory is limited by the limits on peak linear power and burnup reactivity loss. The in-core residence time can only be increased when the fuel inventory is hardly influenced, which is the case as long as the limits on burnup reactivity loss and peak burnup are not reached.

This systematic optimization process is used to develop a metallic and oxide fueled burner. These burners burn approximately the same amount of transuranics per year, which is about 60 kg per year for the 471 MW_t reactor power, which equals to 0.39 kg/MW_e·y. This amount is about 1.5 times the amount discharged yearly by an ordinary Light Water Reactor operated at the same power level. The amount of transuranics burned is maximally 1.2 kg/MW_e·y for reactors without uranium. The uranium is necessary for a safe and cost effective operation. The time to halve the inventory represented by the Inventory Transmutation Time is calculated to be about 42 years.

It is concluded that a smaller reactor power will lead to a higher amount of transuranics burned per unit of reactor power. An explanation that the metallic and oxide fueled ALMR burners burn equally well is presented: Although the transuranics enrichment is lower for the metallic fuel, the burning capability is the same as for the oxide fueled burner, because the transmutation rate of U-238 is the same. This is caused by the lower microscopic capture cross section for U-238 for metallic fuel.

In this study, the safety of the designs are studied. Concluded is that the burner cores will lead to lower temperature changes due to Anticipated Transients Without Scram than the IFR breeder designs due to the lower linear power and the smaller sodium density coefficient. The oxide cores lead to higher temperature changes for ATWS events due to the higher fuel temperatures caused by the lower heat conductivity of the oxide fuel compared to the metallic fuel. The only exception is the Transient OverPower event, in which a control rod is pulled out. For this

event, the metallic fueled cores react more violently, leading to higher average coolant outlet temperatures. This is, however, not the limiting event.

One major difference with the original ALMR breeder reactor is the large burnup reactivity loss. This leads to a large overreactivity at startup of the reactor, which is potentially unsafe. One way to reduce this effect is the use of burnable absorber rods to lower the overreactivity and to flatten the power profile. The implications of such absorber rods on reactor characteristics should be studied. Another advantage of absorber rods is that the transuranics enrichment can be increased without lowering the fuel inventory. This might be needed to obtain a high enrichment for reactors with a higher thermal power than the ones considered in this study.

In general, the optimization of burning potential in the ALMR will lead to fuel inventory reduction and in-core residence time maximization. This will increase the cost effectiveness of the design. However, optimization leads also to a small cycle length, which will increase costs. Also, optimization on burning will lead to a decrease in reactor power, which will increase the cost per unit of energy produced. It is expected that reprocessing losses for the oxide fueled burner will be lower. Also, the technology for this reprocessing technique is already developed. The choice between metallic or oxide fueled burner cores for burning transuranics depends on the difference in safety behavior and the difference in cost but not on the burning capability for burning transuranics.

Chapter 4

Molten Salt Transmuter

4.1 Introduction

In chapter two, the dependence of burner capability on neutron spectrum and uranium content is discussed. An empirical relationship between enrichment and burner capability showed that reactors without uranium (or thorium) burn at the highest rate. In chapter three, the possibilities for a fast reactor burner on the basis of a practical design are presented. The advanced liquid metal reactor operated as burner still contains fertile material for economics and safety. The time to reduce the actinide inventory is long due to this fertile inventory. The time to reduce an amount equal to the inventory, the Inventory Transmutation Time, for the ALMR is equal to 42 years.

In this chapter, a thermal burner design is presented without fertile material based on an old design of Oak Ridge National Laboratory (ORNL). Both designs use a molten salt as fuel, and operate with continuous reprocessing and refueling, and use a molten salt based reprocessing technique. The usage of a molten salt fuel has many advantages:

1. By continuous refueling and reprocessing, there is no burnup reactivity loss.
2. By continuous reprocessing, the neutron absorption by fission products is reduced due to the relatively short time between production and removal of the fission products.
3. The absorption in the neutron 'poison' Xe-135 is reduced, because the solubility of noble gases in molten salts is low.

4. The molten salt reactor can be designed with a negative temperature coefficient, independent of the fuel content; fuel heating leads to a loss of fuel by expansion, which will lead to a reactivity loss when the reactor core is overmoderated.
5. A high α -activity and heat production poses many problems in aqueous reprocessing used for solid oxide fuel. These problems can be avoided by using a molten salt reprocessing technique.
6. Molten salt fuel fabrication is much simpler.

For a burner design, the burnup reactivity loss, the neutron absorption by fission products (especially for thermal reactors), the temperature reactivity feedback, and the reprocessing may pose difficult problems which can be solved by using a molten salt reactor.

Without continuous refueling, fuel without fertile material leads to large reactivity changes during a cycle because fissioned fissile material is not replaced by fissile material produced by neutron captures in fertile material. One might accommodate for this reactivity change by adding burnable poisons to the fuel at the beginning of cycle. However, the overreactivity for a transuranics based thermal reactor at the beginning of cycle is low, leading to a very short cycle length (see chapter 2).

For this different reactor and fuel concept, many questions can be asked: Is reprocessing of molten salt fuel possible and can it be operated continuously; how is the interaction of the molten salt with materials in the reactor; and how much is it going to cost? Many of these questions have been addressed by the molten salt reactor program operated by ORNL from 1947 to 1976, described in many papers and reports. In the next section, the history of the molten salt reactor development, mainly carried out by ORNL, will be presented⁶⁵.

As determined in chapter two, the optimal burner is the one which reduces the largest amount of transuranics in the shortest time to the smallest residue at a certain power level. This results in a burner without uranium, operated at the highest power density. For a molten salt reactor, the power density is limited by the characteristics of the salt and the capacity of the primary pumps which circulate the fuel salt.

In this chapter, a molten salt transmuter is designed. Normally, one would proceed by choosing the power density and the other design parameters, but in this chapter, the power density is determined as a function of three input parameters. This method is followed because the calculational method makes it impossible to take the salt power density as input parameter. The approach used allows three input parameters to be used in a systematic study. The input parameters are the total flux, the fuel volume fraction, and the fraction of transuranics in the salt. The output

parameters are the isotopic composition of the fuel salt, the salt power density, the total equilibrium critical power, the equilibrium critical core volume, the Inventory Transmutation Time, and the temperature reactivity coefficient. The equilibrium critical power and volume are defined as the power and volume at which the reactor will run at the desired flux level, fuel volume fraction, and transuranics fraction in the salt. Using these results and limits on these output parameters, a range of input parameters is determined, for which safe operation is possible. Two limits are to be imposed:

1. The power density has to be smaller than a certain value determined by the cooling system and the flow characteristics.
2. The temperature feedback coefficients should be negative.

Furthermore, the total power should be reasonable, for instance between 100 MW_t and 3000 MW_t.

The burner dimensions are determined by the neutron balance: neutron production by fission on the one side and neutron leakage and absorption on the other side. Absorption of neutrons occurs in fission products, construction material, and in components of the fuel salt including the fuel itself. The isotopic composition of the fuel salt is dependent on the design parameters and on the isotopic composition of the feed material. The flux level influences the fission product densities, whereas the neutron spectrum, mainly determined by the fuel volume fraction, influences the relative amount of neutron absorptions in the non-fuel parts of the core. The transuranics fraction in the salt influences the ratio of the neutron absorption in the actinides and the non-fuel parts of the fuel salt. Therefore, variation of these design parameters will influence the core dimension and other performance parameters of the molten salt transmuter.

Then, for one particular design, the safety characteristics are determined, especially the temperature coefficient. Also, the startup of such a reactor completely with transuranics from LWR discharges is considered. The isotopic composition of the fuel salt and the critical transuranics fraction in the fuel salt are determined. For this startup core, the safety characteristics are determined also.

For a transuranics fueled reactor, large uncertainties in the neutron data of transuranics will lead to large design uncertainties. For many nuclides, the available data is scarce, or based on calculations only. Normally, these uncertainties will be unimportant due to the large contribution to neutron absorption and fission of well-studied isotopes like U-235, U-238, and Pu-239. For a transuranics fueled reactor, however, a large uncertainty in the multiplication factor is expected. The magnitude of this uncertainty and the influence on the reactor size are estimated with adjoint calculational techniques.

4.2 History of the Molten Salt Reactor Development

Fluid fueled reactors received attention in the past because of the possibilities of continuous reprocessing and recycling. In this way, the neutron absorption in fission products could be reduced and these extra neutrons could be used for breeding new fissile material. Fluid fueled thermal reactors operated on the thorium/uranium cycle might be able to produce more fissile material than is consumed: breeding. A thermal breeder reactor has the advantage of a small fissile inventory compared to that of a fast reactor. One of these fluid fueled designs was studied in the Netherlands since 1951. A prototype reactor was the Kema Suspension Test Reactor operated on an aqueous suspension of UO_2/ThO_2 particles from 1974 to 1977⁶⁶. In 1956, research started in ORNL to design another type of fluid fueled reactor for commercial use: The molten salt reactor.

In 1960, the Molten Salt Reactor Experiment (MSRE) was started to prove that a safe, reliable, and maintainable molten salt reactor could be operated. The experiment was a 8 MW_t, graphite moderated molten salt fueled reactor, which operated on U-235, U-233, and Pu-239, from 1964 to 1969. The reactor operated without problems: the fuel salt was not damaged by irradiation, the graphite was stable, and the alloy (Hastelloy N) which was used in all equipment was resistant to the fuel salt. Noble gases were stripped from the salt by a helium spray system, which reduced xenon poisoning by a factor of 6. Also, the reprocessing of uranium by fluorination was proven to be adequate. The experiment was stopped in 1969 because it had provided all the requested information, and the funds were to be used for the development of the Molten Salt Breeder Reactor.

After the MSRE was stopped, ORNL studied on a proposal for a Molten Salt Breeder Reactor. In 1976, funds were lost to the fast breeder sodium cooled reactor program.

In recent years, the molten salt reactor has gained interest from scientists outside the US. Especially, the breeding capabilities and the operation on thorium has been studied^{67,68,69,70,71,72}. It is an alternative to the fast reactor technology. Very recently, some proposals have been made to use the molten salt reactor as a burner of transuranics^{73,74,75,76}.

The program by Furukawa in Japan is based on the program of ORNL, but its goal is the design of a small molten salt reactor, in which the power density is low and continuous reprocessing is not used except for the removal of fission gases like xenon and krypton. In the MSBR, every four years, some of the graphite moderator had to be removed, because of swelling due to radiation damage. This will be reduced at a lower power density. Continuous reprocessing is abandoned because of cost and the proliferation risk.

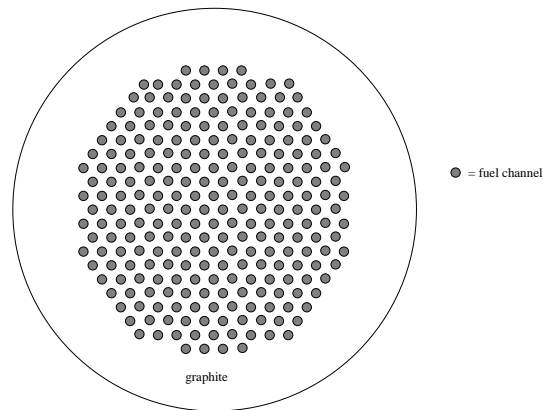


Figure 4.1: *Core map of the Molten Salt Transmuter.*

Kasma and Kazaritsky studied burner concepts based on the ORNL experience of molten salt reactors. They propose transuranics to U-233 converters^{74,75}. These designs are not of interest for this thesis, because transition to another actinide is not a solution of the actinide waste problem.

Hughes studied a transuranics fueled concept of a molten salt reactor, which uses heavy water as moderator⁷⁶. In his paper, Hughes showed that it is possible to transmute 1.3 times the transuranics inventory annually equal to an Inventory Transmutation Time of 0.77 years. This is almost two orders of magnitude less than for the ALMR designs, which had ITTs of about 42 years. Many questions remain, for instance is a salt power density of 10 GW/m³ possible (Three cubic meters produce all the electric power for the Netherlands)? We will come back to this question when we discuss the cooling system of the reactor. Another question is how to isolate the salt from the water: The only possible material available right now, is Hastelloy N which is not radiation resistant⁷⁷.

4.3 Systems Description

4.3.1 Core

The core of the Molten Salt Transmuter consists of two regions: The fuel region and the radial graphite reflector. An axial reflector is not considered. The relative fuel salt content for the fuel salt in graphite is one of the design parameters. The radius of the fuel ring is varied between 150 cm and 400 cm whereas the reflector

thickness is always 50 cm. The core height will be determined in this chapter. In figure 4.1, the core map is shown. The core consists of graphite with fuel channels with a radius of 1.7 cm.

4.3.2 Reprocessing

Reprocessing is an important part of the Molten Salt Transmuter. In this section, some of the features of the reprocessing are described. The systems described in literature are either based upon the thorium breeder reactor for which protactinium extraction is important, or for the denatured molten salt reactor, for which extraction of uranium is important. Five processes can be distinguished^{77,78}:

1. Removal of all gases by a sparging process,
2. The fluoride volatility process: UF_4 is contacted to fluorine to produce the gaseous UF_6 ,
3. The separation of protactinium by reduction in a salt-bismuth mixture,
4. The separation of the rare earths from thorium by reduction in a salt-bismuth mixture and salt-LiCl mixture,
5. Reduction of UF_6 with hydrogen to produce UF_4 .

For a Molten Salt Transmuter, the reprocessing will be different, because the only objective is to separate the fission products. Engel et al show a processing sheet for a denatured molten salt converter reactor⁷⁹. This reactor was designed to make the molten salt reactor more proliferation resistant by keeping one the actinide stream. Nothing can be said about reprocessing losses or whether reprocessing is possible with other salts. Clearly a lot of work is required to proof these processes to be feasible.

4.3.3 Materials

The most important materials are graphite, Hastelloy N, and the fuel salt. For the fuel salt, FLIBE is not suited because not more than 1% of plutonium can be added to this salt. According to Hughes in reference 76, two other salts are available to act as fuel salt:

1. The $TRUF_3$ -NaF- ZrF_4 , with the relative contents of NaF and ZrF_4 according to reference 72. So, the mole fractions are x:3.5:2.4 for $TRUF_3$:NaF: ZrF_4 .

2. The $\text{TRUF}_3\text{-NaF-KF-BeF}_2$, with relative contents of NaF, KF, and BeF_2 according to reference 75. So, the mole fractions are x:2.2:5.2:1.3 for $\text{TRUF}_3\text{:NaF:KF:BeF}_2$.

For core calculations, the density of the salt is needed as a function of the relative TRUF_3 content. To determine the temperature coefficient, the density as a function of the temperature is needed. In reference 80, a method is presented to calculate the density of a salt composition from a table of measured molar volumes at two temperatures (600 and 800 °C). Assumed was that the density in a restricted temperature range important for reactor operation is linear in temperature. Using this table, it is possible to calculate the density of every salt composition as a function of temperature. No molar volume of the TRUF_3 salt is presented. As an estimate, we will use the molar volume of the ThF_4 salt.

In figure 4.2, the density of a thorium based salt is presented as a function of the ThF_4 content. In the calculations presented in this thesis, it is assumed that the density of the thorium based salt is the same as the density of a transuranics based salt.

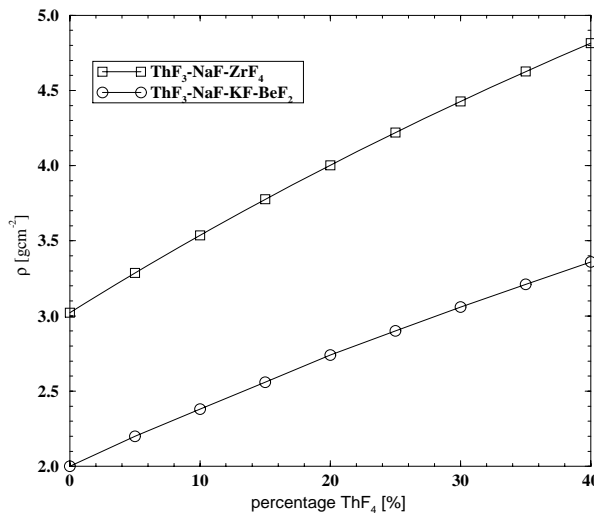


Figure 4.2: Density of $\text{ThF}_4\text{-NaF-ZrF}_4$ and $\text{ThF}_4\text{-NaF-KF-BeF}_2$ salts as a function of ThF_4 mole percentage.

This figure shows that the fuel density increases strongly with actinide content. Other important characteristics, like viscosity, heat conductivity, and heat capacity, determine the suitability of the fuel salt. The heat capacity and the heat conductivity

are decreasing with actinide percentage, and are always lower than for FLIBE for the ThF₄-NaF-ZrF₄. For the ThF₄-NaF-KF-BeF₂ salt, the heat capacity and the heat conductivity are higher than for FLIBE for percentages of ThF₄ lower than 30%. The viscosity of the salts as a function of ThF₄ mole fraction could not be calculated. This quantity has to be determined experimentally. In this study, only the data of the ThF₄-NaF-ZrF₄ salt is used representing the TRUF₄-NaF-ZrF₄ salt.

4.3.4 Cooling

This section describes the cooling of the Molten Salt Breeder Reactor. The average temperature increase of the coolant from inlet to outlet is 140 K. The heat capacity C_p is 1.4 Jg⁻¹K⁻¹, and the density is 3.3 g/cm³. So, the maximum energy production per unit of coolant volume is 647 J/cm³ and for a core height of 4 meters and a maximal flow speed of 3 m/s, the maximum power density is 0.49 GW/m³, which is the value presented by the MSBR research group⁸¹. It is hard to tell if any higher value of this maximum power density is possible, but a factor 20 as is proposed by Hughes⁷⁶ seems impossible. For this study, the maximum power density is chosen as 1 GW/m³ counting on new developments.

4.4 Calculational Methods

4.4.1 Neutron Balance

The objective of this study on the molten salt transmuted is to obtain the value of the output parameters (equilibrium critical core size, equilibrium critical power, salt power density, the inventory transmutation time, and the temperature reactivity feedback) as a function of the three input parameters (total flux, fuel volume fraction, and the transuranics content of the salt). The equilibrium critical core size is determined from the neutron balance equation, describing neutron production and loss.

To determine the equilibrium critical core size, equation 4.1 with core size V and design parameters p_i as variables is solved using the multigroup one-dimensional transport code XSDRN.

$$k(p_i, V) = k_\infty(p_i) \cdot P_{NL}(p_i, V) = 1, \quad (4.1)$$

with k_∞ the infinite multiplication factor, and P_{NL} the neutron non leakage probability. The infinite multiplication factor is equal to:

$$k_\infty = \frac{\nu \Sigma_f}{\Sigma_a^{AC} + \Sigma_c^{FP} + \Sigma_c^{PAR}} = \frac{\nu}{1 + \alpha^{AC} + \alpha^{FP} + \alpha^{PAR}}, \quad (4.2)$$

where ν is the number of neutrons emitted per fission, Σ_f is the macroscopic fission cross section, Σ_a^{AC} is the macroscopic absorption cross section of the actinides, Σ_c^{FP} is the macroscopic absorption cross section of the fission products, and Σ_c^{PAR} is the macroscopic absorption cross section of the parasitic absorbers, for instance in some elements in the salt and the graphite. The α s are the ratios of the respective macroscopic capture cross sections and the macroscopic fission cross section.

The α -values have to be calculated to determine the equilibrium critical core size. α^{FP} is calculated independently from α^{AC} and α^{PAR} . The influence of the fission products on the reactivity is included in the determination of the infinite multiplication factor of an infinite array of system cells with one pseudo fission product using the multigroup transport equation. In the next section, the method to determine α^{FP} as a function of flux level is explained

4.4.2 Calculation of Fission Product Densities

The fission products are treated independently from the actinides to simplify the calculational method. The fission products are treated in the calculation of the equilibrium critical core size as one isotope with a microscopic capture cross section with a $(1/v)$ energy dependence, with v the neutron speed. This method can be used as long as the isotopic composition of the fission products is not important.

ORIGEN-S is used to study the buildup of fission products during reactor operation; it contains data for about 800 fission products^{31,82}. Continuous reprocessing of the fission products is assumed in which all fission products are separated from the actinides. Then, ORIGEN-S solves the equation for production and loss of each fission product i :

$$\frac{dN_i}{dt} = \gamma_i \Sigma_f \phi + \sum_j (\lambda_{ji} + \sigma_{ji} \phi) N_j - N_i \sigma_i \phi - \lambda_i N_i - \frac{N_i}{T}, \quad (4.3)$$

with N_i , the density of i nuclide, γ_i the yield for this fission product, λ_{ji} is the radioactive decay constant for isotope j which decays to isotope i , σ_{ji} is a neutron cross section for isotope j which will lead to isotope i , λ_i the radioactive decay constant for isotope i , and T the mean residence time in the system. The time t of "reactor operation" in ORIGEN-S was long enough to reach equilibrium for most fission products.

The fission product densities are calculated as a function of flux and of the mean residence time. A constant production of fission products as a function of time t is obtained by taking constant Pu-239 density and flux. This is possible because

the fission product yields for all other transuranics are zero in the ORIGEN library for the molten salt reactor. We assumed that the xenon and krypton are removed from the reactor immediately when they are formed, because the noble gases are not soluble in the salt, so no neutron captures in xenon and krypton atoms occur. Then, α^{FP} is equal to:

$$\alpha^{FP} = \frac{\sum_{i=1}^N N_i \sigma_c^i}{N^{Pu9} \sigma_f^{Pu9}}. \quad (4.4)$$

Some assumptions have been made by using ORIGEN in this way and not including the fission product calculation in the neutron transport calculations of the cell:

1. The production of the fission products is independent of the actinide composition,
2. the influence of flux spectrum changes on the microscopic and macroscopic cross section for the fission products is neglected,
3. the fission product cross sections of the ORIGEN-S data files for the molten salt reactor are used.

The first assumption is due to the fact that only Pu-239 was used for fuel. This was necessary because no fission product yields for other transuranics are present in the ORIGEN-S data files for the Molten Salt Reactor. Using ORIGEN-S will lead to underestimation of the fission product densities when other transuranics are used as fuel.

A spectrum change will change the microscopic cross sections, but a change in microscopic cross section will partly be canceled out by a change in density resulting in a smaller change in the macroscopic cross section. For instance, an increase of a microscopic cross section will increase the neutron capture for that specific isotope reducing its density.

4.4.3 Calculation of the Actinide Densities

The SCALE-4.1 code system and the code EQUI were used to calculate the actinide densities. The SCALE-4.1 code system calculates the neutron spectrum and the corresponding microscopic cross sections for an infinite lattice of fuel "pins". These "pins" consist of a graphite cylinder with a central hole filled with fuel salt. EQUI is introduced in chapter 2 of this thesis and a more extensive description is given in appendix B. It calculates the actinide densities based on the microscopic cross sections. These calculations provided the ratio of macroscopic capture cross

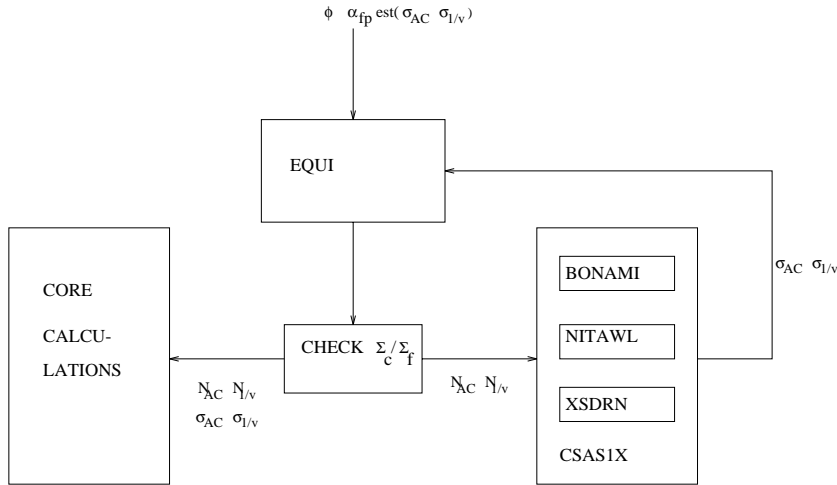


Figure 4.3: Flow schedule for the calculations on the molten salt transmuter.

section and fission cross section of all actinides. Furthermore, cell-averaged cross sections were determined, which were used to determine the equilibrium critical core size.

In figure 4.3, the flow diagram of the actinide density calculations is shown. The calculation starts with estimated one-group cross sections for the actinides and the $(1/\nu)$ -pseudo fission product, a fixed flux level, and a fixed α^{FP} dependent on the flux level. In EQUI, the actinides equilibrium densities, N_{AC} , are calculated based on the estimated actinide cross section data, the total flux level and the feed composition of transuranic material, which is spent fuel from once-through LWRs. These densities and the density of the $(1/\nu)$ -pseudo fission product, which is calculated from the microscopic cross section, the macroscopic fission cross section and the α^{FP} , are used in the cell calculation controlled by the CSASIX-module⁸³. This module generates the input for the BONAMI, NITAWL and XSDRN codes^{84,85,86}. This set of codes generates one-group cross sections, σ^{AC} and $\sigma_{1/\nu}$ (the microscopic one-group absorption cross section of the $(1/\nu)$ -pseudo fission product), which will be used to recalculate the actinide densities with EQUI and the density of the $(1/\nu)$ -pseudo fission product. This process continues until the ratio of Σ_a^{AC} and Σ_f from step to step changes less than 0.05%. The cross section of the $(1/\nu)$ -pseudo fission product is determined every step from which a new input density for the $(1/\nu)$ -pseudo fission product is calculated. The nuclear data is based on the JEF2.2 data, generated into a 172 fine-group data file by NJOY91⁸⁷.

4.4.4 Core Calculation

The equilibrium critical core size is calculated with XSDRN in the direct buckling search. In XSDRN, the core height is adjusted to obtain a critical core. The core radius is varied by hand depending whether a critical core is obtained between 150 cm and 400 cm

4.4.5 Calculation of Reactivity Coefficients

Temperature increase will lead to expansion of both the graphite and the fuel salt. Fuel expansion reduces the in-core fuel amount and the fuel-moderator ratio. Graphite expansion will be a very small effect compared to the fuel expansion effect because the graphite expansion coefficient is small ($1.3 \cdot 10^{-6} \text{K}^{-1}$).

The effects of a fuel temperature increase from operating temperature (908K) to a temperature of 1000 K have been determined with a direct calculation of the temperature effect (Doppler effect) and with a direct calculation of the fuel density decrease. The influence of these effects on the infinite multiplication factor were determined and do not include the effect of increased neutron leakage, which might be important especially for the fuel density effect.

The effects of a graphite temperature increase have only been determined for one case with a direct calculation of the influence on the infinite multiplication factor for radial expansion and the influence on the effective multiplication factor for axial expansion. The reactivity coefficients for these effects were about a factor 20 and 200 smaller than the effects due to a fuel temperature increase and are not considered in the rest of this chapter.

4.5 Design of the Molten Salt Transmuter

4.5.1 Role of Fission Products

The results of the ORIGEN-S calculations as function of thermal flux, and for four mean residence times are presented in figure 4.4.

Clearly, the ratio of Σ_c^{FP} and Σ_f increases with flux level according to equation 4.3. When the production of a certain fission product i by decay or neutron capture of other isotopes is neglected, the solution of this equation in equilibrium ($dN/dt = 0$) is:

$$N_i(t \rightarrow \infty) = \frac{\gamma_i \Sigma_f \phi}{\sigma_i \phi + \lambda_i + 1/T}, \quad (4.5)$$

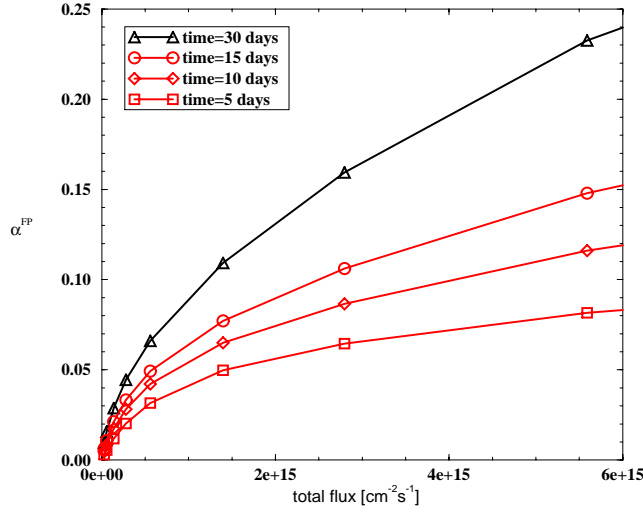


Figure 4.4: The ratio of Σ_c^{FP} and Σ_f , α^{FP} , as a function of total flux and the mean residence time.

and the ratio α_i^{FP} for this isotope is given by:

$$\alpha_i^{FP} = \frac{\gamma_i}{1 + \frac{\lambda_i + 1/T}{\sigma_i \phi}}. \quad (4.6)$$

The density will increase with increasing flux to a constant value equal to $\gamma_i \Sigma_f / \sigma_i$. α^{FP} is a summation of α_i^{FP} of all fission products. The function α_i^{FP} has a decreasing positive slope with increasing flux for all isotopes. The influence of a smaller mean residence time T is a decrease in α^{FP} .

It is noted that the noble gases were not taken into account. For a thermal flux of $10^{14} \text{ cm}^{-2} \text{ s}^{-1}$, α^{NG} for the noble gases is about two times higher than α^{FP} without the noble gases. The maximum value for α^{NG} is about 0.12. These results are similar to the results by Davidson⁸⁸, who calculated the fission product densities for an accelerator-based transmutation system.

In table 4.1, the ten most important fission products for neutron capture are presented for three flux levels for the ten day reprocessing time. For reference, the ten most important fission products after three years in a normal LWR core are presented. These results were obtained with ORIGEN-S as well. For low flux levels, the neutron capture for the molten salt transmuter is dominated by Rh-105,

whereas for a normal LWR, Xe-135 is most important for neutron capture in fission products. To explain the behavior of Rh-105 and Sm-149, we will make use of equation 4.6. Rh-105 is short-lived and has an extremely high capture cross section, whereas Sm-149 is stable and has an extremely high capture cross section as well. So, Sm-149 is at its maximum value for relatively low fluxes due to the decay constant equal to zero and the high cross section. The relative mass of Sm-149 will therefore decrease with increasing flux, because other isotopes will increase with flux. For instance, Rh-105 is for low fluxes not at its maximum value and will increase.

Table 4.1: Ten most important fission products for neutron capture (C) for three flux levels and for a normal LWR after three years in core.

flux	$3 \cdot 10^{13} \text{ cm}^{-2} \text{ s}^{-1}$		$3 \cdot 10^{14} \text{ cm}^{-2} \text{ s}^{-1}$		$3 \cdot 10^{15} \text{ cm}^{-2} \text{ s}^{-1}$		LWR	
rank	Nuclide	C [%]	Nuclide	C [%]	Nuclide	C [%]	Nuclide	C [%]
1	Rh-105	43.1	Rh-105	53.1	Rh-105	49.1	Xe-135	19.9
2	Sm-149	31.2	Sm-149	22.3	Sm-149	10.9	Rh-103	14.4
3	Sm-151	8.9	Sm-151	9.6	Sm-151	7.7	Nd-143	10.8
4	Gd-157	8.1	Eu-155	3.2	Sm-152	4.1	Sm-149	8.3
5	Eu-155	2.9	Gd-157	2.4	Eu-155	2.9	Xe-131	8.0
6	Cd-113	1.1	Sm-152	1.1	Pm-147	2.7	Cs-133	7.5
7	Pm-147	0.7	Pm-147	1.1	Pm-149	2.6	Pm-147	6.8
8	Sm-152	0.5	Cd-113	1.1	Ag-109	2.3	Sm-152	5.5
9	Ag-109	0.5	Ag-109	0.8	Nd-143	1.8	Sm-151	4.8
10	Pm-149	0.5	Pm-149	0.8	Eu-153	1.6	Eu-153	4.0

4.5.2 Flux Dependence

In this section, the results of a variation in flux level are presented. The other input parameters were constant. The TRU fraction in the salt was 20%, the fuel volume fraction was 2.3%, and the mean residence time was 10 days. Furthermore, it was assumed that the out-of-core residence time could be neglected for the actinides.

The ratio of the capture to fission cross section for the actinides (lowest curve in figure 4.5) is a continuous decreasing function with flux level, ranging between 2.0 and 1.5. The most pronounced decrease in α^{AC} is for low flux. The densities of the short-lived isotopes increase linearly with flux as long as the product of flux and microscopic absorption cross section is much smaller than the decay constant. This is similar to the result for the fission products explained in section 4.5.1. Therefore, the relative mass of the short-lived isotopes and their activation

products, Cm-245 in particular, increase with flux level. The ratio of fission to capture cross section is higher for Cm-245 than for the plutonium isotopes.

In figure 4.6, this phenomenon is shown. The higher actinides, activation products of short-lived isotopes, increase with flux level, whereas the plutonium isotopes decrease with flux level.

The lower content of the absorbing plutonium isotopes (Pu-239, Pu-240, and Pu-241) causes a spectral softening because these isotopes have high thermal cross sections. Also, it causes a decrease in selfshielding for these isotopes. The microscopic one-group absorption cross sections increase due to the higher thermal flux.

In figure 4.5, the ratio of the total capture and fission cross section including the actinides, fission products, and the parasitic absorptions is presented. The minimum value depends strongly on the mean residence time and is between a flux of $5 \cdot 10^{14} \text{ cm}^{-2} \text{ s}^{-1}$ and $10^{16} \text{ cm}^{-2} \text{ s}^{-1}$. A mean residence time of 10 days was assumed for the equilibrium critical core volume calculations.

In figure 4.7, the equilibrium critical core volume for a mean residence time of 10 days is presented as determined with the code system. The minimal equilibrium critical core volume is for a flux of $5 \cdot 10^{15} \text{ cm}^{-2} \text{ s}^{-1}$. This is somewhat higher than the minimum in α^{tot} due to the increase in ν caused by the increased fission rate of Cm-245 with increasing flux level. First, the equilibrium critical core volume decreases with flux due to the decrease in α^{AC} , which is for higher fluxes compensated by the increase in α^{FP} . For fluxes lower than $10^{14} \text{ cm}^{-2} \text{ s}^{-1}$, no equilibrium critical core volume could be obtained.

In figures 4.8 and 4.9, the power density and the equilibrium critical reactor power of the burner are presented. The power density increases with flux level and is for fluxes higher than $10^{15} \text{ cm}^{-2} \text{ s}^{-1}$ higher than the limit of 1 GW/m^3 . Due to the increased equilibrium critical core volume and the higher flux, the power increases strongly above $3 \cdot 10^{15} \text{ cm}^{-2} \text{ s}^{-1}$.

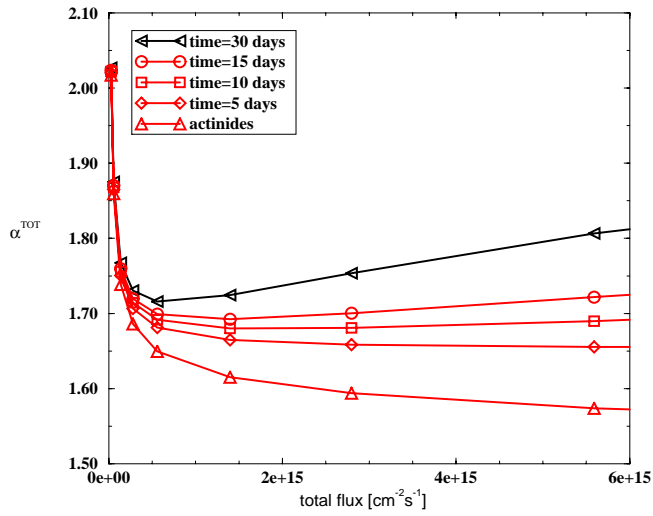


Figure 4.5: The α_{tot} as a function of flux level.

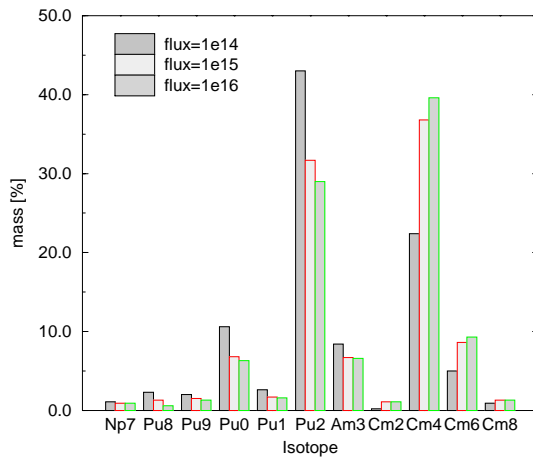


Figure 4.6: Relative isotopic mass of some actinide isotopes for three flux levels.

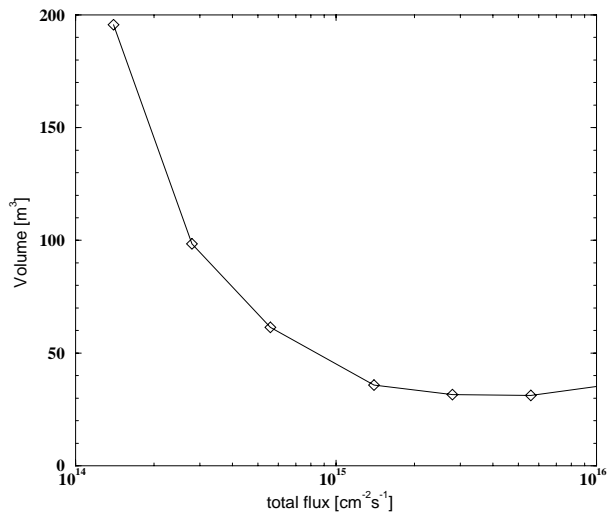


Figure 4.7: *The equilibrium critical core volume as a function of flux level.*

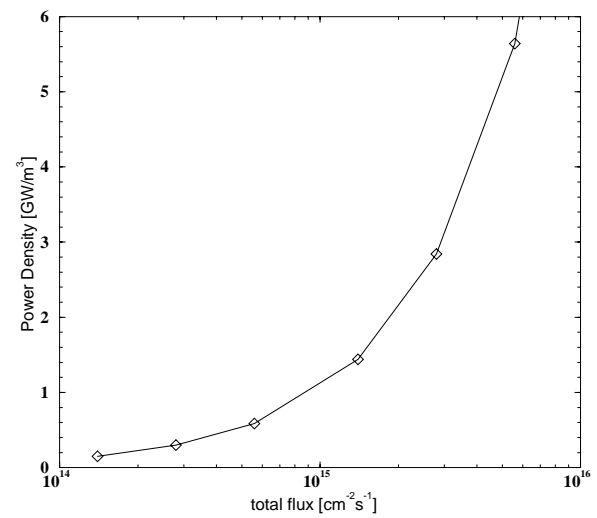


Figure 4.8: *The average power density in the fuel salt as a function of flux level.*

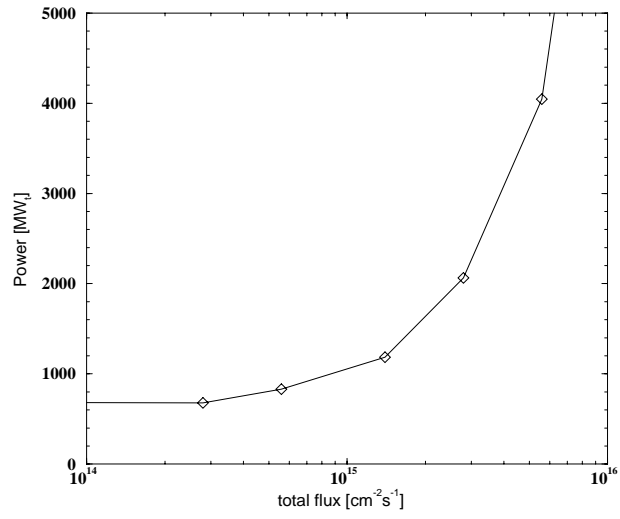


Figure 4.9: *The equilibrium critical thermal reactor power as a function of flux level.*

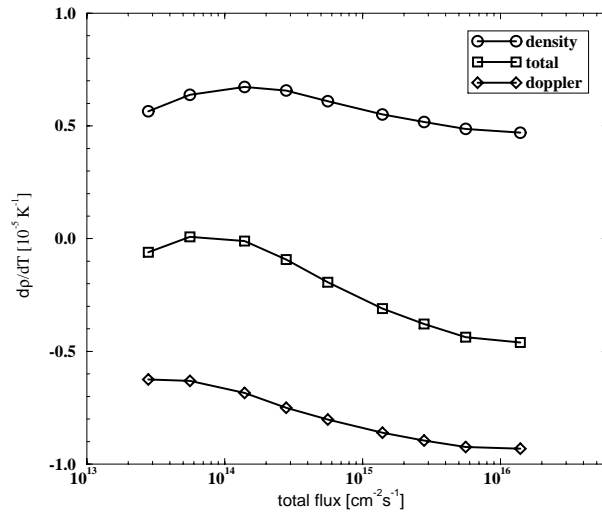


Figure 4.10: *The Doppler coefficient, the fuel expansion reactivity coefficient, and the total fuel temperature reactivity coefficient as function of flux level.*

In figure 4.10, the fuel temperature reactivity feedback coefficients are presented as a function of the total flux level. The Doppler coefficient is negative and its absolute value is increasing with flux. It is negative due to the increase in absorption in the fissionable Pu-242 and Cm-244 in particular. The absolute value increases with flux level due to the increased influence of Cm-245. This isotope has a much lower increase of resonance absorption with increasing temperature than the plutonium isotopes it is replacing. The temperature reactivity coefficient for the fuel density is positive, and for low flux increasing with flux, and for higher flux values decreasing with flux. The differences are too small to come up with a clear reason for this behavior, because too many isotopes have changing densities. The total reactivity coefficient is positive for low fluxes, and negative for flux values higher than $10^{14} \text{ cm}^{-2} \text{ s}^{-1}$.

In conclusion, for a fuel volume fraction of 2.3%, the total flux should be in the range from $10^{14} \text{ cm}^{-2} \text{ s}^{-1}$ to $10^{15} \text{ cm}^{-2} \text{ s}^{-1}$, where the largest reactivity feedback is for a flux value of $10^{15} \text{ cm}^{-2} \text{ s}^{-1}$.

4.5.3 Fuel Volume Fraction Dependence

For a total flux value of $3 \cdot 10^{15} \text{ cm}^{-2} \text{ s}^{-1}$, a transuranics fraction of 20%, and a mean residence time of 10 days, the dependence of the burner performance on fuel volume fraction has been studied. The fuel volume fraction has been changed by varying the pitch between fuel cells, while maintaining the same radius for the fuel channels of 1.7 cm. In the following graphs, the results are presented. In figure 4.11, the relative masses of some of the most important actinides are presented for three fuel volume fractions. The relative mass of the plutonium isotopes increases with increasing fuel volume fraction due to the decreased cross sections caused by spectrum hardening. Therefore, the feed composition is more important.

Figure 4.12 shows the equilibrium critical core volume and the equilibrium critical salt volume of the molten salt transmuter as a function of fuel volume fraction. The decrease in equilibrium critical core volume is caused by two effects:

- 1 Relative decrease of absorptions in graphite,
- 2 Spectrum hardening.

Both effects are caused by the increase of absorptions in the fuel. The influence of fuel volume fraction above 4% on equilibrium critical core volume is small. The neutron spectrum in the fuel of the burner is similar to the spectrum of a fast reactor for fuel fractions above approximately 10%. Up to a fuel volume fraction of 6%, the decrease in equilibrium critical core volume is mainly caused by the reduced absorption in graphite relative to that of fuel. Above 10%, the decrease in equilibrium critical core volume is mainly caused by the spectrum hardening. The total equilibrium critical salt volume has a minimum value at 4% fuel volume

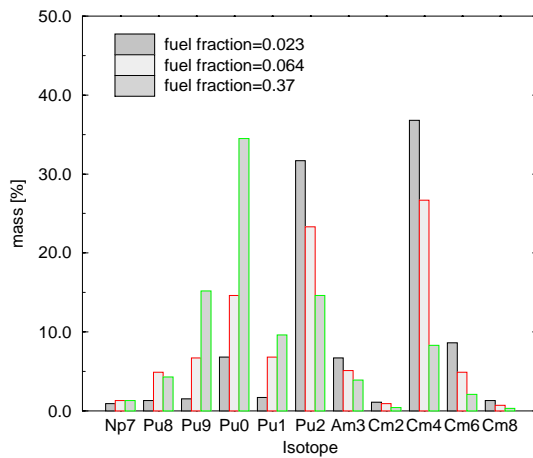


Figure 4.11: *Relative isotopic mass of the actinide isotopes for three fuel volume fractions.*

fraction. Above this value, the increase in fuel volume fraction is stronger than the decrease in equilibrium critical core volume. Up to a fuel volume fraction of 4%, the decrease in equilibrium critical core volume is much stronger than the increase in fuel volume fraction.

In figure 4.13 and 4.14, the power density and the equilibrium critical reactor power are plotted as function of the fuel volume fraction. The power density decreases continuously with fuel volume fraction due to the decrease in macroscopic fission cross section. Due to spectrum hardening, the microscopic fission cross section decreases. The equilibrium critical reactor power decreases strongly with fuel volume fraction until a fraction of 4% due to the strong decrease in equilibrium critical core volume. For higher fuel volume fractions, the decrease in power density and the increase in salt volume cancel out and the equilibrium critical reactor power is about 1600 MW_t.

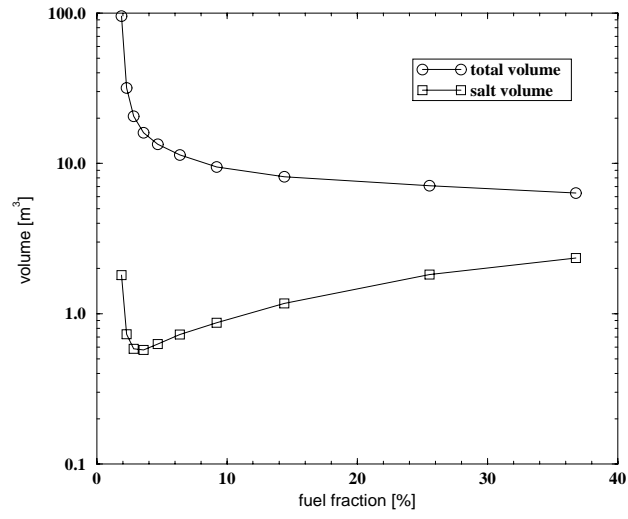


Figure 4.12: *The equilibrium critical core volume as a function of fuel volume fraction.*

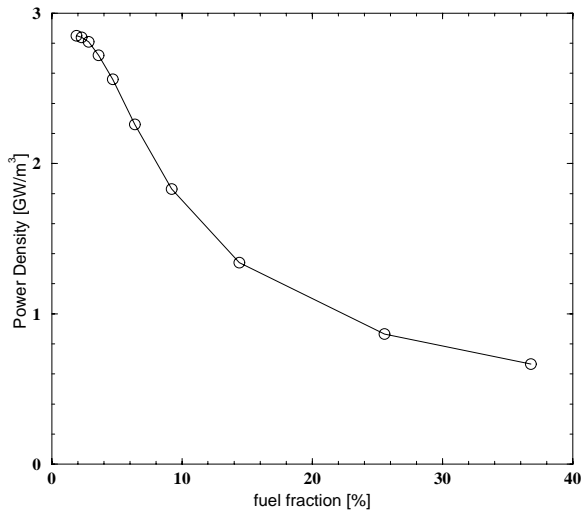


Figure 4.13: *The average power density in the fuel salt as a function of fuel volume fraction.*

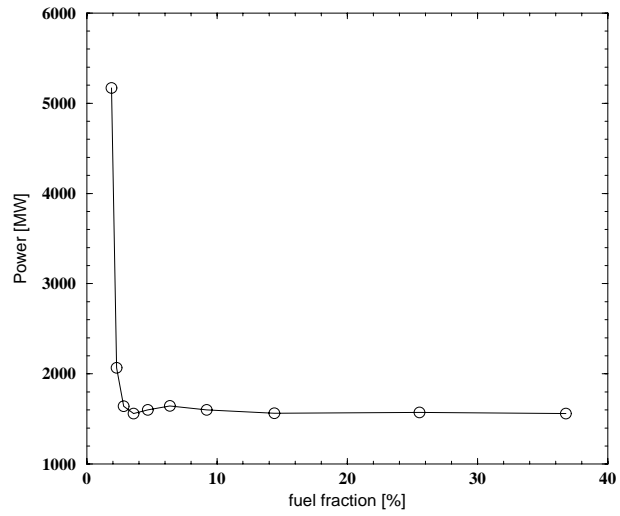


Figure 4.14: *The equilibrium critical reactor power as a function of fuel volume fraction.*

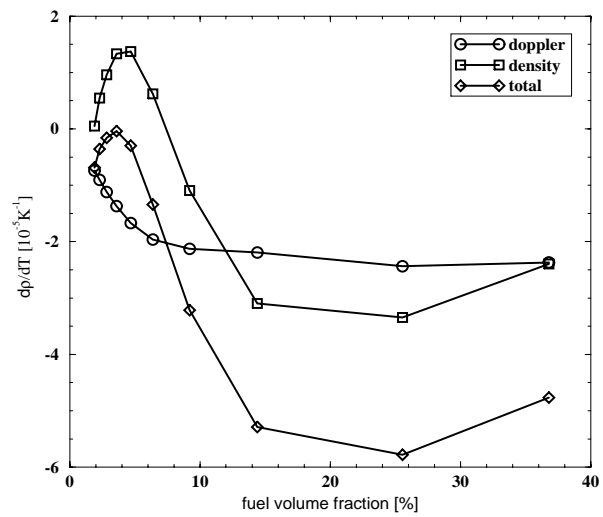


Figure 4.15: *The Doppler coefficient, the fuel expansion reactivity coefficient, and the total fuel temperature reactivity coefficient as function of fuel volume fraction.*

In figure 4.15, the fuel temperature reactivity feedback coefficients are presented as a function of the fuel volume fraction. The Doppler coefficient is negative and its absolute value is increasing with fuel volume fraction. This is caused by the decrease of the resonance escape probability with reduced moderation, which leads to an increased influence of the resonances and thus the Doppler effect.

Three regions can be seen in the graph of the temperature reactivity coefficient for the fuel density as a function of the fuel volume fraction. Below a fuel volume fraction of 2%, the temperature reactivity coefficient is negative, which means that the reactor is overmoderated. For fuel volume fractions between 2% and 7%, the temperature reactivity coefficient for fuel density is positive, which means that the reactor is undermoderated. And for fuel volume fractions larger than 7%, the reactivity coefficient is negative. In this case, we can not speak of overmoderated, because the reactor behaves effectively as a fast reactor.

The temperature reactivity coefficient for the fuel density is increasing for low fuel volume fractions due to the decreased influence of the absorptions in graphite. That it is decreasing for higher fuel volume fractions shows that the reactor more or less is operating as a fast reactor. A decrease in fuel density leads to an increased thermalization and a softer spectrum. A softer spectrum leads to a decrease in the infinite multiplication factor due to the decrease in the number of fissions per absorption for both the fissile and the fissionable isotopes. The total temperature reactivity coefficient is always negative, with its maximum at 4%, for which the reactivity coefficient is almost zero.

In conclusion, an increase in fuel volume fraction leads to a decrease in power density of maximally a factor of three. The temperature reactivity coefficient has a maximum value at 4% and is increasingly negative for higher fuel volume fractions.

4.5.4 Transuranics Salt Fraction Dependence

The third parameter which can be varied is the TRUF_3 fraction of the salt. For a total flux value of $3 \cdot 10^{15} \text{ cm}^{-2} \text{ s}^{-1}$, a fuel volume fraction of 2.3%, and a mean residence time of 10 days, the dependence of the transuranics fraction in the salt has been studied. The salt density is dependent on the transuranics fraction according to figure 4.2. In figure 4.16, the power density is presented as a function of the transuranics salt fraction. The power density increases with the transuranics salt fraction due to the increased density of transuranics in the salt. One would expect the power density to be linearly dependent on this fraction, but this is not the case. The thermal flux decreases with increasing transuranics salt fraction due to the higher macroscopic absorption cross section of the fuel. Due to this decrease in thermal flux, the microscopic fission cross section decreases with increasing

transuranics salt fraction, which reduces the power density. Therefore, the power density increases with increasing transuranics salt fraction with a decreasing slope.

In figure 4.17, the equilibrium critical reactor power is presented as a function of the transuranics salt fraction. The equilibrium critical reactor power decreases with increasing transuranics salt fraction due to the relative decrease in absorption in the non-actinide salt isotopes and the graphite.

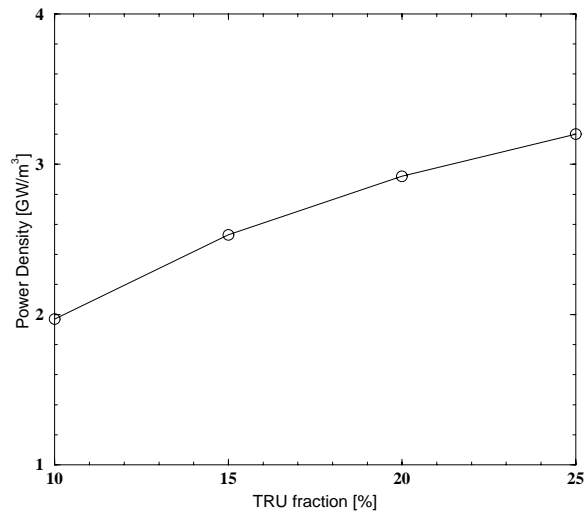


Figure 4.16: *The average power density in the fuel salt as a function of transuranics salt fraction.*

In figure 4.18, the fuel temperature reactivity feedback coefficients are presented as a function of the transuranics fraction. The Doppler coefficient is negative and constant with transuranics fraction. The temperature reactivity coefficient for the fuel density is negative for low transuranics fractions and increasing continuously with transuranics fraction. For transuranics fractions higher than 11%, it is positive. It is increasing with transuranics fractions due to reduced influence of the absorptions in graphite. The total temperature reactivity coefficient is always negative.

In conclusion, reducing the transuranics fraction in the salt reduces power density, but it increases equilibrium critical reactor power considerably. The temperature reactivity coefficient is negative and its absolute value is reduced by a factor of two by increasing the transuranics fraction from 10% to 20%.

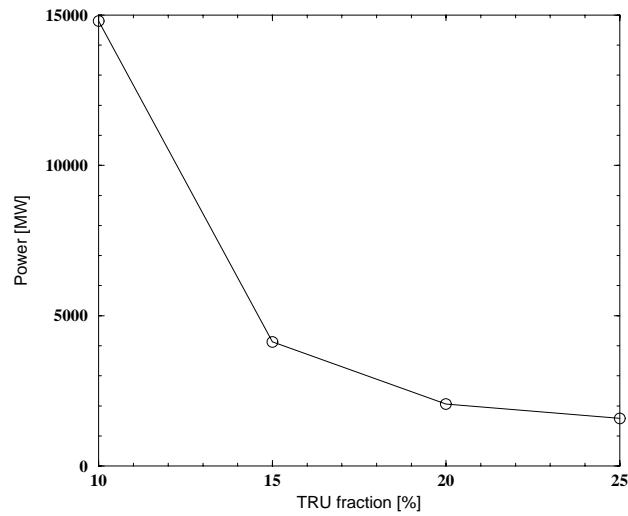


Figure 4.17: *The equilibrium critical reactor power as a function of transuranics salt fraction.*

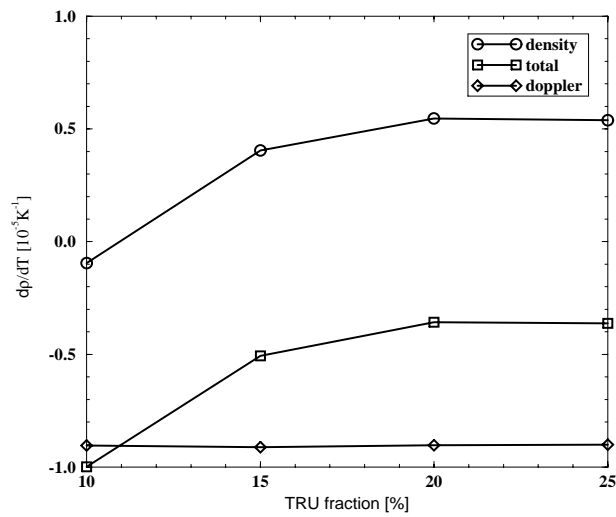


Figure 4.18: *The Doppler coefficient, the fuel expansion reactivity coefficient, and the total fuel temperature reactivity coefficient as function of transuranics fraction.*

4.5.5 Startup of the Molten Salt Transmuter

The startup procedure of the Molten Salt Transmuter is to add slowly transuranics from LWR discharges to the salt without transuranics. The reactor will start producing power when the equilibrium critical concentration is reached. This concentration is determined assuming that no fission products are present in the salt and that the isotopic composition of the transuranics in the salt is equal to that of LWR discharges for a core volume of 50 m^3 and a fuel volume fraction of 2.3%. Then, the critical TRUF_3 fraction in the fuel salt is equal to 0.1%. The total flux value and the salt power density will be determined by the power subtracted from the core.

For the Molten Salt Transmuter with startup concentrations, the reactivity effects are determined. These are:

1. the Doppler coefficient is equal to $+1.1 \cdot 10^{-5} \delta k/K$,
2. the fuel expansion coefficient is equal to $-6.4 \cdot 10^{-5} \delta k/K$,
3. and the net reactivity effect is equal to $-5.3 \cdot 10^{-5} \delta k/K$ assuming that the reactivity effects of graphite expansion are negligible.

The Doppler coefficient is rather positive due to the large content of Pu-239. For the equilibrium core, the effect is negative due to the large content of fissionable isotopes like Pu-240. On the other hand, the fuel expansion coefficient is negative, because the reactor is overmoderated due to the small percentage of transuranics in the fuel salt.

After startup, other actinides and fission products will buildup, which will increase the need for a higher transuranics content in-core. The Doppler coefficient will decrease and eventually become negative. The fuel expansion coefficient will increase and become positive. Overall, the net reactivity effect of a temperature increase might remain negative in going from startup concentration to equilibrium concentration, but this is not clear on beforehand.

For other flux values and fuel volume fractions, the effects might be different, although we expect that the enrichment and the reactivity coefficients will be quite similar at startup. For higher fuel volume fractions, the fuel density coefficient is negative for equilibrium concentrations too. Therefore, we expect that the total temperature coefficient will be negative from startup to equilibrium operation.

4.5.6 Discussion of the Results

Normally, one would design a reactor based on a certain power density. In this chapter, a different approach is followed, because our set of codes is not able to

work with a fixed power density. This approach has the advantage to show clearly the dependencies of the reactor design on three parameters: The flux level, the fuel volume fraction, and the transuranics salt fraction. The power density in the salt is limited to 1 GW/m^3 . Power density can be reduced by reducing the total flux value (in practice by increasing the salt volume), by increasing the fuel volume fraction, and by reducing the transuranics fraction in the salt. However, increasing the fuel volume fraction will lead to an increase of the fast flux above 50 keV which damages the graphite. For the MSBR, the graphite has to be renewed every four years at a fast flux of $4 \cdot 10^{14} \text{ cm}^{-2} \text{ s}^{-1}$ ⁸¹.

For the Molten Salt Transmuter at a power density of 1 GW/m^3 , the Inventory Transmutation Time is between five and ten years, which is a significant reduction compared to about 42 years for the ALMR. The minimal reactor power is about 800 MW_t assuming that all noble gases are removed from the core instantaneously. When some of the xenon remains in-core, the equilibrium critical core volume and reactor power might be considerably larger.

The main concern for this design is safety. At startup, the reactor is overmoderated due to the small transuranics salt fraction, but at equilibrium, the reactor will be undermoderated for fuel volume fractions between 2% and 7%. For fuel volume fractions smaller than 2%, the equilibrium critical reactor power and reactor volume is very large, which seems not practical. So, the fuel volume fraction should be larger than 7%.

4.6 Influence of Uncertainty in Actinide Cross Sections

4.6.1 Adjoint Calculational Method

The Molten Salt Transmuter is a reactor which operates only on transuranics. Normally, a main isotope in a reactor core would be U-238, for which the cross sections are well known. For this transmuter, U-238 is not present at all. Cross sections of some important transuranics are not well known. Therefore, the uncertainty in the core calculations is expected to be high⁸⁹. In this section, the uncertainty in the equilibrium critical core size due to uncertainties in cross sections is studied using the adjoint method. This method is used to determine the influence of uncertainties on the multiplication factor, which can be translated to the equilibrium critical core size. By using the adjoint method, the influence of uncertainties in all cross sections can be determined by solving the adjoint equation.

The problem for the calculations including density and reactivity determination is that these are not determined by one calculation, but by two. First, the densities

are calculated, and second, the multi-group flux and the multiplication factor are determined. So, an uncertainty in a cross section, translates into uncertainty in density, which together with the uncertainty in the cross section translates into uncertainty in the multiplication factor.

The nuclide density is calculated according to the matrix equation:

$$\mathbf{A}\underline{N} = \underline{b} \quad (4.7)$$

where \mathbf{A} the transition matrix, \underline{N} the nuclide density vector, and \underline{b} the feed vector which is linear with reactor power. Suppose a variation in one element α_i of the transition matrix. Then, the derivative of the matrix equation to α_i becomes:

$$\frac{d}{d\alpha_i}(\mathbf{A}\underline{N} - \underline{b}) = \frac{d}{d\alpha_i}\mathbf{A}\underline{N} = \frac{\partial\mathbf{A}}{\partial\alpha_i}\underline{N} + \mathbf{A}\frac{\partial\underline{N}}{\partial\alpha_i} = 0 \quad (4.8)$$

The equation adjoint to equation 4.7 reads:

$$\mathbf{A}^*\underline{N}_j^* = -\frac{\partial R_j}{\partial\underline{N}}, \quad (4.9)$$

where \mathbf{A}^* is the adjoint of \mathbf{A} , equal to the transposed, \underline{N}_j^* is the adjoint function which meaning depends on the right-hand side of equation 4.9, and R_j is the response function, which is in this case the density of isotope j. To determine the meaning of the adjoint \underline{N}_j^* , we take the inner product of \underline{N}_j^* and equation 4.8 and the inner product of \underline{N} and equation 4.7 and subtract the results. Then, we arrive at:

$$\langle \underline{N}, \frac{\partial R_j}{\partial\underline{N}} \rangle = \langle \underline{N}_j^*, \underline{b} \rangle \quad (4.10)$$

So, \underline{N}_j^* is the contribution to the response function R_j per unit of feed.

To obtain a relation between the response function and the uncertainty in α_i , we progress by taking the inner product of \underline{N}_j^* and equation 4.8 and the inner product of $\partial\underline{N}/\partial\alpha_i$ and equation 4.9 and subtract the results:

$$\begin{aligned} \langle \underline{N}_j^*, \frac{\partial\mathbf{A}}{\partial\alpha_i}\underline{N} \rangle + \langle \underline{N}_j^*, \mathbf{A}\frac{\partial\underline{N}}{\partial\alpha_i} \rangle - \langle \mathbf{A}^*\underline{N}_j^*, \frac{\partial\underline{N}}{\partial\alpha_i} \rangle \\ - \langle \frac{\partial R_j}{\partial\underline{N}}, \frac{\partial\underline{N}}{\partial\alpha_i} \rangle = 0 \end{aligned} \quad (4.11)$$

and use $\langle \underline{N}_j^*, \mathbf{A}\frac{\partial\underline{N}}{\partial\alpha_i} \rangle = \langle \mathbf{A}^*\underline{N}_j^*, \frac{\partial\underline{N}}{\partial\alpha_i} \rangle$ to obtain:

$$\langle \underline{N}_j^*, \frac{\partial\mathbf{A}}{\partial\alpha_i}\underline{N} \rangle - \langle \frac{\partial R_j}{\partial\underline{N}}, \frac{\partial\underline{N}}{\partial\alpha_i} \rangle = 0 \quad (4.12)$$

The differential of the response function R_j to α_i can be written as:

$$\frac{dR_j}{d\alpha_i} = \left(\frac{\partial R_j}{\partial \underline{h}}\right)^T \frac{d\underline{h}}{d\alpha_i} + \left(\frac{\partial R_j}{\partial \underline{N}}\right)^T \frac{d\underline{N}}{d\alpha_i} + \frac{\partial R_j}{\partial \phi} \frac{d\phi}{d\alpha_i} \quad (4.13)$$

where \underline{h} is the "realization function" which selects the appropriate nuclides i for the response function when h_i is one. So, the first term represents the direct effect of change of α_i on the response function, which is zero when the response function is the density itself. The last term is the direct influence of flux on the response function, which will be zero for the response functions considered in this section. So, using equation 4.12, equation 4.13 becomes:

$$\frac{dR_j}{d\alpha_i} = \langle \underline{N}_j^*, \frac{\partial \mathbf{A}}{\partial \alpha_i} \underline{N} \rangle . \quad (4.14)$$

Equation 4.14 gives the relation between an uncertainty in an element α_i of the transition matrix and the uncertainty in the response function R_j . Using first-order Taylor expansion, this uncertainty can be expressed by⁹⁰:

$$\frac{\Delta R_j}{R_j} \approx S_{ij} \frac{\Delta \alpha_i}{\alpha_i}, \quad (4.15)$$

where S_{ij} is the relative sensitivity coefficient given by:

$$S_{ij} = \frac{\alpha_i}{R_j} \langle \underline{N}_j^*, \frac{\partial \mathbf{A}}{\partial \alpha_i} \underline{N} \rangle . \quad (4.16)$$

In this section, the response function R_j is the density of isotope j . Then, the fractional mean squared error $FMSE$ of k_∞ due to uncertainties in the cross sections of all isotopes is determined with the uncertainty in the densities by:

$$FMSE^2 = \sum_{i=1}^N \left(\frac{k_\infty - k_\infty(\Delta \alpha_i, \underline{\Delta N}(\alpha_i))}{k_\infty} \right)^2 . \quad (4.17)$$

4.6.2 Method Verification

The adjoint method is verified by comparing the results of a direct and an adjoint calculation of the influence of a variation in one cross section, in this case, the capture cross section of Pu-239. The density changes for the forward calculations are obtained by comparing the results with a set of cross sections for the Molten Salt Transmuter and the results with the same set except for a 10% increase of the

Pu-239 capture cross section. The result for the adjoint calculation are obtained using equation 4.15 for a 10% uncertainty in the capture cross section of Pu-239.

Table 4.2 shows that the results for the forward calculation and the adjoint calculation are in reasonable agreement. The differences are caused by the first-order approximation used in deriving equation 4.15.

The adjoint calculations overestimate the changes in densities by about 3%, the change in k_{∞} is overestimated by 1.4%. Note that an increase in the capture cross section of Pu-239 leads to a decrease in Pu-239 density and an increase of all other densities.

Table 4.2: *Nuclide density changes for the forward calculation and adjoint calculation of a 10% increase of the capture cross section for Pu-239.*

Isotope	change [%]		relative difference [%]
	Forward	Adjoint	
Pu-239	-3.51	-3.62	3.1
Pu-240	2.86	3.01	5.2
Pu-241	2.47	2.59	4.9
Pu-242	1.82	1.87	2.7
Cm-244	1.69	1.73	2.4
Cm-246	1.69	1.76	2.4
k_{∞}	-1.43	-1.45	1.4

4.6.3 Reactivity and Core Size

Two sets of cross section uncertainties were applied to the calculation of the uncertainty in the multiplication factor. The first set was the low uncertainty case with 5% uncertainties in the cross sections of the uranium and plutonium isotopes and 10% for all other actinides. The high uncertainty case used 10% for the uranium and plutonium isotopes and 50% for all other actinides. The influences of uncertainties in cross sections on the infinite multiplication factor are presented in table 4.3 per isotope for the most important isotopes. The signs of the presented numbers are related to a cross section increase.

In going from the low uncertainty set to the high uncertainty set, the uncertainties in k_{∞} are about a factor of two higher for the plutonium isotopes, but much higher than five for other isotopes. This is probably due to the high uncertainties which invalidates the first-order perturbation approximation. Clearly, this is the case for the uncertainty calculation due to fission in Cm-245. A higher fission cross section should always have a positive reactivity effect, but for a five times

higher uncertainty the reactivity effect is negative, because the Cm-245 density is decreased linearly, which means that for a 50% increase in fission cross section the density is almost halved. For such a large density effect, the first-order approximation is invalid.

In table 4.4, the fractional mean squared errors are presented for the two sets. The results of the direct variation, the influence on k_{∞} due to the change in cross section, and the indirect variation, the influence on k_{∞} due to the change in isotope densities, are presented also. The fractional mean squared error $FMSE$ due to the direct and indirect effect are approximately equal, but much higher than the total fractional mean squared error. This is due to the fact that the indirect effect partly cancels out the direct effect. For instance, an increase in the capture cross section of Pu-239 causes the density of Pu-239 to decrease, and therefore the effect of the increase in cross section on k_{∞} is partly canceled out as is shown in table 4.2. The uncertainty in the equilibrium critical core volume due to the uncertainty in the k_{∞} can be determined with the relation between volume and the effective multiplication factor.

Table 4.3: *Influence of uncertainties in cross sections on k_{∞} for the low and high uncertainty set for the most important isotopes.*

Isotope	$\Delta k/k$ [%]			
	Low Uncertainty		High Uncertainty	
	Capture	Fission	Capture	Fission
Pu-239	-0.73	+0.72	-1.43	+1.38
Pu-241	-0.68	+0.65	-1.34	+1.22
Am-243	+0.05	+0.02	+1.61	+0.09
Cm-244	+0.02	+0.11	+1.06	+0.48
Cm-245	-0.22	+0.12	-1.05	-1.47

The effective multiplication factor is the product of k_{∞} and the non-leakage probability P_{NL} . According to one-group diffusion theory, this probability is equal to¹¹:

$$P_{NL} = \frac{1}{1 + L^2 B_g^2}, \quad (4.18)$$

where L is the diffusion length. The geometrical buckling B_g^2 for a bare cylindrical core with core height H and core radius R is given by¹¹:

$$B_g^2 = \left(\frac{\pi}{H}\right)^2 + \left(\frac{\nu_0}{R}\right)^2, \quad (4.19)$$

where ν_0 , equal to 2.405, is the smallest zero of the zeroth order Bessel function¹¹. We neglected the extrapolation length to be added to the height and radius. This

Table 4.4: Influence of uncertainties in cross sections on k_{∞} for the low and high uncertainty set for the most important isotopes.

Variation	FMSE [%]	
	Low Uncertainty	High Uncertainty
Direct	2.4	8.3
Indirect	1.8	7.3
Total	1.4	3.9

extrapolation length accounts for the fact that the flux at the core boundary is not exactly zero and is equal to $2D$, with D the diffusion coefficient equal to about 1 cm for graphite in a purely thermal spectrum ¹¹.

R and H are inversely proportional to B_g , and the volume of a bare cylindrical core is inversely proportional to the third power of B_g ¹¹. For an effective multiplication factor of one, the relation between B_g and k_{∞} is:

$$B_g = \frac{1}{L}(k_{\infty} - 1)^{1/2}. \quad (4.20)$$

If the uncertainty in the diffusion length due to uncertainties in cross sections is neglected, the uncertainty in the equilibrium critical core volume due to Δk is equal to:

$$\frac{V \pm \Delta V}{V} \approx \left(1 \pm \frac{\Delta k}{k_{\infty} - 1}\right)^{-3/2}. \quad (4.21)$$

This result is used to calculate the uncertainty in the volume for the Molten Salt Transmuter. The influence of the reflector is neglected and a k_{∞} of 1.1 was assumed, which is the k_{∞} for the Molten Salt Transmuter at a total flux of $3 \cdot 10^{15} \text{ cm}^{-2} \text{ s}^{-1}$, a fuel volume fraction of 2.3%, and a transuranics fraction of 20%. The results are presented in table 4.5.

Table 4.5: Maximum increase and decrease in the equilibrium critical core volume of the Molten Salt Transmuter due to uncertainties in the cross sections.

Uncertainty Set	Max	Min
Low	+25%	-18%
High	+110%	-39%

Due to the small k_{∞} and the relatively large uncertainty in k_{∞} , the uncertainty in the equilibrium critical core volume is large. The same uncertainty holds for the

equilibrium critical power. It is clear that the assumed uncertainties in the data for the transuranics is too high to predict the behavior of the Molten Salt Transmuter with reasonable accuracy.

4.7 Conclusions

The Molten Salt Transmuter is developed in this chapter because it is ideal as a transuranics burner due to the continuous fueling and reprocessing capabilities, the reprocessing technique based on a reduction process, and the low content of fission products. The low content of fission products is of major importance because the infinite multiplication factor is close to unity for the equilibrium isotope concentrations. Assumed was that xenon gas leaves the reactor immediately after production, which reduces the neutron absorption rate in the fission products by almost a factor of two. All fuel is reprocessed within 10 days to reduce the concentration of fission products further. Still, the maximum infinite multiplication factor for a thermal molten salt transmuter is only about 1.1 leading to a large equilibrium critical core size. Thermal reactor operation on only transuranics is possible for total flux values between $10^{14} \text{ cm}^{-2} \text{ s}^{-1}$ and $10^{15} \text{ cm}^{-2} \text{ s}^{-1}$.

The equilibrium critical reactor power depends strongly on the flux level of which the maximum value is completely determined by the maximum power density allowed in the salt. For a power density of 0.5 GW/m^3 which is equal to the one for the Molten Salt Breeder Reactor designed by ORNL, the flux level is equal to $5 \cdot 10^{14} \text{ cm}^{-2} \text{ s}^{-1}$ and the equilibrium critical reactor power is about 800 MW_t . It is shown that due to uncertainties in the cross sections of the transuranics, the reactor power might have been under- or overestimated by a factor of two, for uncertainties up to 50%. Uncertainties in cross sections should not exceed 10% for accurate reactor design.

The molten salt fuel was also chosen to make a negative fuel temperature reactivity coefficient possible by overmoderating the reactor. Due to the high cross sections of the plutonium isotopes, overmoderation can only be achieved for fuel volume fractions smaller than 2% leading to high core volumes or for fuel volume fractions higher than 7% for which the reactor spectrum is much harder than for lower fuel volume fractions. In equilibrium, the Doppler coefficient is always negative. For startup, the reactor is overmoderated and the fuel temperature reactivity coefficient is negative even though the Doppler coefficient is positive due to the large concentration of Pu-239. Of course, these reactivity coefficients are determined by the energy-dependent cross sections. For many isotopes important for the Molten Salt Transmuter, the data is very scarce, and the discussed results have very large uncertainties.

Chapter 5

Final Conclusions and Recommendations

To make possible the reduction of nuclear waste transuranics, two requirements must be met:

1. The losses in reprocessing should be smaller than 0.5%. In this thesis, it is assumed that these low losses can be obtained.
2. Special burner reactors should be operated at the end of the nuclear era to reduce the transuranics inventory. Up to then, one may use the transuranics in commercial power plants, which will significantly reduce the growth of transuranics.

A major part of this thesis deals with the design of special transuranics burners. An important conclusion is that no uranium should be present in the burner reactor in order to maximize the burned amount of transuranics per unit of energy. Furthermore, the specific power should be high to obtain a short reduction time for the transuranics inventory.

Two important issues result from reactor operation without uranium. First, fissioned material is not replaced by the fissile material formed by neutron capture in fertile uranium; this leads to a large reactivity loss during a cycle. Second, the Doppler coefficient which results from the broadening of neutron absorption resonances will be very different, thereby changing the reactivity feedback. Both issues might have serious implications on the safety of the design.

In this work, two reactor designs have been studied for burning transuranics:

- 1- A standard fast reactor operated in batch mode with a solid fuel and liquid sodium coolant,
- 2- A Molten Salt Transmuter, operated on a molten salt fuel with continuous refueling and reprocessing.

For the designed fast reactor, a large portion of uranium was necessary. The presence of uranium in the fuel reduces the burning efficiency of this reactor type considerably. Still, the burnup reactivity loss during a cycle was large in order to obtain a large net burnup of transuranics. This high reactivity leads to a high reactivity control requirement, which is in contradiction with modern safety philosophies. However, other safety implications are positive: the sodium void worth is reduced, and the coolant outlet temperatures for Anticipated Transients Without Scram are lower than for standard fast reactors.

The molten salt reactor is able to transmute transuranics at a rate four times higher than the ALMR burners. The burnup reactivity loss of the molten salt reactor is zero by definition. Operation as a thermal reactor is possible when the fission products are continuously removed. An additional advantage of using a fuel salt is that xenon can be removed easily due to its low solubility in the fuel salt. A negative temperature reactivity coefficient for the fuel density could only be obtained for fuel volume fractions below 2%, which makes the equilibrium critical reactor power and volume impractical. A negative temperature reactivity coefficient for the fuel density could also be obtained for fuel volume fractions higher than 7%. Then, the reactor is more or less a fast reactor. The increased fast fluence will make graphite exchange more frequent. A complete safety analysis of the Molten Salt Transmuter is yet to be performed.

Considering the follow up of this thesis, we recommend that the safety and the economics of the Molten Salt Transmuter are studied further. Especially of concern is the safety at start up of such a reactor.

The Molten Salt Reactor is not the only reactor type with continuous refueling. Other reactors to be considered in a follow up study are the suspension reactor, the CANDU reactor, and the High Temperature Gas Cooled Reactor (HTGR). The suspension reactor is of special interest to the Netherlands because of our history in the development of such a system, which resulted in the Kema Suspension Test Reactor. The CANDU is a commercially operated design developed in Canada. The use of inert matrices with transuranics seems to be possible for this design. It is yet to be proven that safety is sufficient and reprocessing is possible or that reprocessing is not necessary. The HTGR is a reactor operated with a helium gas as coolant and graphite as moderator. For the HTGR, reprocessing is very difficult because of the special graphite encapsulation of the fuel grains. This encapsulation is very hard to remove. The HTGR seems to be a viable burner

option when reprocessing is not necessary. A high transuranics burning rate can only be obtained at a very high burnup.

For fast reactors, the possibilities of designs without continuous refueling are not fully researched yet. The application of inert matrices in conjunction with burnable poisons might facilitate a non-fertile design with only a small reactivity change during a cycle.

REFERENCES

- 1 F. von Hippel, *Eliminating Nuclear Warheads*, Scientific American, August, 1993.
- 2 N. News, *World List of Nuclear Power Plants*, Nuclear News, **Vol. 35/No. 10** (August 1992), p. 74.
- 3 J. H. Bultman, *Reduction of Nuclear Waste by Introducing Advanced Liquid Metal Reactors*, in Global'93: Future Nuclear Systems: Emerging Fuel Cycles and Waste Disposal Options, Seattle, Washington (USA) , September 12-17, 1993.
- 4 K. D. B. Johnson and N. J. Keen, *Is the Nuclear Transmutation of the Actinides Justifiable?*, Proc. 2nd. Tech. Mtg. Nuclear Transmutation of Actinides, Ispra, 1980.
- 5 J. O. Blomeke, A. G. Croff, B. C. Finney and D. W. Tedder, *An overall assessment of actinide partitioning and transmutation for waste management purposes*, Proc. 2nd. Tech. Mtg. Nuclear Transmutation of Actinides, Ispra, 1980.
- 6 A. G. Croff, J. O. Blomeke and D. W. Tedder, *Actinide partitioning-transmutation program final report*, ORNL-5566, .
- 7 J. Prij, *Safety Evaluation of Disposal Concepts in Rock Salt*, IL-369/OPLA 89-08, Petten , 1989.
- 8 J. Prij, B. M. Blok, G. M. H. Laheij, W. van Rheenen, W. Slagter, G. J. M. Uffink, P. U. de Haag, A. F. B. Wildenberg and D. A. Zanstra, *PROSA, Probabilistic Safety Assessment*, RIVM, ECN, RGD, OPLA-1A , Petten , 1993.
- 9 R. Stack, J. Aschenbach, R. P. Hirsekom, A. Nies and N. Steltz, *PAGIS Performance Assessment of Geological Isolation Systems for Radioactive Waste, Disposal in Salt*, GSF report 23/88, München, 1988.
- 10 L. Burris, W. E. Miller, E. C. Gay, J. P. Ackerman, Z. Tomczuk, J. E. Herceg and J. Kann, *Update on Development of the IFR Reprocessing*, in Transactions of the American Nuclear Society, **Vol. 56**, 1988, pp. 68–70.
- 11 J. J. Duderstadt and L. J. Hamilton, *Nuclear Reactor Analysis*, J. Wiley & Sons, Toronto, Canada, 1976.
- 12 A. G. Elayi, *Plutonium and reactor transmutation*, Rad. Waste Man. Nuc. fuel cycle, **14**(1990), pp. 275–284.
- 13 A. G. Croff, C. W. Forsberg and S. B. Ludwig, *A Reexamination of the Incentives for Actinide Burning*, in Transactions of the American Nuclear Society, **Vol. 62**, 1990, pp. 76–78.
- 14 T. Mukaiyama, *Higher actinides transmutation using Higher Actinides Burner Reactors* , in Proc. Int. Conf. on the Physics of Reactors, Marseille, 1990, pp. I-97-107.
- 15 W. Takano, H. Akui, K. Kaneko and J. Saito, *Higher actinide confinement/transmutation fuel cycles in fission reactors*, in Proc. Int. Conf. on the Physics of Reactors, 1990, pp. PIII.145–155.
- 16 G. Oliva, *Neutronic transmutation of transuranium isotopes in a fast breeder power reactor*, Proc. 2nd. Tech. Mtg. Nuclear Transmutation of Actinides, Ispra, 1980.
- 17 S. Guardini and B. G. R. Smith, *Calculations for the assessment of actinide transmutation in LWRs*, Proc. 2nd. Tech. Mtg. Nuclear Transmutation of Actinides, Ispra, 1980.
- 18 S. F. Mobbs, M. P. Harvey, J. S. Martin, A. Mayall and M. E. Jones, *Comparison of the waste management aspects of spent fuel disposal and reprocessing: post-disposal radiological impact*, EUR 13561 EN, 1991.

- 19 Y. I. Chang, *Use of Fast Reactors for Actinide Burning*, in First MIT Int. Conf. on the Next Generation of Nuclear Power Technology, **CONF-9010305-1**, Cambridge (MA USA), 4-5 October, 1990.
- 20 B. Cohen, *Effects of ICRP-30 and the 1980 BEIR report on hazard assessments of HLW*, Health Physics, **42** (1982), p. 133.
- 21 A. G. Elayi and J. P. Schapira, *Impact of the changes from ICRP-26 to ICRP-48 recommendations on the potential radiotoxicity of the discharges of LWR, FBR and CANDU fuels*, Rad. Waste Man. Nuc. fuel cycle, **8** (1987), pp. 327–338.
- 22 L. H. Baetstlé, *Partitioning and Transmutation of Actinides and Fission Products*, Atomwirtschaft, April, 1993.
- 23 J. H. Bultman, *Calculation of the Transmutation Rates of Tc-99, I-129, and Cs-135 in the High Flux Reactor, in the Phenix Reactor, and in a Light Water Reactor*, ECN-I-92-013, 1992.
- 24 A. J. Janssen, *Transmutation of Fission Products in Reactors and Accelerator-Driven Systems*, ECN-R-94-001, Petten, 1994.
- 25 D. Lancaster, *Actinide Burning in a Standard Pressurized Water Reactor*, in GLOBAL'93: Future Nuclear Systems, Seattle (Washington USA), 12-17 September, 1993, pp. 609–614.
- 26 H. W. Wiese and B. Krieg, *Comparative Analysis of Actinide Burning in Multiple Recycling FBRs and PWRs*, in GLOBAL'93: Future Nuclear Systems, Seattle (Washington USA), 12-17 September, 1993, pp. 609–614.
- 27 H. W. Wiese, *Investigation of the Nuclear Inventories of High-Exposure PWR Mixed Oxide Fuels with Multiple Recycling of Self-Generated Plutonium*, Nucl.Tech., **102** (April, 1993), pp. 68–80.
- 28 G. Kessler, D. Faude and H. W. Wiese, *Direct Disposal Versus Multiple Recycling of Plutonium*, in GLOBAL'93: Future Nuclear Systems, Seattle (Washington USA), 12-17 September, 1993, pp. 275–282.
- 29 A. Strömich and W. Timm, *Semi-Annual Progress Report on "Transmutation of long-lived radionuclides by advanced converters"*, Siemens AG Power Generation Group (KWU), KWU BT71/92/0041, Bergisch Gladbach (Germany), 5-10-1992.
- 30 A. G. Croff, M. A. Bjerke, G. W. Morrison and L. M. Petrie, *Revised Uranium-Plutonium cycle PWR and BWR Models for the ORIGEN computer code*, ORNL/TM-6051, 1978.
- 31 M. J. Bell, *ORIGEN: The ORNL Isotope Generation and Depletion Code*, ORNL-4628, 1973.
- 32 J. L. Kloosterman, *New Working Libraries for Transmutation Studies*, in GLOBAL'93: Future Nuclear Systems, Seattle (Washington USA), 12-17 September, 1993, pp. 1229–1236.
- 33 M. L. Thompson, *Actinide recycle in the advanced liquid metal reactor*, Nucl.Eng.Int., October 1991.
- 34 C. L. Cockey, *Actinide Transmutation in the Advanced Liquid Metal Reactor*, in IAEA Int. Working Group on Fast Reactors: Specialists Meeting on Use of Fast Breeder Reactors for Actinide Transmutation, Obninsk, Russian Federation, september, 1992.
- 35 C. L. Cockey and M. L. Thompson, *ALMR Potential for Actinide Consumption*, in Proc. Int. Conf. Design & Safety of Advanced Nuclear Power Plants, Tokyo, Japan, October 25-29, 1992, pp. Paper P3–4.
- 36 T. H. Pigford and J. S. Choi, *Reduction in Transuranic Inventory by Actinide-Burning Liquid-Metal Reactors*, UCB-NE-4183, Berkeley (USA), June, 1991.

- 37 T. H. Pigford and J. S. Choi, *Inventory Reduction Factors for Actinide-Burning Liquid-Metal Reactors*, in Transactions of the American Nuclear Society, **Vol. 64**, San Francisco (USA), November, 1991, pp. 123–125.
- 38 J. H. Bultman, C. L. Cockey and T. Wu, *Actinide Breeding and Burning in Metallic Fueled and Oxide Fueled ALMR Cores*, in Global'93: Future Nuclear Systems: Emerging Fuel Cycles and Waste Disposal Options, Seattle, Washington (USA), September 12-17, 1993.
- 39 M. L. Thompson and I. N. Taylor, *Projected Waste Packages from Alternative Spent-Fuel Separation Processes*, EPRI-NP-7262, Palo Alto (USA), 1991.
- 40 M. Salvatores, I. Slessarev and M. Uematsu, *A Global Physics Approach to Transmutation of Radioactive Nuclei*, Nucl.Sci.Eng., **116**(1994), pp. 1–18.
- 41 R. I. Slessarev, N. Salvatores and M. Uematsu, *Transmutation Potential of Current and Innovative Nuclear Power Systems*, in GLOBAL'93: Future Nuclear Systems, Seattle (Washington USA), 12-17 September, 1993, pp. 1044–1049.
- 42 A. G. Croff and M. A. Bjerke, *LMFBR models for the ORIGEN2 computer code*, ORNL/TM-7176, 1981.
- 43 A. G. Croff and M. A. Bjerke, *Once-through CANDU reactor models for the ORIGEN2 computer code*, ORNL/TM-7177, 1980.
- 44 R. N. Hill, D. C. Wade, E. K. Fujita and H. Khalil, *Physics studies of higher actinide consumption in an LMR*, in Proc. Int. Conf. on the Physics of Reactors, Marseille, 1990, pp. I-83-96.
- 45 W. Timm, U. Strehlen and F. Sperber, *Semi-Annual Progress Report on "Transmutation of long-lived radionuclides by advanced converters"*, Siemens AG Power Generation Group (KWU), KWU BT71/93/0015, Bergisch Gladbach (Germany), 8-3-1993.
- 46 M. L. Thompson and J. E. Quinn, *The ALMR System's Missions for Transmuting Waste into Energy*, in GLOBAL'93: Future Nuclear Systems, Seattle (Washington USA), 12-17 September, 1993, pp. 110–117.
- 47 C. L. Cowan, A. E. Dubberley, E. L. Gluekler, R. E. Murata and D. M. Switick, *Core Design and Performance Characteristics for the Sodium Cooled Power Reactor Inherently Safe Module (PRISM)*, Proc.Int.Topl.Mtg.Advances in Reactor Physics Mathematics and Computation, Paris, France, April, 1987.
- 48 J. J. Laidler, J. E. Battles, W. E. Miller and E. C. Gay, *Development of IFR reprocessing technology*, in GLOBAL'93: Future Nuclear Systems, Seattle (Washington USA), 12-17 September, 1993, pp. 1061–1065.
- 49 V. A. Wichers and R. J. Heyboer, *INFCE Review Part A. Introduction, Fuel Cycles and Technologies*, ECN-I-93-001, 1993.
- 50 V. A. Wichers, *Evaluation of Reprocessing in the IFR with respect to Actinide Waste and Non-Proliferation*, ECN-R-93-018, 1993.
- 51 D. C. Wade, *Advanced Liquid Metal Reactor Development at Argonne National Laboratory during the 1980s*, in Transactions of the American Nuclear Society, **Vol. 62**, 1990.
- 52 I. N. Taylor, *private communication*, GE Nuclear Energy, San Jose, USA, 1993.
- 53 C. L. Cockey, T. Wu, A. J. Lipps and R. N. Hill, *Higher Actinide Transmutation in the ALMR*, in GLOBAL'93: Future Nuclear Systems, Seattle (Washington USA), 12-17 September, 1993, pp. 123–130.
- 54 R. Kinsey, *ENDF/B Summary Documentation*, Brookhaven National Laboratory, BNL-NCS-17541 (ENDF-201), July 1979.

- 55 R. E. Macfarlane, D. W. Muir and R. M. Boicourt, *The NJOY Nuclear Data Processing System*, Los Alamos National Laboratory, LA-9303-M (ENDF 324), 1982.
- 56 M. Salvatores, *Fast Reactor Calculations*, in Handbook of Reactors Calculations, Y. Ronen, ed., **III**, Boca Raton, Florida (USA), 1986, pp. 263–363.
- 57 K. L. Derstine, *DIF3D: A Code to Solve One-, Two-, and Three-dimensional Finite-Difference Diffusion Theory Problems*, Argonne National Laboratory, ANL-8144 (ENDF-239), 1976.
- 58 H. H. Hummel and D. Okrent, *Reactivity Coefficients in Large Fast Power Reactors*, 1970.
- 59 W. H. Press, B. P. Flannery, S. A. Teukolsky and W. T. Vetterling, *Numerical Recipes, The Art of Scientific Computing*, 1989.
- 60 J. Lewins, *Nuclear Reactor Kinetics and Control*, Pergamon Press, 1978.
- 61 D. C. Wade and E. K. Fujita, *Trends Versus Reactor Size of Passive Reactivity Shutdown and Control Performance*, Nucl.Sci.Eng., **103**(Oct. 1989), pp. 182–195.
- 62 D. C. Wade and Y. I. Chang, *The Integral Fast Reactor (IFR) Concept: Physics of Operation and Safety*, Proc.Int.Topl.Mtg.Advances in Reactor Physics Mathematics and Computation, Paris, France, April, 1987.
- 63 G. L. Gyorey, R. W. Hardy and P. M. Magee, *Safety and Licensing of the PRISM Liquid Metal Cooled Reactor*, Nucl.Eng.Des., **137**(1992), pp. 181–189.
- 64 A. J. Janssen, *On the Safety of the ALMR; Some Physics Aspects*, ECN-R-94-011, Petten, 1994.
- 65 H. G. MacPherson, *The Molten Salt Reactor Adventure*, Nucl.Sci.Eng., **90**(1985), pp. 374–380.
- 66 KEMA, *Final Report on the Aqueous Homogeneous Suspension Reactor Project*, Kema Sci.Techn.Rep., **5**(1987), pp. 1–48.
- 67 K. Furukawa, A. Lecocq, Y. Kato and K. Mitachi, *Thorium Molten-Salt Nuclear Energy Synergetics*, J.Nucl.Sci.Tech., **27**(1990), pp. 1157–1176.
- 68 K. Furukawa, *Symbiotic Molten-Salt Systems Coupled with Accelerator Molten-Salt Breeder (AMSB) or Inertial-Confined Fusion Hybrid Molten-Salt Breeder (IHMSB) and their Comparison*, Atomkernenergie/Kerntechnik, **44**(1984), pp. 42–45.
- 69 K. Furukawa, A. Lecocq, Y. Kato and K. Mitachi, *New Global Energy Strategy By Thorium Molten Salt Nuclear Energy Synergetics*, in Proc. Int. Conf. Design & Safety of Advanced Nuclear Power Plants, Tokyo (Japan), 25-29 Oct, 1992, pp. P3.9–1, 7.
- 70 K. Furukawa, Y. Kato and K. Mitachi, *Small Molten-Salt Reactors with a Rational Thorium Fuel-cycle*, Nucl.Eng.&Design, **136**(1992), pp. 157–165.
- 71 V. M. Novikov, *Molten Salt Advanced and Emerging Nuclear Systems: Flexible Energy Option*, Atomkernenergie/Kerntechnik, **45**(1984), pp. 45–49.
- 72 M. Taube, *The Transmutation of Strontium-90 and Cs-137 in a High-Flux Fast Reactor with a Thermalized Central Region*, Nucl.Sci.Eng., **61**(1976), pp. 212–221.
- 73 U. Gat, J. R. Engel and H. L. Dodds, *Molten Salt Reactors for Burning Dismantled Weapons Fuel*, Nucl.Tech., **100**(December, 1992), pp. 248–252.
- 74 E. Kasma and N. Hirakawa, *Conceptual Design of Molten Salt Reactor Fueled Partly By Transuranics*, in GLOBAL'93: Future Nuclear Systems, Seattle (Washington USA), 12-17 September, 1993, pp. 240–247.
- 75 V. D. Kazaritsky, K. Furukawa, G. V. Kiselev and N. Hirakawa, *Practical Treatment of Minor Actinides by Single Fluid Molten Salt Reactor Concepts*, in Proc. Int. Conf. Design & Safety of Advanced Nuclear Power Plants, Tokyo (Japan), 25-29 Oct, 1992, pp. P3.8–1, 5.

- 76 J. Hughes, I. Soares, E. Greenspan, W. F. Miller and Z. Shayer, *Molten Salt Critical Reactors for the Transmutation of Transuranics and Fission Products*, in GLOBAL'93: Future Nuclear Systems, Seattle (Washington USA), 12-17 September, 1993, pp. 644–651 .
- 77 M. W. Rosenthal, P. N. Haubenreich and R. B. Briggs, *The Development Status of a Molten-Salt Breeder Reactors*, ORNL-4812, 1972.
- 78 U. Gat and H. L. Dodds, *The Source Term and Waste Optimization of Molten Salt Reactors with Processing*, in GLOBAL'93: Future Nuclear Systems, Seattle (Washington USA), 12-17 September, 1993, pp. 248–252 .
- 79 J. R. Engel, W. A. Rhoades, W. R. Grimes and J. F. Dearing, *Molten-Salt Reactors for Efficient Nuclear Fuel Utilization without Plutonium Separation*, Nucl.Sci.Eng., **46**(1979), pp. 30–43.
- 80 ORNL, *Reactor Chemistry Division Annual Progress Report for Period Ending Dec. 31, 1965*, ORNL-3913, 1966.
- 81 R. C. Robertson, *Conceptual Design Study of a Single Fluid Molten-Salt Breeder Reactor*, ORNL-4541, 1971.
- 82 J. C. Ryman, *ORIGEN-S Data Libraries*, NUREG/CR-0200, 1981.
- 83 N. F. Launders and I. M. Petrie, *CSAS4: An Enhanced Criticality Safety Analysis Module with an Optimum Pitch Search Option*, NUREG/CR-0200, 1981.
- 84 N. M. Greene, *BONAMI-S: Resonance Self-Shielding by the Bondarenko Method*, NUREG/CR-0200, 1981.
- 85 R. M. Westfall, I. M. Petrie, N. M. Greene and J. L. Julius, *NITAWL-S: Scale System Module for Performing Resonance Self-Shielding and Working Library Production*, NUREG/CR-0200, 1981.
- 86 L. M. Petrie and N. M. Greene, *XSDRNPM: AMPX Moduel with One Dimensional S_n Capability for Spatial Weighting*, ORNL/RSIC-PSR-63, 1978.
- 87 R. C. L. vander Stad, C. Chonghai, H. Gruppelaar and V. L. Lalov, *EJ2-XMAS, a JEF2.2 Based Neutron Cross Section Library in the XMAS Group Structure; User Manual*, ECN-I-94-049 , Petten, The Netherlands, 1994.
- 88 J. W. Davidson and M. E. Battat, *Neutronics-Processing Interface Analysis for the Accelerator Transmutation of Waste (ATW) Aqueous Blanket System*, in GLOBAL'93: Future Nuclear Systems, Seattle (Washington USA), 12-17 September, 1993, pp. 387–396 .
- 89 G. Palmiotti, N. Salvatore and R. N. Hill, *Transmutation Potential of Current and Innovative Nuclear Power Systems*, in GLOBAL'93: Future Nuclear Systems, Seattle (Washington USA), 12-17 September, 1993, pp. 461–466 .
- 90 M. L. Williams, *Perturbation Theory for Nuclear Reactor Analysis*, in Handbook of Reactors Calculations, Y. Ronen, ed., **III**, 1986, pp. 108–133.
- 91 F. M. Mann and R. E. Schenter, *Calculated neutron capture cross sections to the Americium ground and isomeric states*, Nucl. Sci. Eng., **63**(1977), pp. 242–249.
- 92 ICRP, *ICRP Publication 61: Annual limits on intake of radionuclides for workers based on the 1990 recommendations*, Pergamon Press, New York, 1990 .
- 93 D. Nosske, B. Gerich and S. Langner, *Dosisfaktoren für inhalation oder ingestion von radionuklid verbindungen (Erwachsene)*, Institut für Strahlenhygiene des Bundesgesundheitsamtes, ISH-heft 63, 1985.

Appendix A

EQUI: Calculation of Equilibrium Actinide Densities

A.1 Calculational Method

For each isotope in the nuclear fuel cycle, the change in density is described by the difference in production and loss of this isotope. Each actinide isotope is produced either by decay of the mother or by neutron interaction in an isotope which will produce the isotope studied. Loss is caused by decay, by neutron absorption, or by loss in reprocessing. The loss of the isotope depends on the isotopic density of this isotope itself and the production depends on the isotopic density of other isotopes. When the densities of some isotopes are constant from cycle to cycle the densities of all the other isotopes will reach saturation values as soon as the loss will be equal to the production (equilibrium).

A special code EQUI has been developed for the calculation of equilibrium densities. To obtain the basic equations used in EQUI, several assumptions were made:

1. Constant cross-sections, which are independent on the problems calculated (no selfshielding anomalies),
2. One cycle exists of three years in core and three years of cooling and reprocessing,

3. Linear behavior of the isotopic densities during a cycle,
4. Constant loss of isotopes during the out-of-core periods to account for reprocessing losses,
5. Constant flux during in-core periods,
6. Exponential behavior of the basic fuel isotopes U-235 and U-238, during the in-core periods (no influence of other isotopes),
7. The same beginning of cycle (BOC) mass for each cycle for U-238.

Two periods were distinguished: the irradiation period, in which the nuclides are in-core, and the cooling period, in which cooling and reprocessing take place. Then, two differential equations are obtained.

$$irradiation : \frac{dN_i}{dt} = \sum_{j=1}^N (\lambda_{ji} + \phi(t)\sigma_{ji})N_j(t) - (\lambda_i + \phi(t)\sigma_i^{abs})N_i, \quad (A.1)$$

$$cooling : \frac{dN_i}{dt} = \sum_{j=1}^N \lambda_{ji}N_j(t) - \lambda_iN_i(t) - a_iN_i(t), \quad (A.2)$$

where $\phi(t)$ is the time dependent flux, σ_{ji} is the cross-section for producing nuclide i by neutron capture in nuclide j , σ_i^{abs} is the absorption cross-section, λ_{ji} is the decay constant for decay from nuclide j to i , and a_i is the loss rate during reprocessing. If one assumes a linear dependence on time of the isotopic densities as well as a constant loss rate, a constant flux and constant cross-sections, the equations A.1 and A.2 may be integrated to obtain the mean isotopic densities \overline{N}_i . Then, the following difference equations are derived.

$$\Delta N_i|_{t_{rad}} = \sum_{j=1}^N (\phi\sigma_{ji} + \lambda_{ji})\overline{N}_j t_{rad} - (\lambda_i + \phi\sigma_i^{abs})\overline{N}_i t_{rad}, \quad (A.3)$$

$$\Delta N_i|_{t_{cool}} = \sum_{j=1}^N \lambda_{ji}\overline{N}_j t_{cool} - (\lambda_i + a_i)\overline{N}_i t_{cool}. \quad (A.4)$$

In these equations, t_{rad} and t_{cool} are the durations of the irradiation and cooling periods. Equations A.3 and A.4 are added up and for equilibrium, $\Delta N_i|_{t_{rad}}$ and $\Delta N_i|_{t_{cool}}$ have to be equal, but of opposite sign, thus:

$$(a_i t_{cool} + \lambda_i t_{tot} + \phi \sigma_i^{abs} t_{rad}) \overline{N}_i = \sum_{j=1}^N \phi \sigma_{ji} \overline{N}_j t_{rad} + \sum_{j=1}^N \lambda_j \overline{N}_j t_{tot}. \quad (\text{A.5})$$

First, the behavior of U-235 and U-238 will be considered. For these nuclides, the production by decay and neutron interactions by other nuclides was assumed to be zero. U-235 is only produced by decay of Pu-239 with a half life of $2.4 \cdot 10^4$ years. So, in six years, only a fraction of $1.7 \cdot 10^{-4}$ of the Pu-239 decays to U-235. U-238 is produced by decay of Pu-242 with a half life of $3.8 \cdot 10^5$ years and by neutron capture in the short-lived U-237. These nuclides hardly influence the U-238 mass. Also, the half lives of U-235 and U-238 were assumed to be infinite (both are of the order of 10^9 years). Then, equation A.1 may be integrated immediately for U-235 and U-238:

$$N_i(t) = N_i(0) \exp(-\phi \sigma_{abs}^i t). \quad (\text{A.6})$$

The production by U-235 and U-238 is given by integration of these equations when multiplied by the neutron cross-section of the production path of interest. Equations for the production P of U-236, U-237 and U-239 are:

$$P(^5U \rightarrow ^6U) = \frac{N_5(0) \sigma_{cap}^5}{\sigma_{abs}^5} (1 - \exp(-\phi \sigma_{abs}^5 t_{rad})), \quad (\text{A.7})$$

$$P(^8U \rightarrow ^7U) = \frac{N_8(0) \sigma_{n \rightarrow 2n}^8}{\sigma_{abs}^8} (1 - \exp(-\phi \sigma_{abs}^8 t_{rad})), \quad (\text{A.8})$$

$$P(^8U \rightarrow ^9U) = \frac{N_8(0) \sigma_{cap}^8}{\sigma_{abs}^8} (1 - \exp(-\phi \sigma_{abs}^8 t_{rad})). \quad (\text{A.9})$$

A special case is Am-241. Neutron capture gives two states for Am-242. A ground state which decays quickly to Cm-242 (82.7%) and Pu-242 (17.3%) and a metastable state which decays to the ground state with a half life of 152 years. According to reference 91, about 15% of the metastable state is formed by capture in Am-241. In ORIGEN-S, approximately 16% of the metastable state is formed by capture in Am-241⁸².

In EQUI, an iteration processor is available to obtain the user-specified k_∞ at the end of cycle and/or the burnup at end of cycle by varying the density of specified nuclides and the total flux value.

The total and alpha activities and the radiotoxicity for ingestion and inhalation according to both the ICRP⁹² and ISH standards⁹³ are calculated for the fuel and the waste as a function of time according to equation A.10:

$$Z(t) = \sum_{i=1}^N N_i Z_i(t) \quad (\text{A.10})$$

Here $Z_i(t)$ is the activity or radiotoxicity Z of nuclide i and its daughters as a function of time. At $t=0$, the contributions of the daughters to Z are zero. The activity and radiotoxicity of the fuel, the losses, and the added mass are calculated.

In EQUI, the energy H produced during a cycle is calculated by multiplying the number of fissions during the irradiation with the energy production w_f^i per fission of nuclide i , as given in equation A.11

$$H = \sum_{i=1}^N w_f^i \phi t_{rad} \sigma_f^i \overline{N}_i + H(^8U) + H(^5U). \quad (\text{A.11})$$

The energy produced in U-235 and U-238 is calculated using the time dependence of the density of these nuclides. The result is shown in equation A.12

$$H(^5U \text{ or } ^8U) = \frac{N_i(0) \sigma_f^i w_f^i}{\sigma_{abs}^i} (1 - \exp(-\phi \sigma_{abs}^i t_{rad})). \quad (\text{A.12})$$

The energy produced by neutron capture (about 10 MeV per capture) is neglected because w_f^i is approximately 200 MeV.

The k_∞ at BOC and EOC due to the actinides is calculated according to equation A.13:

$$k_\infty = \frac{\sum_{i=1}^N \nu_i \sigma_f^i N_i}{\sum_{i=1}^N (\sigma_a^i + \sigma_f^i) N_i}, \quad (\text{A.13})$$

with ν_i , the number of neutrons released per fission in nuclide i and N_i the isotopic densities at BOC or EOC. At BOC, the isotopic density is approximated by $(1 - \frac{1}{2} a_i t_{cool}) \overline{N}_i$ and at EOC, the isotopic density is approximated by $(1 + \frac{1}{2} a_i t_{cool}) \overline{N}_i$.

A.2 Cross Section and Decay Data

In table A.1, the cross-sections and the half lives of the relevant nuclides are presented. Cross-section data for EQUI were obtained from reference³⁰ (the PWR-U reactor type). These data were selected to obtain maximum traceability. The half lives were obtained from reference 82.

Also the (n,2n) reaction in U-238 is considered, with a value of 0.005 barn⁸². The amount of neutrons per fission, ν , and the corresponding energy production per fission in MeV, w_f , were obtained from reference⁸².

Table A.1: *Half lives and cross-sections for the nuclides for an LWR.*

nuclide	half-life [y]	σ_{cap} [b]	σ_{fis} [b]	ν	w_f [MeV]
U-234	$2.45 \cdot 10^5$	19.2	0.45	2.42	190.3
U-235		10.5	46.7	2.42	192.9
U-236	$2.346 \cdot 10^7$	7.54	0.197	2.75	191.4
U-238		0.9	0.1	2.82	193.9
Np-237	$2.142 \cdot 10^6$	32.1	0.52	3.01	193.6
Pu-238	87.81	34.7	2.46	2.82	196.9
Pu-239	$2.408 \cdot 10^4$	58.6	106	2.87	198.5
Pu-240	6541	104	0.58	3.12	196.9
Pu-241	14.71	38.7	118	2.93	200.3
Pu-242	$3.7605 \cdot 10^5$	29.4	0.46	3.13	200
Am-241	432.49	111.5	1.32	3.21	200
Am-242m	151.99	155	770	3.21	200
Am-243	7385	38	0.36	3.21	200
Cm-242	0.4471	5.48	0.22	3.36	200
Cm-243	28.52	9.92	97.6	3.36	200
Cm-244	18.123	3.44	0.85	3.36	200
Cm-245	8505.8	184.0	172	3.35	200
Cm-246	4733.3	1.32	0.49	3.35	200
Cm-247	$1.561 \cdot 10^7$	13.3	9.36	3.35	200

A.3 Program Description

A short description of the program and the subroutines used is presented in this section.

Subroutines and their functions:

- **INPUT:** data preparation from input file CHAIN_INPUT. Reading isotopes and half lives and daughters. Reading all possible cross-section data sets which are available in the file. Reading selected data: fission cross-section, energy production per fission, neutrons per fission, capture cross-section (the subroutine assumes that the product of capture is the next isotope in the chain), and finally cross-sections for other reaction types. After that all sets of BOC masses plus the options on exponential behavior, which are available in the file are printed as well as the input data to be selected.
- **PRODUCTION:** calculation of the production of isotopes by isotopes with fixed exponential behavior (equations A.7, A.8 and A.9)

- MATRIX: preparing equation A.5 for all isotopes for which equilibrium densities are needed.
- LUDCMP of reference 59 calculating the triangular factorization of the coefficient matrix A.
- LUBKSB of reference 59 calculating the solution of the triangular factorization of matrix A.
- OUTEQ: calculating and printing in file OUTPUT all possible functions: isotopic masses at BOC and at EOC, energy production per isotope per cycle, burnup, total masses of MA and of plutonium isotopes and of all actinides, k_{∞} at BOC and at EOC, total and alpha activity of fuel and waste as calculated by ACTIV and radiotoxicity for ingestion and inhalation of fuel and waste as calculated by DOSE.
- DOSE: radiotoxicity for ingestion and inhalation according to ISH or ICRP for 1, 3, 10, 100, 200, 1000, 10^4 , 10^5 , 10^6 and 10^7 years of decay. The daughters have zero mass at discharge. The radiotoxicity is calculated from the isotopic density array.
- ACTIVITY: total and alpha activity for 1, 3, 10, 100, 200, 1000, 10^4 , 10^5 , 10^6 and 10^7 years of decay. The daughters have zero mass at discharge. The activity is calculated from the isotopic density array.

Commands of the main program EQUI:

1. Calling INPUT
2. Input of several parameters: losses, flux/burnup, in- and out-of-core period.
3. Calling MATRIX, PRODUCTION, LUDCMP and LUBKSB
4. memorizing isotopic densities
5. calculation of k_{∞} (ETA) and burnup (MASSHEAT)
6. adjustment of flux and mass of specific isotopes to obtain fixed burnup and/or k_{∞} at EOC (if asked)
7. recalculation with new flux and densities (if asked)
8. calling OUTEQ

A.4 Verification of EQUI

A.4.1 Nuclide Densities

Table A.2 presents the end of cycle (EOC) masses for the once-through scenario as calculated by EQUI with the cross sections of Croff, and compared to results of Croff calculated with ORIGEN³⁰. In EQUI, the k_{∞} at EOC was 1.2, which is

Table A.2: *Mass of nuclides at EOC for the once-through scenario per 1000 kg heavy mass at the BOC.*

nuclide	mass at EOC [kg]	
	EQUI	Croff
U-234	0.174	0.180
U-235	8.87	7.94
U-236	4.65	3.94
U-238	944.9	944.1
Np-237	0.408	0.441
Pu-238	0.147	0.127
Pu-239	6.24	5.03
Pu-240	1.42	2.32
Pu-241	1.21	1.22
Pu-242	0.450	0.461
Am-241	0.069	0.031
Am-243	0.114	0.085
Cm-242	0.012	0.011
Cm-244	0.055	0.019
Total Pu	9.47	9.16
Total TRU	10.20	9.75
Total MA	0.729	0.587
Total ARA	15.02	13.87
Total	964.1	967.7

the same as the k_{∞} for the EOC mass of the actinides according to Croff³⁰. The same burnup of U-238 as Croff was obtained at a flux of $3.76 \cdot 10^{13} \text{ cm}^{-2} \text{ s}^{-1}$. The same burnup of 33 MWd/kg(HM) was used. In general, the results seem to be in reasonable agreement. Exceptions are:

1. U-235 mass at BOC is 36.9 kg for EQUI compared to 32 kg for Croff due to the higher flux needed to obtain the same burnup of U-238 as Croff.
2. The Pu-240 mass is underestimated.

3. Cm-244 is overestimated.

The burnup is lower for EQUI at the same flux level, due to the buildup of especially Pu-239. In EQUI, it is assumed that Pu-239 builds up linearly, which is not the case in a once-through system. So, the average density of Pu-239 calculated by EQUI is lower than for the once-through system, and the energy production by Pu-239 is underestimated. The reason why the flux had to be higher to obtain the same burnup of U-238 is not clear, because the same cross sections were used.

In table A.3, the nuclide densities for the total recycling scheme are presented calculated with EQUI and with ORIGEN-S with continuous concentration of U-235 and U-238. The same ORIGEN-S cross-sections were used. The ORIGEN-S calculations was 15 cycles long with recycling of all actinides. The ORIGEN results are separated in BOC, EOI and EOC. Here, EOI means at the end of the 3 years of irradiation and EOC means after 3 years decay. For total recycling, the EOC masses are the same as the BOC masses of the next cycle. So, if the BOC and EOC masses are not the same, these nuclides did not reach their equilibrium masses yet.

The following discrepancies for the total recycling calculations were observed:

1. For the following nuclides, the BOC masses of two following cycles were not the same as calculated by ORIGEN-S: U-236, Np-237, Pu-238, Cm-246 and Cm-247. Differences between EQUI and ORIGEN for these nuclides are probably caused by the fact that these nuclides are not in equilibrium after 15 cycles in the ORIGEN calculation.
2. The Cm-242 mass calculated by EQUI is equal to the EOI mass of ORIGEN. This is probably caused by the linear approximations in EQUI, which is not correct for short-lived nuclides.
3. The Am-241 mass in EQUI is approximately equal to the average mass in the ORIGEN case, probably due to the decay of Pu-241, which is only present in EQUI by taken an average during the whole cycle, including the cooling time.

Table A.3: Equilibrium masses of nuclides for total recycling calculated by EQUI compared to ORIGEN-S calculations with the same ORIGEN-S cross-sections.

nuclide	Mass [kg]			
	EQUI	ORIGEN		
		BOC	EOI	EOC
U-234	0.49	0.524	0.364	0.54
U-235	32.0	32.0	32.0	32.0
U-236	48.7	45.8	46.5	46.5
U-238	968.0	968.0	968.0	968.0
Np-237	9.56	8.91	8.98	9.06
Pu-238	8.14	7.27	7.48	7.38
Pu-239	6.68	6.52	6.50	6.57
Pu-240	4.01	4.13	3.82	4.15
Pu-241	2.02	1.71	1.98	1.72
Pu-242	2.16	2.14	2.16	2.16
Am-241	0.154	0.339	0.082	0.343
Am-242m	0.00523	0.0031	0.00317	0.00313
Am-243	1.64	1.64	1.65	1.65
Cm-242	0.0517	$5 \cdot 10^{-4}$	0.051	$5 \cdot 10^{-4}$
Cm-243	$8.28 \cdot 10^{-4}$	$9.2 \cdot 10^{-4}$	0.001	$9.3 \cdot 10^{-4}$
Cm-244	3.01	2.76	3.13	2.79
Cm-245	0.337	0.340	0.345	0.345
Cm-246	2.47	1.44	1.54	1.54
Cm-247	0.157	0.086	0.093	0.093
Total Pu	23.0	21.8	21.9	22.0
Total TRU	40.4	37.4	37.7	37.9
Total MA	17.4	15.6	15.8	15.9
Total RAA	89.6	83.7	84.6	84.9
Total	1089.6	1083.7	1084.6	1084.9

A.5 Conclusions

For most cases, the results of the program EQUI and ORIGEN with continuous feeding of U-235 and U-238 are in agreement with each other. Except for a few isotopes, EQUI can produce good results for the once-through case. Especially for Pu-239 and the higher curium isotopes, the results were different, because this program was developed to calculate equilibrium concentrations. The results for the total recycling case with constant U-235 and U-238 concentrations are in good agreement.

Curriculum Vitae

Jan Bultman werd op 19 juni 1964 geboren te Renkum. In 1982 behaalde hij het Atheneum diploma aan het Christelijk Atheneum te Arnhem. In dat jaar begon hij zijn studie Natuurkunde aan de Rijks Universiteit Utrecht. In 1988 studeerde hij af met het *judicium cum laude* op zijn onderzoek naar het neutralentransport in tokamak plasma's bij het FOM-instituut Rhijnhuizen bij de vakgroep plasmafysica van Professor Dr. H. de Kluiver. Daarna werkte hij twee jaar bij het Rijks Instituut voor Volksgezondheid en Milieuhygiëne te Bilthoven bij de afdeling Standaarddosimetrie van Drs. A.H.L. Aalbers aan de verbetering van meetmethoden voor de calibratie van radioactieve bronnen gebruikt bij Radiotherapie. In 1990 kwam hij als promovendus in dienst van het Energieonderzoek Centrum Nederland, hetgeen leidde tot dit proefschrift. Vanaf 1 september 1994 is hij in dienst van het ECN als post-doc.